

2012

## PERFORMANCE PREDICTION OF PAVEMENTS WITH COLD IN-PLACE RECYCLING ASPHALT MIXTURES

Max Benjamin Müller  
*University of Rhode Island, max\_mueller@my.uri.edu*

Follow this and additional works at: <https://digitalcommons.uri.edu/theses>

Terms of Use

All rights reserved under copyright.

---

### Recommended Citation

Müller, Max Benjamin, "PERFORMANCE PREDICTION OF PAVEMENTS WITH COLD IN-PLACE RECYCLING ASPHALT MIXTURES" (2012). *Open Access Master's Theses*. Paper 105.  
<https://digitalcommons.uri.edu/theses/105>

This Thesis is brought to you by the University of Rhode Island. It has been accepted for inclusion in Open Access Master's Theses by an authorized administrator of DigitalCommons@URI. For more information, please contact [digitalcommons-group@uri.edu](mailto:digitalcommons-group@uri.edu). For permission to reuse copyrighted content, contact the author directly.

PERFORMANCE PREDICTION OF  
PAVEMENTS WITH COLD IN-PLACE RECYCLING  
ASPHALT MIXTURES

BY

MAX BENJAMIN MÜLLER

A THESIS SUBMITTED IN PARTIAL FULFILLMENT OF THE  
REQUIREMENTS FOR THE DEGREE OF  
MASTER OF SCIENCE  
IN  
CIVIL AND ENVIRONMENTAL ENGINEERING

THE UNIVERSITY OF RHODE ISLAND

2012

MASTER OF SCIENCE  
OF  
MAX BENJAMIN MÜLLER

APPROVED:

Thesis Committee:

Major Professor      K. Wayne Lee

Natacha Thomas

Arun Shukla

Martin Sadd

Nasser H. Zawia  
DEAN OF THE GRADUATE SCHOOL

THE UNIVERSITY OF RHODE ISLAND

2012

## **ABSTRACT**

The pavement rehabilitation and reconstruction method with Cold In-Place Recycling (CIR) is an alternative that can effectively conserve materials and energy, preserve the environment and reduce the cost. An attempt was made to predict the performance, particularly low-temperature cracking resistance characteristics of CIR mixtures prepared with the mix design procedure developed at the University of Rhode Island (URI) for the Federal Highway Administration (FHWA). The mix design procedure was developed to reduce wide variations in CIR mixture production and to develop a nation-wide standard.

This standard was applied to a Rhode Island (RI) reclaimed asphalt pavement (RAP) to produce CIR mixtures with CSS-1h asphalt emulsion as the additive. By adjusting the number of gyrations of the Superpave Gyratory Compactor (SGC) for compaction, the field density of 130 pcf was achieved in the laboratory. To secure a base line, hot mix asphalt (HMA) samples were produced first according to the Superpave volumetric mix design procedure with an air void content of 4.0%. These were tested and analyzed parallel to the CIR specimens to compare the performances.

The specimens were tested using the Indirect Tensile (IDT) tester at temperatures of -20, -10 and 0°C (-4, 14, and 32°F, respectively) in accordance with the AASHTO T 322 procedure. The creep compliance and tensile strength values were used as input data for the Mechanistic Empirical Pavement Design Guide (MEPDG) analysis. This software predicts the performance of roadways with different pavement structures, traffic, environmental conditions, and material properties using several mathematical models for different types of distresses.

The analysis results indicated that no thermal or low-temperature cracking is expected over the entire analysis period of 20 years for both HMA and CIR mixtures. It confirms with the field performance in Arizona. Thus, it appears that CIR is a sustainable rehabilitation technique, and it justifies further research on and investigation of load-related distresses such as rutting and fatigue cracking.

## **ACKNOWLEDGEMENTS**

I would like to express my sincere thanks to my supervisor, Professor K. Wayne Lee, for his guidance and encouragement throughout this study. I consider it an honor to have Prof. Natacha Thomas and Prof. Arun Shukla on my thesis committee. I am also thankful to Prof. Martin Sadd for agreeing to be the chairman of my thesis defense committee. Also, I would like to acknowledge the general assistance provided by Ajay Singh and technical support by Kevin Broccolo with the laboratory equipment.

A research team at the University of Connecticut supported this research effort, and I appreciate the assistance by Prof. Adam Zofka and his research assistant Ramandeep Josen. Also, the support from the research from the University of Illinois at Urbana-Champaign with the software TCMODEL is highly appreciated.

Personal thanks go to my parents as well as my sister, Laura Amelie. Without their support and understanding I would not have been able to complete this work.

## TABLE OF CONTENTS

Abstract.....	ii
Acknowledgements .....	iv
Table Of Contents.....	v
List Of Tables.....	viii
List Of Figures.....	x
1 Introduction .....	1
1.1 Cold In-Place Recycling (CIR).....	2
1.2 Research Plan.....	3
2 Current Status of Knowledge .....	5
2.1 Earlier Works by URI Research Team .....	5
2.2 Asphalt Emulsions .....	9
2.3 Indirect Tensile Testing .....	10
2.4 Mechanistic-Empirical Pavement Design Guide.....	16
3 Asphalt Pavement Materials.....	19
3.1 Hot-Mix Asphalt (HMA) Specimens.....	19
3.2 Cold In-Place Recycled (CIR) Mixtures.....	25
4 Indirect Tensile (IDT) Testing.....	32
4.1 Specimen Preparations.....	32
4.2 IDT Testing.....	35

4.3	Data Analysis.....	38
4.3.1	Creep Compliance, $D(t)$ .....	38
4.3.2	Tensile Strength, $S$ .....	47
5	Performance Prediction of Both Mixtures.....	51
5.1	Input for TCMODEL and MEPDG.....	51
5.2	Prediction Results and Interpretation.....	57
6	Conclusions and Recommendations.....	61
6.1	Conclusions.....	61
6.2	Recommendations.....	62
	References.....	64
APPENDIX A	Modified Superpave Mix Design for CIR Mixtures.....	67
APPENDIX B	New Test Machine Documentation.....	71
APPENDIX C	Gradation Requirements for RI Class I-1.....	82
APPENDIX D	Exemplary Compaction Calculations for HMA Sample.....	85
APPENDIX E	RAP Material Analysis.....	92
APPENDIX F	Necessary Number of Gyration for CIR Material.....	95
APPENDIX G	Determination of Optimum Contents of CIR Material.....	102
APPENDIX H	Masses of Ingredients for Produced CIR Specimens.....	106
APPENDIX I	Planned Testing Schedule.....	108
APPENDIX J	Specimen Labels.....	110



APPENDIX K	Normalized Horizontal Deformations .....	112
APPENDIX L	Creep Compliance Summary .....	116
APPENDIX M	Tensile Strength Summary .....	122
APPENDIX N	Traffic and Weather Data for Construction Site .....	127
APPENDIX O	Simulation Results .....	132
Bibliography	.....	135

## LIST OF TABLES

Table 2-1 Work Plan of the URI Study to Develop Mix Design Procedure .....	6
Table 3-1 Maximum and Bulk SG Test Results over Binder Content .....	22
Table 3-2 Masses of Ingredients for OEC Determination Samples .....	28
Table 3-3 Ingredients for OWC Determination Samples .....	30
Table 4-1 PID-Settings for Conducted Testing .....	36
Table 4-2 Creep Test Steps.....	38
Table 4-3 Calculations prior to Creep Compliance at -10°C (14°F).....	45
Table 4-4 Creep Compliance of HMA at -10°C.....	46
Table 4-5 Creep Compliance of HMA Mixture with Respect to Creep Time $t$ .....	47
Table 4-6 Creep Compliance of CIR Mixture with Respect to Creep Time $t$ .....	47
Table 4-7 Average Tensile Strength $S_t$ [psi] of both Mixtures.....	49
Table 5-1 General Parameters for Bituminous Mixtures .....	56
Table 5-2 CIR (1) Simulation Output.....	58
Table A-1 Sieve sizes for RAP gradation.....	67
Table C-1 Gradation Required for Class I-1 classification .....	82
Table C-2 Required Material Amounts for Preparation of Specimens .....	83
Table D-1 Compaction Calculations for first 5.5% BC Sample .....	85
Table D-2 Bulk SG Computations .....	90
Table D-3 Theoretical Maximum SG Computations .....	90
Table E-1 Moisture Test.....	92
Table E-2 Sieve Analysis Measurements .....	93
Table F-1 Calculations for Determination of Number of Gyration for CIR Materials.	95

Table F-2 Compaction for Determination of Number of Gyration for CIR Materials .	95
Table G-1 Determination of Theoretical Maximum SG for OEC Determination.....	102
Table G-2 Bulk and Theoretical Maximum SG Results and Calculations for OEC Determination .....	103
Table G-3 Determination of Theoretical Maximum SG for OWC Determination .....	103
Table G-4 Bulk and Theoretical Maximum SG Results and Calculations for OWC Determination .....	104
Table H-1 Required Masses of Ingredients for CIR Specimen Production .....	106
Table J-1 Specimen Labels.....	110
Table M-1 Tensile Strength Test Results for HMA .....	122
Table M-2 Tensile Strength Test Results for CIR .....	122
Table N-1 Traffic Amount and Distribution for Route 2 .....	127
Table N-2 Annual Climate Statistics .....	128
Table N-3 Average Monthly Quintile Temperatures - Surface.....	129
Table N-4 Average Monthly Quintile Temperatures - Sublayer 1 .....	129
Table N-5 Average Monthly Quintile Temperatures - Sublayer 2.....	130
Table N-6 Monthly Rainfall Statistics.....	130
Table O-1 HMA Simulation Output.....	132
Table O-2 CIR (1) Simulation Output.....	133
Table O-3 CIR (2) Simulation Output.....	134

## LIST OF FIGURES

Figure 2-1 Liquid Asphalt Dispersed in Water .....	9
Figure 2-2 Indirect Tensile Test setup.....	11
Figure 2-3 Stress States in an Asphalt Concrete Layer under a Wheel Load.....	12
Figure 2-4 Stresses in x- and y- Direction along Horizontal and Vertical Planes.....	13
Figure 3-1 Compaction Level during Compaction for 5.5% Binder Content Specimen	23
Figure 3-2 Averaged Air Voids over Binder Content .....	24
Figure 3-3 Gradation of RAP Material.....	25
Figure 3-4 Compaction Behavior of CIR Sample during Compaction .....	27
Figure 3-5 Determination of OEC at 3.0% Water Content .....	29
Figure 3-6 Determination of OWC at 0.7% Emulsion Content .....	30
Figure 4-1 Specimens in Saw Fixture and during Sawing .....	34
Figure 4-2 Attaching Buttons for Strain Gauge Attachment.....	35
Figure 4-3 IDT Specimen during Creep Test.....	37
Figure 4-4 Loading over Time for Specimen 004 .....	39
Figure 4-5 Displacements of both Axes on both Faces of Specimen 004 over Time ....	40
Figure 4-6 Normalized Horizontal Deformations of three HMA Specimens at -10 °C.	42
Figure 4-7 Averaged Tensile Stress over Time for HMA Material .....	49
Figure 5-1 MEPDG Input Checklist.....	52
Figure 5-2 Climate File Generation via Interpolation .....	54
Figure 5-3 MEPDG Pavement Setups .....	56
Figure 5-4 Thermal Cracking Parameters Input Window .....	57
Figure B-1 Instron® Quotation for Test Machine Upgrades, page 1/5.....	76

Figure B-2 Instron® Quotation for Test Machine Upgrades, page 2/5 .....	77
Figure B-3 Instron® Quotation for Test Machine Upgrades, page 3/5 .....	78
Figure B-4 Instron® Quotation for Test Machine Upgrades, page 4/5 .....	79
Figure B-5 Instron® Quotation for Test Machine Upgrades, page 5/5 .....	80
Figure I-1 Planned Testing Schedule .....	108
Figure K-1 Normalized Horizontal Deformations of HMA Specimens at -20 °C .....	112
Figure K-2 Normalized Horizontal Deformations of HMA Specimens at -10 °C .....	112
Figure K-3 Normalized Horizontal Deformations of HMA Specimens at 0 °C .....	113
Figure K-4 Normalized Horizontal Deformations of CIR Specimens at -20 °C .....	113
Figure K-5 Normalized Horizontal Deformations of two CIR Specimens at -10 °C ...	114
Figure K-6 Normalized Horizontal Deformations of two CIR Specimens at 0 °C .....	114
Figure L-1 Specimen Dimensions for HMA Mixture .....	116
Figure L-2 Specimen Dimensions for CIR Mixture .....	117
Figure L-3 Creep Compliance Calculations for HMA Specimens .....	118
Figure L-4 Creep Compliance Calculations for CIR Specimens .....	119
Figure L-5 Creep Compliance of HMA for Superpave Software Input .....	120
Figure L-6 Creep Compliance of CIR for Superpave Software Input .....	120
Figure M-1 Averaged Tensile Stress over Time for CIR Mixture .....	123
Figure M-2 Detailed Strength Test Data for HMA Mixtures .....	124
Figure M-3 Detailed Strength Test Data for CIR Mixtures .....	125

## 1 INTRODUCTION

Roadways are exposed to various loadings and stresses that reduce their serviceability like other infrastructures. Traffic as well as environmental stresses wear out pavement structures. Despite careful consideration in the design and construction process, distresses cannot be avoided in the pavement surfaces. The most efficient means to deal with these distresses and wearing appears to be rehabilitating the pavement at a point where its condition can be improved with a reasonably affordable amount of resources. This could be an adequate maintenance practice in order to avoid expensive reconstruction, and it needs to be planned over the expected pavement service period.

Whenever rehabilitation or reconstruction is required, it is necessary to rebuild portions of the pavement structure. Certain layers of the roadway are typically milled up to a determined depth, which can include the surface and even the base course. If the milled materials are replaced with virgin materials, it requires purchasing and transporting new material which consumes time, energy, and money. Furthermore, the old material becomes waste, harming the environment and incurring further costs tied to disposal.

A method of reducing these issues is in-place recycling. It allows the user to re-use materials that are already in the pavement. This process includes milling, screening and crushing of the broken pavement materials. Additives such as emulsified asphalt or fly ash are then incorporated. This mixture is put back in place and compacted. Finally,

a protective overlay is placed above the recycled layer of asphalt concrete, which is typically Hot Mix Asphalt (HMA).

In general, major advantages of this recycling procedure are as follows:

- Less trucking
- Conservation of materials, energy, and time
- Preservation of the environment
- Cost reduction

These advantages pose major incentives to promote and support in-place recycling and allow the roadway rebuilding procedure to be conducted in a sustainable way.

In-place recycling can be performed at different temperatures. Cold recycling typically uses materials at ambient temperatures, i.e., at around 25°C (77°F). The absence of the necessity to heat up the material provides major advantages. Furthermore, pollution in the form of smoke, heat and noise is reduced. Less time is needed for cooling off, therefore allowing sooner openings for traffic. Thus, in-place recycling is an approach for green highways and streets.

### 1.1 COLD IN-PLACE RECYCLING (CIR)

While various pavement construction practices have been used for centuries and a considerable amount of empirical experiences has been accumulated, in-place recycling is a relatively new technique, and performance records are limited. The special feature of this technique is the use of reclaimed asphalt pavement (RAP), and its properties and behavior are not uniform. Assumptions used for virgin material may not necessarily be applicable for RAP.

Standardized regulations for procedures, testing, and quality control are still needed for a wide-spread application of this technique. Based on the URI Mix Design procedure, this Master thesis deals with the prediction of performance of pavements with CIR, particularly, low-temperature cracking resistance characteristics. In order to fairly evaluate the predictions, the pavement structures with CIR materials were compared to the ones with virgin materials, or HMA, with the same boundary conditions. Even with varying thicknesses of different layers in the pavement structure (which are explained in section 5.1), exposure to the same environmental conditions ensure a fair comparison.

## 1.2 RESEARCH PLAN

To evaluate the performance of pavement for CIR materials, the first step was to get accustomed to this construction method and to investigate the current status of knowledge.

A parallel HMA base line had to be established to which the results of the CIR materials could be compared. The results, obtained similarly to those with CIR material, represent the performance of materials which are being used presently for a variety of road construction or rehabilitation projects. The results for the CIR mixture give expectations in a situation where CIR materials can be used instead of the HMA using raw materials.

Cylindrical specimens with almost equal dimensions were prepared for HMA and CIR materials. These are then tested with the Indirect Tensile (IDT) testing device, which allows the user to prepare input data for performance prediction. After a data



analysis, the creep compliance, a measure to determine resistance against deformation with respect to time, and the tensile strength, were obtained. These are the input data for a software which can predict the performance of both materials for a given analysis period. Comparing the outputs for both materials give the user the expectable performance. Interpretations of these were used for a technical recommendation for not only future road construction projects, but also further research.

## **2 CURRENT STATUS OF KNOWLEDGE**

The literature review comprised many fields of pavement engineering, starting from the specimen preparation, i.e., basic material handling, all the way to software-based predictions on the basis of analyzed test data. This chapter also explains why certain decisions were made and why certain steps were taken in order to accomplish the objective. It includes steps of the CIR Mix Design, the indirect tensile test, and application of gained data in the computer software.

### **2.1 EARLIER WORKS BY URI RESEARCH TEAM**

A URI research team developed a performance-based mix design for bituminous materials with CIR under the contract of the Federal Highway Administration (FHWA) (Lee, Brayton and Milton 2002). Firstly, they analyzed the difficulties that existed for the standardized application of this technique. Overall it was found that there were wide variations concerning procedures, testing and quality control, e.g., Oregon and California have state-wide methods which differ considerably from one another. Hence, the main objective was to develop a standard procedure to use throughout the US.

The research project started with forming an expert task group (ETG) whose members comprised representatives from CIR contractors, universities and state agencies. They assisted setting up a work plan consisting of five phases which are shown in Table 2-1.

Table 2-1 Work Plan of the URI Study to Develop Mix Design Procedure

Phase	Task
I	Identify Sensitivity Factors
II	Procure and test RAP + Emulsion
III	Evaluation of Modified Marshall Mix Design
IV	Development of Performance Based Mix Design
V	Limited Field Evaluation

Past specimen production procedures with CIR were typically based on the Marshall Method, which compacts the specimens by dropping a weight of 4,536 g (10 lbs.) from a height of 457.2 mm (18 in.) 35 to 75 times, depending on the assumed traffic loading (Asphalt Institute 1984). However, it was found out that this method does not simulate field conditions well. The Marshall hammer did not seem to be the method of choice for CIR samples, since it did not compact specimens with small amounts of fine materials appropriately. That led, inter alia, to air voids of approx.  $16.5 \pm 1.0$  %. Furthermore, preparation of those samples could exceed 8 days, and the mass of a specimen could easily fall below 1,000 g, whereas a mass of 1,150 g is the suggested minimum. Together with further problematic disadvantages such as missing guidelines and lack of performance prediction, the Marshall mix design was found to be inappropriate for CIR mixtures.

Unlike the hammer blows with the Marshall compactor, the Superpave gyratory compactor “imparts a constant vertical pressure of 600 kPa to the sample while rotating (or gyrating) the sample with an eccentricity of  $1.25^\circ$  from the vertical axis” (Coree and VanDerHorst 1998). After every gyration, the height of the sample is determined, which

allows any desired density, once the initial mass was measured. With field densities known, representative specimens can be prepared.

Since curing plays an important role, the appropriate duration and temperature needed to be determined. In the study, two levels for both curing time as well as temperature were compared. Results showed that the temperature of 60°C (140°F) was more effective than 25°C (77°F), and a curing time of 24 hours was more practical than 6 hours. It was decided to add an asphalt emulsion as the additive in the study. Once the RAP with the asphalt emulsion is put back in place, compaction causes the emulsion to break and the asphalt eventually coats the aggregate particles. What needed to be determined was the adequate amount of water as well as emulsion.

To optimize both parameters, a criterion was chosen. In this case, the bulk specific gravity was supposed to become maximum. Optimizing both parameters with only one criterion is a very challenging task, thus the parameters were optimized one at a time.

Initially, the water content is to be kept constant (3.0% suggested) while the amount of emulsion varies. Four different amounts of emulsion are to be used with 2 specimens each for improved reliability. For both contents, values may be based on experience, but the procedure suggests starting values that are expected to surround the optimum contents. After specimen production and determination of unit weight (or bulk specific gravity) according to the procedure of AASHTO T 166 (AASHTO 2011) and theoretical maximum specific gravity according to AASHTO T 209 (AASHTO 2011), both values are plotted over the percentage of emulsion in the first, or water in the second step.

For both the emulsion and water content, the optimum levels are determined by selecting the “content at which the unit weight is at its maximum value” or, “if a maximum unit weight is not achieved, the content at which the unit weight is similar to those found in the field” should be the optimum value (Lee, Brayton and Milton 2002).

The Superpave design method was recommended to prepare specimens for the prediction of future performance of the pavement with CIR. Software, such as VESYS® or the Mechanistic-Empirical Pavement Design Guide (MEPDG®) which includes more comprehensive prediction models, can be used to predict performance of the roadway in the future using the input data of the materials and environmental conditions.

A visco-elastic model, VESYS, requires two parameters,  $K_{1q}$  and  $K_{2q}$ , which describe the material’s fatigue characteristics, to predict the area that is expected to crack, with certain stochastic deviation. These parameters can be determined from material testing; the flexure fatigue test on beams (Steen 2001). Those parameters need to be determined at a set of different temperatures because the behavior of asphalt concrete, as a viscoelastic material, is highly dependent on the temperature. The test results are utilized to determine the parameters with which the models predict the performance.

For field verification, a test site was constructed in Arizona. The procedure described above was applied, and the optimum emulsion content (OEC) and optimum water content (OWC) used were 2.5 % and 2.0 %, respectively. A 2-inch milling produced a 2-inch CIR layer, but instead of the planned chip seal, a 1.5-inch HMA overlay was placed on top of CIR base. It has been reported that no significant distresses were found, which proves a very good performance.

For this thesis work, the developed performance-based Mix Design for CIR mixtures was used. The entire procedure can be found in APPENDIX A. However, the concise steps are described in the following chapter.

## 2.2 ASPHALT EMULSIONS

RAP materials still contain some asphalt binder; however it has aged and does not coat the particles well after milling. Without heating, it cannot be distributed evenly throughout the pavement material to glue it together.

Generally, there are several options for the type of additives for CIR projects, but an asphalt emulsion was used in the study. An emulsion's versatility and adjustability to many different boundary conditions was one reason to become the most common additive for CIR projects (California Department of Transportation 2008).

In general, "emulsified asphalt is simply a suspension of small asphalt cement globules in water, which is assisted by an emulsifying agent". As liquid asphalt is based on oil and does not dissolve in water, a chemical agent is needed to disperse the liquid asphalt in water. It forms droplets with a diameter ranging from 1 to 10  $\mu\text{m}$  (Walker 2012). Figure 2-1 visualizes the dispersed phase in the continuous phase.

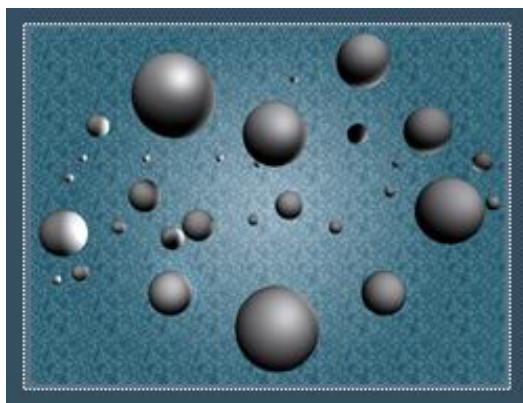


Figure 2-1 Liquid Asphalt Dispersed in Water

Classifications for emulsions have been standardized by the American Society for Testing and Materials (ASTM) as well as the American Association of State Highway and Transportation Officials (AASHTO). Cationic emulsions are positively charged and designated with a "C", while the absence

thereof indicates a negatively charged, anionic emulsion. The latter are not widely used, however. The following label yields information about the “setting”, breaking rate. “RS” stands for rapid set, “SS” for slow set, and “QS” means quick set. Setting or breaking of the emulsion is the process in which the tiny droplets begin to coalesce and form a film to cover the aggregate. Careful handling according to the applicable safety and handling instructions prevent premature breaking.

After breaking, sufficient time must be allowed for curing. This process comprises the attainment of stiffness when the water separates and disperses. Also, the ambient weather can offer good conditions for this while high humidity and low temperatures, on the other hand, can deter proper curing (The Asphalt Institute 1979). For laboratory specimen preparation, a sufficient time for curing must be ensured (24 hours) in an oven.

CSS-1h emulsions are usually a good choice for CIR projects. The slow setting rate is suitable for this type of road construction. The number refers to the emulsion’s viscosity. In this case, the emulsion has a lower viscosity than a “2”. The “h” designates the use of harder base asphalt, which is usually the case.

### 2.3 INDIRECT TENSILE TESTING

When conducting the indirect tension (IDT) test, a cylindrical specimen with a diameter of 150 mm (6 in) and a thickness of 38 to 50 mm (1½ to 2 in) is exposed to a single load imposed perpendicularly to the longitudinal axis with a static support on the opposite side. Figure 2-2<sup>1</sup> offers a front view of the specimen during the test.

---

<sup>1</sup> Source: <http://www.sciencedirect.com/science/article/pii/S0013794407000665>

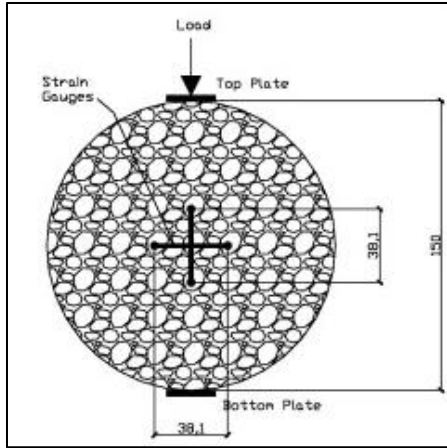


Figure 2-2 Indirect Tensile Test setup

It was found that the IDT test is able to represent the most critical location of a pavement under a wheel load. Roque and Buttlar (1992) stated that, “the critical location for load-induced cracking is generally considered to be at the bottom of the asphalt concrete layer and immediately underneath the load, where the stress state is longitudinal and transverse tension combined with vertical compression (see Figure 2-3). As shown in Figure

2-4, the stress state in the vicinity of the center of the face of an indirect tension specimen is very similar to this stress state, except that tension is induced in one rather than two axes.” Figure 2-3 shows the stress states at different locations in the asphalt layer that evolve from a wheel load. The critical stress state, as described above, is shown in case 2, where the compressive vertical stress due to the wheel load in combination with the deflection of the pavement causes tensile stresses in both of the other axes to build up.



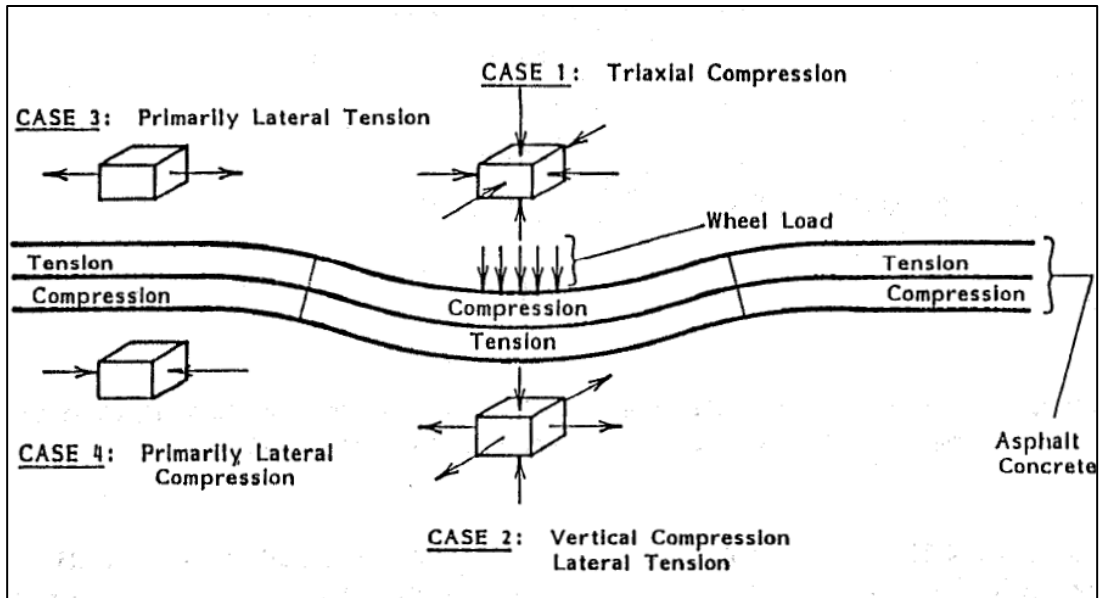


Figure 2-3 Stress States in an Asphalt Concrete Layer under a Wheel Load

Figure 2-4 illustrates the stress intensity along the horizontal and vertical diametric planes of an IDT specimen during testing (Roque and Buttlar 1992). It may be noted how the critical stresses, i.e., where failure can be expected under the assumption of a homogeneous and isotropic material, is along the vertical axis: Along this axis, the tensile stress in the horizontal direction is constant, while the same stress peaks along the horizontal axis. Testing would show that specimen failure occurs along this axis. However certain deviation in the failure path due to material imperfections, uneven distribution of voids, and influence of aggregates can occur.

The location of the failure plane poses another major advantage: Measurements can be taken directly on the failure plane which allow for greater accuracy. Meanwhile, other testing modes only allow determination of average values.

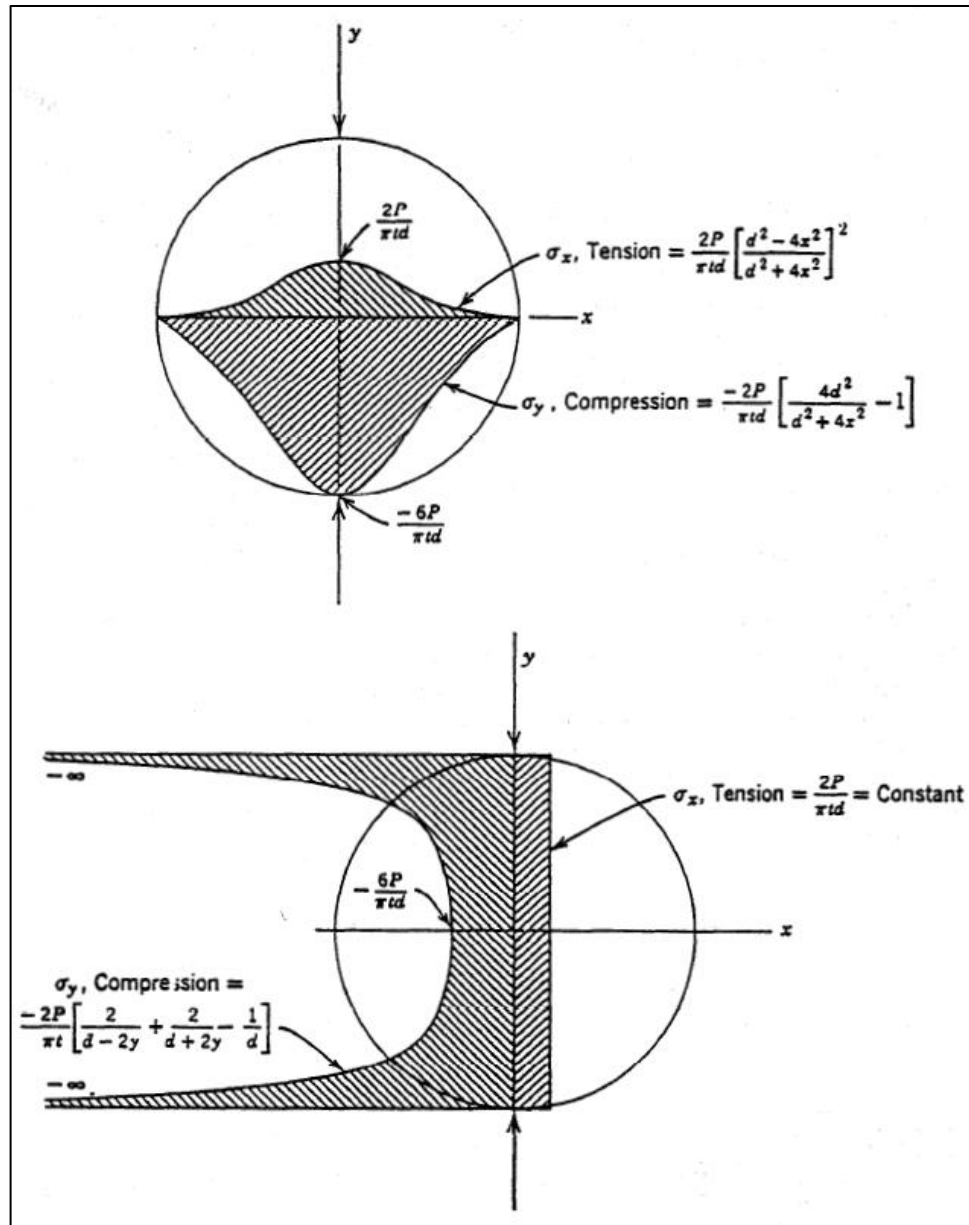


Figure 2-4 Stresses in x- and y- Direction along Horizontal and Vertical Planes

The IDT test is conducted according to the AASHTO T 322 procedure (AASHTO 2011). Its purpose is to determine the creep compliance  $D(t)$  as well as the tensile strength  $S_t$  at low temperatures. Creep compliance is defined as “the time-dependent strain divided by the applied stress” (AASHTO 2011) and therefore has the unit of the reciprocal of stress. A constant load is to be applied on the specimen for a duration of 100 (MEPDG input values) or 1,000 seconds (complete analysis). The

temperature is required to be at or below 0°C (32°F), and the test requires a minimum of three different temperatures. Not only does Superpave mixture analysis specify the temperatures of -20, -10 and 0°C (-4, 14 and 32°F, respectively), but also the input options for MEPDG are at these temperatures. In order to allow the specimen to cool down to the test temperature and establish an appropriate temperature distribution throughout the material, the sample has to remain inside the climate chamber at the test temperature for  $3 \pm 1$  hours prior to testing.

During creep compliance testing, the deformations near the center of the specimen are recorded. This test is considered to be non-destructive; still the specimen shows permanent deformation due to the viscoelastic behavior. The tensile strength test is to be performed immediately after the creep compliance test. Now the loading ram movement is required to be constant with a speed of 12.5 mm/min until the load sustained by the specimen decreases. This is regarded to as failure and the maximum load therefore is the failure load.

Based on the deflections and load recorded during testing, the creep compliance  $D(t)$  as a function of time and the tensile strength  $S_t$  of the material at the test temperatures can be computed.

An up-to date and calibrated testing machine is required to perform the AASHTO T 322 (AASHTO 2011). This includes devices to impose the required loads on the specimens and ensure the required constant ram movement, specimen deformation and load measurement devices as well as a temperature conditioning and a data acquisition system.

A testing machine, an Instron® 5582, that is available in the Transportation Engineering Laboratory at the University of Rhode Island (URI) seemed to meet these

regulations. In close cooperation with the supervisor, Professor K.W. Lee, as well as Mr. K. Broccolo, an attempt was made to calibrate the machine. A malfunction was found in data acquisition system. Several tests showed that the machine could work on a sample, but the deflections and applied force could not be logged during or stored after testing. This way, the data acquisition could be identified as the source of error. Efforts were initiated towards the purchase of a new data acquisition system. The existing machine was purchased before the turn of the millennium and purchasing an entirely new system would exceed the available funding. Therefore, suitable new parts that would work with the old, present machine needed to be identified. In cooperation with the manufacturer Instron with extensive communication via email, the proper upgrades could be found and a quotation was filed (see APPENDIX B). The order was placed, but unfortunately the time frame until delivery and complete installation of the new equipment was too wide for this project to take effect. Therefore, another way of testing needed to be found.

Fortunately, the University of Connecticut (UConn) could provide the required testing environment for this project. With experienced guidance, a total of five appointments were agreed upon first to inspect the testing equipment at the Connecticut Transportation Institute (CTI). Thereafter, four more appointments were made for two different sets of specimens to be sawed and tested. Since sawing the cylindrical specimens to suitable heights of 38 to 50 mm (1½ to 2 in.) from their original heights was accomplished with wet sawing, an appropriate time frame of at least 24 hours was necessary to allow the samples to dry before testing. At this point, gratitude should be expressed to UConn for their generous support towards this project.

## 2.4 MECHANISTIC-EMPIRICAL PAVEMENT DESIGN GUIDE

The Mechanistic-Empirical Pavement Design Guide (MEPDG) was developed based on results of the Long-Term Pavement Performance (LTPP) program. The LTPP program started a comprehensive experiment about pavements in service by monitoring more than 2,400 asphalt and Portland cement concrete roadways across the United States and Canada. The data obtained helped to develop the algorithms for the new performance prediction software. With the weather history known about the location where the future pavement is to be constructed, the pavement structure can be entered into the program. Then, the program output is a prediction of the serviceability of the roadway that can be expected under the given boundary conditions. MEPDG combines a variety of sub-programs that each treat different distresses such as rutting, fatigue cracking and thermal cracking.

TC MODEL is the program which analyzes the stresses due to low temperatures and is able to quantify the thermal distresses. It should be noted at this point, that “TC MODEL does not consider traffic effects” (Marasteanu, et al. 2007). This program is very user-friendly, as it offers a convenient way to enter the data input. It simplifies the problem by using linear elastic fracture mechanics in a one-dimensional stress evaluation model. Newer software aims to treat this problem with nonlinear finite element analysis engines. This allows for better reliability of the predictions due to a more accurate mathematical representation of the problem. This software is still under development for the full-scale deployment (Leon, Dave and Park 2011).

TCMODEL offers a mechanistic approach to treat thermal cracking in flexible pavements by means of mathematical modeling. Unlike a variety of other mechanistic programs, it offers the possibility to quantify the amount of low-temperature cracking

which is a major advantage. However, this is only the final step after first calculating the thermal stress and, second, calculating the crack propagation in the pavement structure over time.

Based on the creep compliance with respect to real time  $t$  determined for different temperatures, master curves are obtained. From that, a 4-parameter Prony series is retrieved for the creep compliance  $D$  with respect to reduced time  $\zeta$ . Using a known strain history, the thermal stress over time can be obtained using a one-dimensional hereditary integral. In order to integrate with respect to real time  $t$  instead of reduced time  $\zeta$ , a finite difference solution was developed. This requires for the solution to be calculated for time intervals  $\Delta t$  in which the strain changes by  $\Delta \varepsilon$ .

The next major step is the calculation of the crack propagation. A crack is modeled as a single vertical crack in the bituminous layer. To express the growth of the crack length, Paris' law is applied and simplified as TC MODEL computes the results on a daily basis. With both the thermal stress and the crack propagation treated mathematically, now the particular step of TC MODEL, the calculation of the crack amount, can be started. The amount of cracking is obtained from a calibrated probability function with respect to the crack length being at least as long as the thickness of the bituminous layer, as shown in Eq 2-1.

$$AC = \beta \cdot P(\log C > \log D) \quad \text{Eq 2-1}$$

where

$AC$	observed amount of thermal cracking
$\beta$	regression coefficient, determined through field calibration
$P( )$	probability function
$D$	thickness of surface layer
$C$	crack length

Field calibration resulted in  $\beta$  to be determined as 353.5. Also, not only the character of the probability function, but the program itself inherits certain restrictions concerning the outputs for crack amount. A crack is only considered a crack if it reaches the bottom of the asphalt layer. Also, the program predicts no more than 50% of the total possible amount of thermal cracking (Marasteanu, et al. 2007).

The results from the performed calculations are shown in the output files. It shows the results after every month for the desired analysis period, which is usually 20 years. So for every month the amount of transverse cracking will be shown in feet per mile. Since MEPDG includes a variety of sub-programs to predict multiple types of distresses, the regular result includes their outputs as well. For the analyses conducted in this thesis, however, the results are limited to the distress of thermal cracking. Then, they are interpreted in order to give an evaluation of the thermal cracking resistance of the recycled material to contribute to a recommendation for the use of CIR in future projects.

### **3 ASPHALT PAVEMENT MATERIALS**

The primary objective of this study was the evaluation of the performance of a CIR material for rehabilitation or reconstruction projects. A base line was established with HMA first. For HMA specimen production, aggregates were acquired from a quarry.

The new type of material was CIR, which makes techniques using this material being more sustainable. The present, old pavement material is milled off the road, screened, and emulsion is added. Then the material is put back in place and compacted. After a sufficient time for curing, the surface needs to be protected by a sealing course or an overlay.

To measure performance in the laboratory, specimens are necessary that represent field conditions as accurately as possible. This chapter explains how this requirement was dealt with, how the material was obtained, how the recipes for both types were developed, and how the final specimens for testing were produced.

#### **3.1 HOT-MIX ASPHALT (HMA) SPECIMENS**

HMA represents the current practice of road construction, and consists of mineral aggregates and asphalt binder. In this study, the aggregates were acquired from the PJ Keating Company in Cranston, Rhode Island. These were sieved and weighed in accordance with the gradation of RI Class I-1 (see APPENDIX C).

Specimens with 4 different binder contents from 5.5 to 7.0% with increments of 0.5% were tested, and the optimum binder content (OBC) was determined at the air void content of 4.0%. The details can be found in APPENDIX C.



A loose (uncompacted) sample with a mass of approximately 1,000 g (2.2 lbs) was used to determine the theoretic maximum specific gravity according to the procedure of AASHTO T 209 (AASHTO 2011). The aggregate particles were separated manually in order to avoid small cavities that would contain air and therefore distort the volume determination. After that, the sample was weighed into a container of known volume. Then, enough water was filled into the container to completely cover the sample. The sealed container was agitated for 15 minutes with a mechanical device while a vacuum pump creates negative pressure to remove all the air that is being expelled from the sample. Finally, the container was filled with water entirely and its mass was measured. The maximum specific gravity could be determined according to Eq 3-1.

$$G_{mm} = \frac{A}{A + D - E} \quad \text{Eq 3-1}$$

where

$G_{mm}$	theoretical maximum specific gravity [-]
$A$	mass of dry sample in air [g]
$D$	mass of container filled with water [g]
$E$	mass of container filled with water and sample [g]

It should be mentioned at this point that the calculated test result is very sensitive to slight deviations concerning the determination of the masses. Not only is it important to avoid any air bubbles when sealing the container with the lid, but also water can be in the tap that is required for the connection of the vacuum pump. That is the reason why this test was repeated several times to get reliable and repeatable results.

This test was performed only for one binder content. Using the correlation between the maximum theoretical specific gravity ( $G_{mm}$ ) and the effective specific

gravity ( $G_{se}$ ) of the mixture,  $G_{mm}$  for the other binder contents can be calculated according to Eq 3-2 (Mamlouk and Zaniewski 2006).

$$G_{se} = \frac{P_s}{\left( \frac{P_{mm}}{G_{mm}} - \frac{P_b}{G_b} \right)} \quad \text{Eq 3-2}$$

$$\Leftrightarrow G_{mm} = \frac{P_{mm}}{\left( \frac{P_s}{G_{se}} + \frac{P_b}{G_b} \right)} \quad \text{Eq 3-3}$$

where

- $G_{se}$  effective specific gravity [-]
- $P_s$  aggregate content (% of total mixture),  $P_s = 100\% - P_b$
- $P_{mm}$  total loose mixture (100 %)
- $P_b$  binder content [%]
- $G_b$  specific gravity of binder (1.03 [-])

These results are the only ones obtained from the uncompacted specimens. The results are shown in Table 3-1. Specimens with all different binder contents need to be compacted with the Superpave gyratory compactor (SGC). A number of 175 gyrations were used. It should be mentioned that the final compaction level is important for calculation purposes only, but not for testing. 175 gyrations would compact the specimens to a point where they would be denser than in the field and would not represent field conditions accurately, since the number of gyrations for design purposes would be 100 according to the procedure of AASHTO R 35 (AASHTO 2011). The obtained test results were only used for back-calculating purposes and not for performance testing.

The compacted specimens were then tested for their bulk specific gravity ( $G_{mb}$ ) and water absorption according to the procedure of AASHTO T 166 (AASHTO 2011). After determining the dry mass of all specimens, they were submersed in water for 4 minutes and the weight under water was determined. Then, they were taken out of the

water and the surface water was removed with a damp towel in order to achieve a saturated surface-dry state. Finally, the mass was determined again. The  $G_{mb}$  was calculated according to Eq 3-4.

$$G_{mb} = \frac{A}{B - C} \quad \text{Eq 3-4}$$

where

- $A$  mass of dry sample in air [g]
- $B$  mass of saturated surface-dry sample in air [g]
- $C$  mass of specimen in water [g]

For this test, duplicate specimen results were averaged, the results are shown in

Table 3-1.

Table 3-1 Maximum and Bulk SG Test Results over Binder Content

Binder Content [%]	$G_{mb}$ [-]	$G_{mm}$ [-]
5.5	2.550	2.638
6.0	2.534	2.617
6.5	2.502	2.595
7.0	2.495	2.574

The bulk SG after every gyration can be estimated because the specimen's mass is known and the gyratory compactor yields the height of the specimen after every gyration in the compaction mold of known dimensions. By dividing the mass by the calculated volume and the density of water at 4.0°C (0.999972 g/cm<sup>3</sup>), the estimated bulk SG ( $G_{sb,est}$ ) can be computed. A correction factor  $C$  is introduced to obtain the corrected bulk SG ( $G_{sb,corr}$ ). It is determined and applied to every gyration according to Eq 3-5 and Eq 3-6.

$$C = \frac{G_{mb,measured}}{G_{mb,best}(N = 175 \text{ gyrations})} \quad \text{Eq 3-5}$$

$$G_{mb,corr} = G_{mb,measured} \cdot C \quad \text{Eq 3-6}$$

By dividing the corrected bulk SG by the theoretical maximum SG, the compaction level as a percentage of the maximum theoretical SG is computed. Figure 3-1 shows the compaction level over the number of gyrations for the first specimen with a binder content of 5.5%.

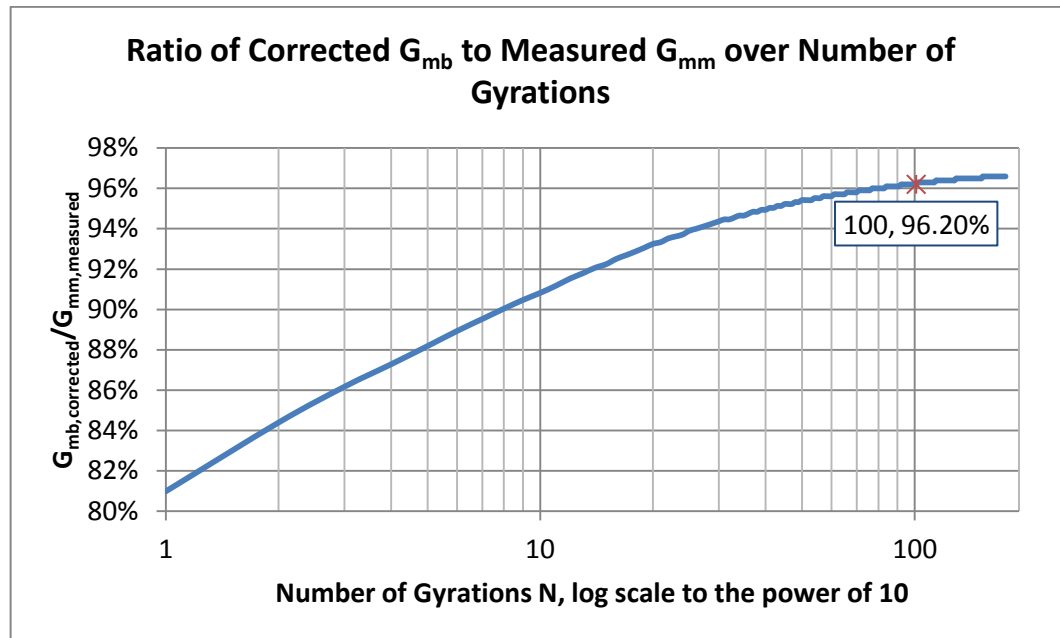


Figure 3-1 Compaction Level during Compaction for 5.5% Binder Content Specimen

As one can see, the compaction level after 100 gyrations is 96.2% which corresponds to an air void content of 3.8%. This calculation was done for duplicate specimens at 4 binder contents. As an example, the spreadsheet for the first sample with a binder content of 5.5% can be found in APPENDIX D.

Finally, the binder content is plotted against the averaged air void contents. The results are shown in Figure 3-2.

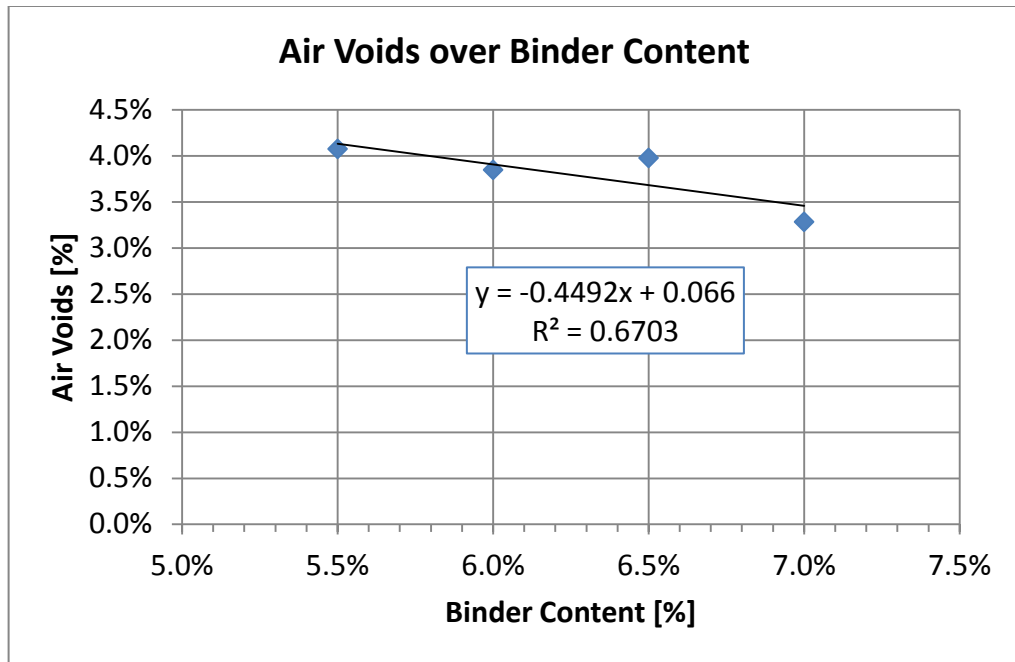


Figure 3-2 Averaged Air Voids over Binder Content

Finally, the OBC at an air void content of 4.0% was determined graphically and numerically to be 5.8%. Therefore, the specimens for the planned indirect tensile testing were produced with this OBC. Also, compaction was accomplished with only 100 instead of 175 gyrations.

### 3.2 COLD IN-PLACE RECYCLED (CIR) MIXTURES

RAP was acquired from a construction site of Rhode Island Route 3. Unfortunately, the material was stored uncovered for an unknown amount of time, and the influence of aging, oxidation and freezing, especially on the binder, may have been significant. However, since another source was not available, the RAP was used despite concerns over different properties from fresh one.

After drying, the moisture content and the gradation were determined in accordance with the procedure of AASHTO T 255 and T 27, respectively (AASHTO 2011). The results indicated that neither the moisture content of 4.1% nor the gradation of Figure 3-3 exhibited any significant deviation from expected ones. The details can be found in APPENDIX E.

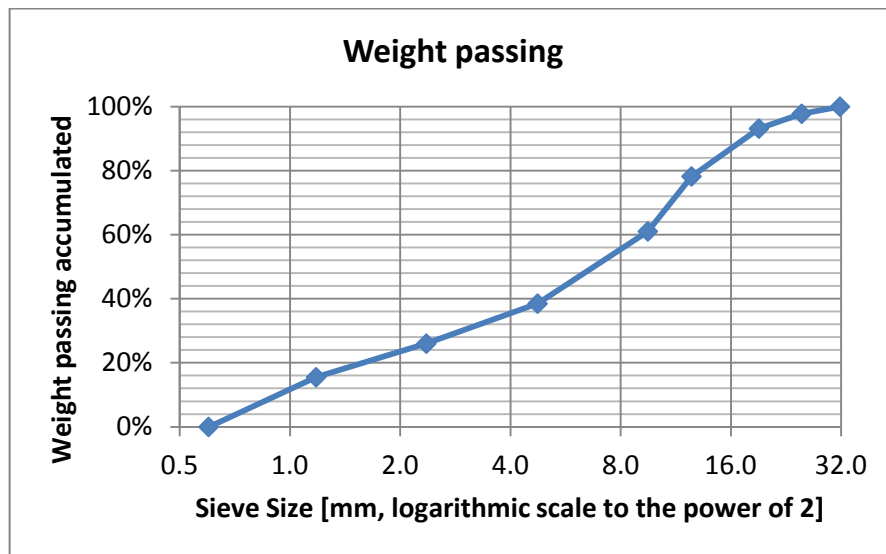


Figure 3-3 Gradation of RAP Material

As reported earlier, the CSS-1h emulsion was used in this study. According to the CIR Mix Design procedure which was developed by a URI research team (Lee, Brayton and Milton 2002), the optimum emulsion and water content needed to be determined. The process was carried out by first keeping the water content constant and

varying the emulsion content. For the determination of the optimum content, the unit weight is the parameter to be compared to field conditions. Either the maximum value or, if a maximum cannot be determined, the best representation of field condition should be chosen. Before any specimen can be produced, the appropriate number of gyrations for compaction needs to be determined. Since the standard procedure for HMA (AASHTO 2011) is not applicable here, another method needed to be used. The URI procedure states that, “The load shall be applied for the number of gyrations that will result in achieving densities similar to those found in the field.” Therefore, a method was used that is somewhat similar to the determination of the amount of air voids for HMA materials (Lee, Brayton and Milton 2002). It is based on representing field density, and the value of previous URI study, i.e., 130 pcf was used (Steen 2001). Following steps were used in this study:

- Determine the mass of the sample (aggregate + water + emulsion)
- Compact with 175 gyrations (like HMA)
- Calculate estimated bulk SG after every gyration
- Measure bulk SG after 175 gyrations (experiment)
- Correction factor  $C = (\text{measured bulk SG after 175 gyrations}) / (\text{estimated bulk SG after 175 gyrations})$
- Multiply bulk SG after every gyration by C to obtain corrected bulk SG
- Find field density
  - Divide corrected bulk SG by field density
  - Look for 100.0%

The test specimen for this procedure was made with a water content of 3.0% and an emulsion content of 1.0%. After compaction, the bulk SG was determined and all the required calculations were completed as seen in APPENDIX F. The compacting behavior of the specimen can be seen in Figure 3-4.

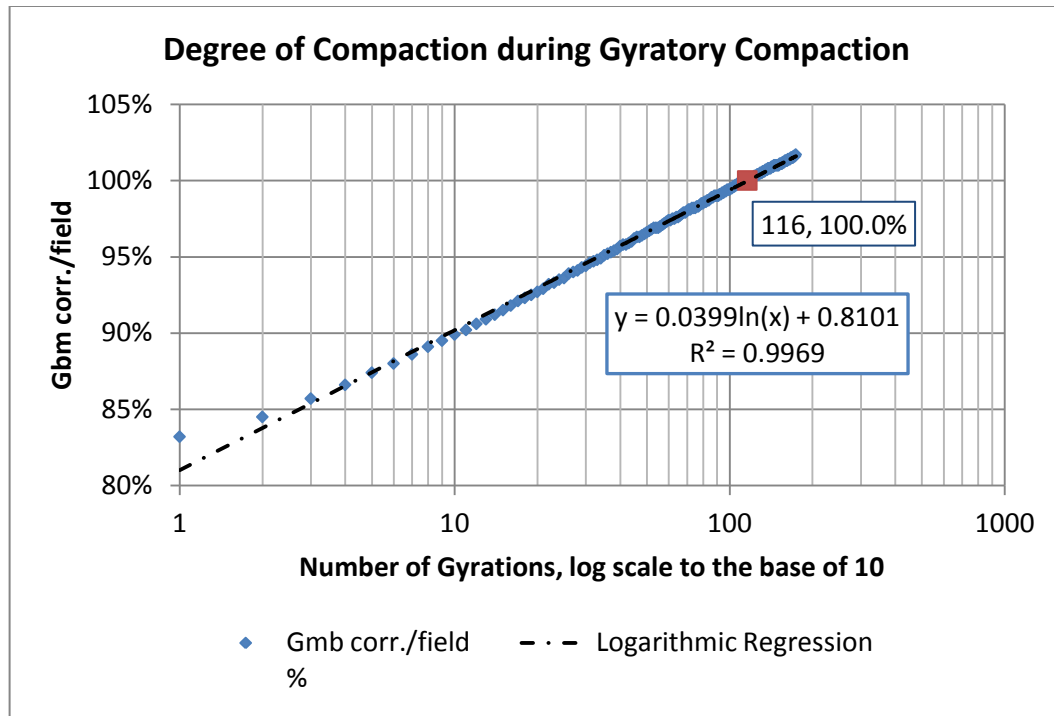


Figure 3-4 Compaction Behavior of CIR Sample during Compaction

As can be seen from this graph, the degree of compaction can very closely be approximated using a logarithmic curve. Based on the values shown in Table F-1 (APPENDIX F), 116 gyrations were used for all following specimens.

For any set of emulsion and water contents, 9,000 g of RAP were used. This was because duplicate specimens for bulk SG determination with about 4,000 g each were needed along with one sample for theoretical maximum SG determination, for which a mass of about 1,000 g was sufficient. To ensure sufficient mass, 9,000 g for the RAP was chosen because emulsion and water still had to be added, which lead to a mass of more than 9,200 g before curing.

For the determination of the OEC, emulsion contents varied from 0.5% (of total mix mass) to 2.0% with increments of 0.5%, while the water content stayed constant at 3.0%. A summary of the masses of ingredients for all specimens that were produced for OEC determination can be found in Table 3-2.



Table 3-2 Masses of Ingredients for OEC Determination Samples

RAP [g]:	9,000			
<b>Water content:</b>	<b>3.0%</b>			
<b>Emulsion contents:</b>	<b>0.5%</b>	<b>1.0%</b>	<b>1.5%</b>	<b>2.0%</b>
Emulsion [g]:	46.6	93.8	141.4	189.5
Water [g]:	279.8	281.3	282.7	284.2
Mass of specimen [g]:	9326.4	9375.0	9424.1	9473.7

After production, specimens were put in an oven at a temperature of 60°C (140°F) for a period of 24 hours for curing. This time was needed for the water to leave the specimen and for the binder to coat RAP and attain stiffness.

While the bulk SG specimens were being cured, the theoretical maximum SG of uncompacted specimens was determined. This was done according to the procedure of AASHTO T 209 (AASHTO 2011). After curing, bulk SG testing was performed, again according to the procedure of AASHTO T 166 (AASHTO 2011). The obtained results and calculations can be found in APPENDIX G. Figure 3-5 shows the unit weight and air voids with respect to emulsion content. The  $R^2$  error is in reference to a parabolic regression curve computed by the spreadsheet program.

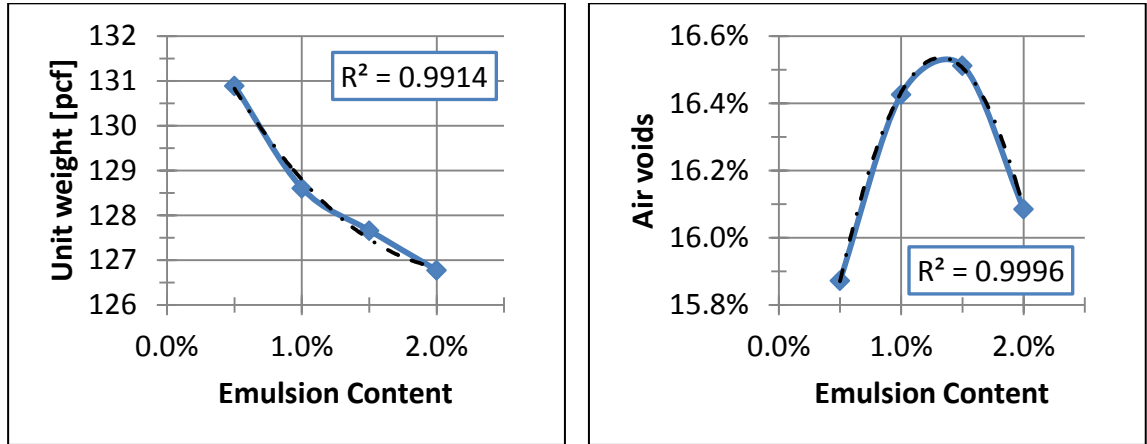


Figure 3-5 Determination of OEC at 3.0% Water Content

In one aspect, the regression fit the data points very well which is indicated by the  $R^2$  value above 0.99 in both cases. However, the behavior of the left curve was somewhat different than expected since it indicated that a higher unit weight was achieved using less emulsion. A similar behavior was observed (Lee, Brayton and Milton 2002) and a solution corresponding to the applied Mix Design procedure was applied:

“Due to the highly variable nature of RAP materials and their mixture with emulsion and water, the relationship between unit weight and emulsion content, as described earlier, occasionally does not hold true for CIR mixtures. Such a case occurred with the Kansas mixture. The highest unit weight was achieved at the lowest emulsion content of 0.5%. However, 0.5% emulsion does not supply enough asphalt to properly coat the RAP particles. Under such conditions, the OEC should be selected at the emulsion content that produces the same unit weight as found in the field.”

In this study, the same option was chosen. Thanks to the close fit of the regression curve, it could be used to numerically determine at which emulsion content a unit weight of 130 pcf was achieved. Thus, the optimum emulsion content was determined to be 0.7%.

With the emulsion content optimized, the next step was to determine the optimum water content (OWC). This was very similar to the previous step with the exception that the emulsion content was kept constant at the optimum level while the

water content was varied. Again, four sets of specimens were produced with 116 gyrations. However, this time the ingredient weights shown in Table 3-3 were used.

Table 3-3 Ingredients for OWC Determination Samples

RAP [g]:	9,000			
<b>Emulsion content:</b>	<b>0.7%</b>	<b>(OEC)</b>		
<b>Water content:</b>	<b>2.0%</b>	<b>2.5%</b>	<b>3.0%</b>	<b>3.5%</b>
Water [g]:	185.0	232.4	280.4	328.8
Emulsion [g]:	64.7	65.1	65.4	65.8
Mass of specimen:	9249.7	9297.5	9345.8	9394.6

After these specimens were produced and cured, testing for the maximum theoretical and bulk SG was performed. The obtained results are shown in APPENDIX G. Figure 3-6 represents the unit weight and the air void content versus the water content. Again, the  $R^2$  error refers to a parabolic regression curve calculated by the spreadsheet program.

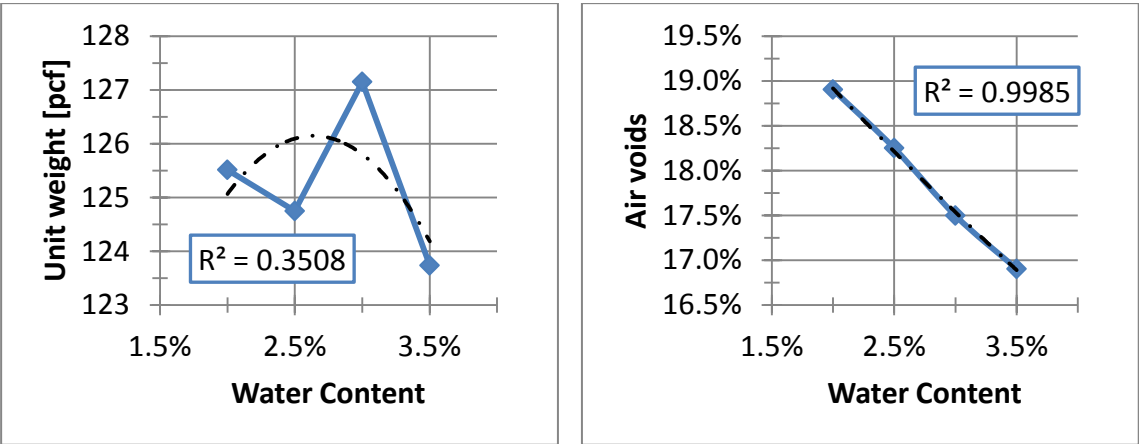


Figure 3-6 Determination of OWC at 0.7% Emulsion Content

Here, a clear maximum can be seen which identifies the optimum water content to be 3.0%.

In summation, the optimum contents for the emulsion and water were determined to be 0.7 and 3.0% of total mix weight, respectively. Another observation was made after the first set of CIR specimens was completed. The specimens, especially in direct comparison between HMA and CIR, revealed that some of the fine particles were not as thoroughly integrated into the material as in the HMA specimens. Even with only slight rubbing motions with a glove or palm over the surface of the CIR specimens, small amounts of fine materials were separated from the specimen. Of course, these amounts were negligible by far, but it was a behavior that suggests a weakness of the material and was expected to be the reason for the absolute necessity of a sealing layer of HMA or seal coat when CIR is applied in a reconstruction project.

Another observation was that even with a limited number of specimens to be produced for both materials, the amount of laboratory work was extensive. The effort for acquiring, drying, and sieving the aggregate as well as specimen production and testing must not be underestimated.

## 4 INDIRECT TENSILE (IDT) TESTING

This chapter describes the different steps from the specimen preparation to the test results.

### 4.1 SPECIMEN PREPARATIONS

A testing machine, Instron® 5582 was available in the Rhode Island Transportation Research Center (RITRC) laboratory at URI. An attempt was made to calibrate the machine. A malfunction was found in data acquisition system. Several tests showed that the machine could work on a sample, but the deflections and applied force could not be logged during or stored after testing. Efforts were initiated towards the purchase of a new data acquisition system. The existing machine was purchased before the turn of the millennium and purchasing an entirely new system would exceed the available funding. Therefore, suitable new parts that would work with the machine needed to be identified. In cooperation with the manufacturer with extensive communication via email, the proper upgrades could be found and a quotation was filed (see APPENDIX B). The order was placed, but unfortunately the delivery and complete installation of the new software was too late for this project to take effect. Therefore, another way of testing needed to be found.

Fortunately, the University of Connecticut (UConn) provided the required testing system for this project. With experienced guidance, a total of five appointments were agreed upon first to inspect the testing equipment at the Connecticut Transportation Institute (CTI). Thereafter, four more appointments were made for two different sets of specimens to be sawed and tested. Since sawing the cylindrical specimens to suitable heights of 38 to 50 mm (1½ to 2 in.) from their original heights

was accomplished with wet sawing, an appropriate time frame of at least 24 hours was necessary to allow the samples to dry before testing. At this point, gratitude should be expressed to UConn for their generous support towards this project.

In cooperation with the University of Connecticut (UConn), five appointments were made. The first meeting was to evaluate the sawing and testing equipment, coordinate future testing, and review requirements and restrictive boundary conditions for performing the test. The following four appointments were sawing and testing both materials.

At least one day was required after sawing as the specimens had to be dried. The cooling water of the saw pervades the specimen. Since testing is conducted at temperatures far below the freezing point of water, the specimens' performance is highly susceptible to any water content.

The cylindrical samples have a height of about 110 mm (4.3 in), thus two specimens with the required height could be produced. Due to the quality of the saw, a high level of accuracy could be maintained. Figure 4-1 shows one HMA and one CIR specimen in the saw fixture and during sawing.



(a) HMA

(b) CIR

Figure 4-1 Specimens in Saw Fixture and during Sawing

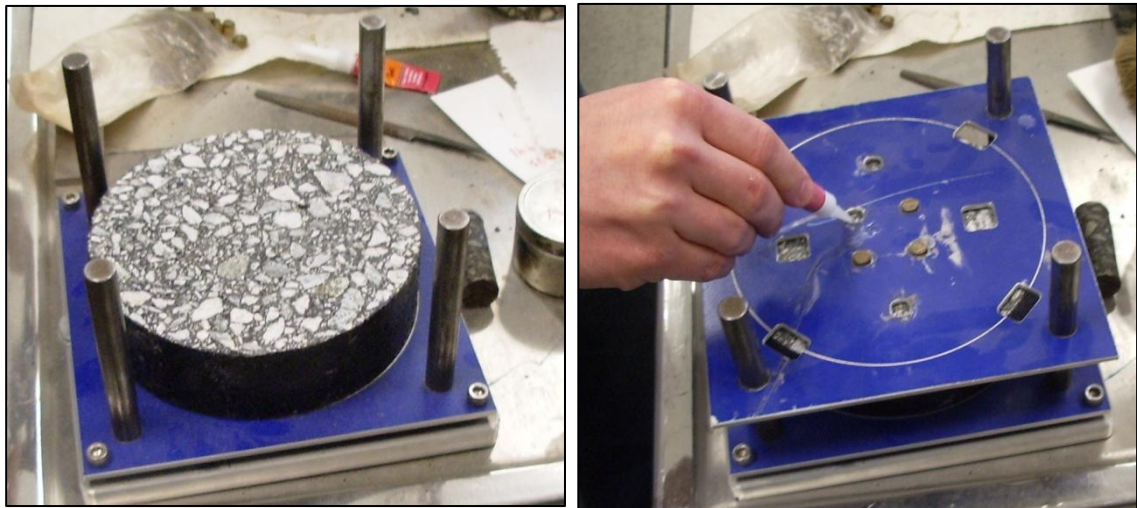
In total, eight different specimens for each material were produced with thicknesses in the range of 41 to 44 mm. These met the requirement of the procedure of T 322, which are 38 to 50 mm (AASHTO 2011).

It was observed that the different behavior of the materials could be seen even during specimen preparation. The fine materials of the recycled samples were less strongly integrated into the material and therefore chipping was increased during sawing. In order to still obtain usable specimens, care had to be taken to saw the specimens fast enough to minimize wobbling of the blade and at the same time slow enough not to rip out particles instead of cutting through them.

After labeling, the average heights were determined and listed. Eight specimens were used from both mixtures for a total of 3 different temperatures. The labels are shown in APPENDIX J.

Next, metal mounting buttons were glued onto the specimens. For testing, strain gauges were attached to them magnetically to detect the horizontal and vertical deflection of the sample in the center of the specimen as shown in Figure 2-2 and Figure

4-2. For an accurate attachment, a template was used (Figure 4-2). After gluing the buttons to the specimens, they were ready for testing.



(a)Alignment of Specimen

(b) Gluing

Figure 4-2 Attaching Buttons for Strain Gauge Attachment

#### 4.2 IDT TESTING

Testing had to be conducted at different temperatures. To ensure an appropriate temperature distribution over the entire cross-section of the specimens, keeping the specimens at test temperatures for  $3 \pm 1$  hours before testing was mandatory according to the procedure of AASHTO T 322 (AASHTO 2011).

The loading ram was lowered onto the specimen as slowly as possible to prevent an impact when the ram came into contact with the specimen. The load was kept constant at such a magnitude that a horizontal displacement, measured by the horizontal strain gauge or linear variable differential transformer (LVDT), was between 1.25 and 19.0  $\mu\text{m}$ , as stated in the procedure of AASHTO T 322 (AASHTO 2011). This ensured that the deflections were within the viscoelastic range.

To achieve this by adjusting the magnitude of the load, it should have been controlled by input from the horizontal deformation measurement device, but this was



difficult to accomplish due to the limitations of the closed-loop control system. Therefore, the load was estimated on the basis of experience and previous testing, and the resulting deformation was verified. In practice, the given range was hard to comply to, and experiences showed that slight exceedances still led to reliable results.

This load was constant for the complete creep test time of 1,000 seconds. During testing, the testing apparatus has to constantly move the loading ram in order to establish a constant load. This is possible electronically through a proportional-integral-derivative (PID) controller. Its task is to minimize the error which is the difference between the desired and the detected load. The loading piston position is corrected constantly; three parameters determine the mode of readjustment. They are chosen mainly based on experience and can be readjusted during testing. The better these values are, the less fluctuation is detected in the course of load over time. Table 4-1 shows the values for the conducted tests.

Table 4-1 PID-Settings for Conducted Testing

	<b>Load Cell</b>	<b>Strain Gauge</b>
<b>Proportional</b>	0.95	14.00
<b>Integral</b>	0.20	0.50
<b>Derivative</b>	0.10	0.00

After establishing this constant load, the deflections were measured for both faces of the specimen. This is intended to reduce influences on the obtained measurements due to material inhomogeneities by allowing the user to average them. Figure 4-3 shows the arrangement of a specimen in the climate chamber during testing.



Figure 4-3 IDT Specimen during Creep Test

After this testing phase, the load was removed. Although the specimen was not destroyed, it exhibited permanent deformation. However, it can still be used for the tensile strength test, as can be seen in the standard test method (AASHTO 2011). In this test, the loading ram had to maintain a constant movement of 12.5 mm/min (0.5 in/min), while only the imposed load needed to be measured. The deflections did not matter here. Since this test destroys the specimen, the strain gauges were removed to prevent damage that might have occurred due to the specimen's collapse. The ram movement must be maintained until the load sustained by the specimen starts to decrease. This is regarded to as failure, and the maximum load is used to calculate the failure load. When testing for the material's strength at different temperatures, it was observed that the temperature had a significant influence on the behavior. The lower the temperature, the more brittle failing occurred. While the material allowed some rather ductile deflection before completely falling apart rather slowly at freezing point. At  $-20^{\circ}\text{C}$  ( $-4^{\circ}\text{F}$ ) there was mainly one sudden, loud crack, and the specimen collapsed.

APPENDIX I shows the testing schedule. The first testing took more time than the schedule. But, the experience helped tremendously to shorten the testing time at the following meeting. The data were retrieved and analyzed to obtain the creep compliance as well as the tensile strength for the planned simulations.

### 4.3 DATA ANALYSIS

It should be noted that the testing software includes analysis algorithms. However, since academic testing is mostly used for educational purposes, in this study only raw data were used. Also, in order to understand the entire sequence of events and to check for any mistakes that may have happened during testing, manual calculations were more useful than automated processing.

#### 4.3.1 CREEP COMPLIANCE, $D(t)$

Table 4-2 shows 5 steps of testing.

Table 4-2 Creep Test Steps

Step 1	<ul style="list-style-type: none"> <li>• Balance strain gauges and load cell</li> </ul>
Step 2	<ul style="list-style-type: none"> <li>• Lower loading ram</li> <li>• Load <math>\leq 0.5</math> kN ('noise')</li> </ul>
Step 3	<ul style="list-style-type: none"> <li>• Load <math>&gt; 0.5</math> kN</li> <li>• Increase load to desired level</li> </ul>
Step 4	<ul style="list-style-type: none"> <li>• Keep load constant for test duration of 1,000 s</li> </ul>
Step 5	<ul style="list-style-type: none"> <li>• Remove load</li> <li>• End test</li> </ul>

The first three steps had to precede the actual testing. The strain gauges and the load cell were zeroed and the loading piston was moved towards the specimen. The important data for the analysis were produced in step 4. For supervisory reasons; however, data from all steps were checked first and only step 4 data was used for the creep analysis.

First, the behavior of the load was checked for every specimen to see its deviation around the desired load. As explained earlier, the PID controller algorithm constantly attempts to minimize the error which in this case is the difference between the desired and the detected load. However, this can practically never be perfect and it gets worse with PID settings that are not optimized. Figure 4-4 shows the course of the load for specimen 004. Here, the load exhibits almost no fluctuation around the creep load of 5.0 kN, but the value was varied. Its magnitude for every test is shown in APPENDIX L.

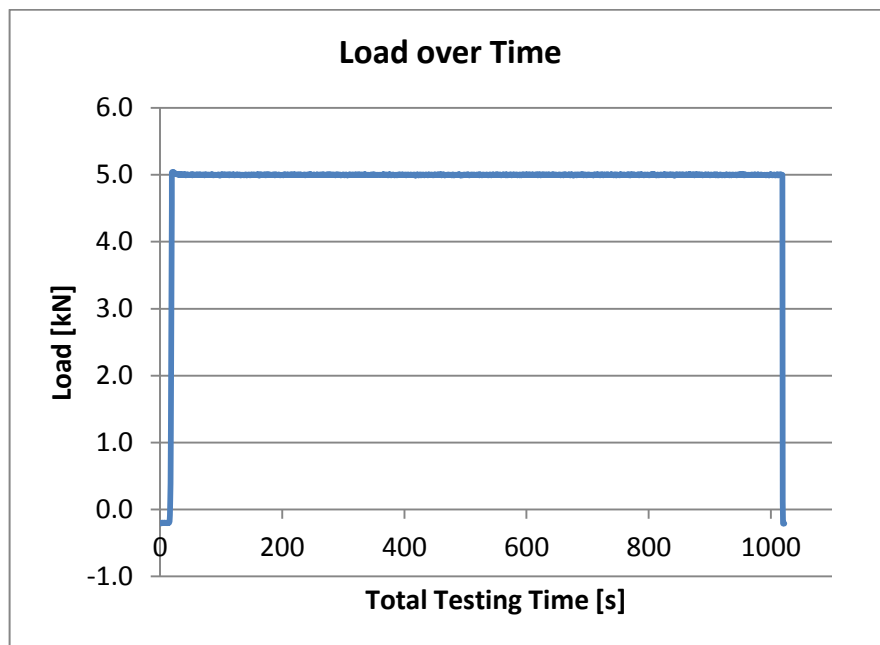


Figure 4-4 Loading over Time for Specimen 004

It is obvious how initially the load was close to 0 while the loading ram was moved slowly in order to reach the specimen but at the same time prevent an impact in the first instance of contact. It should be noted that any force below a magnitude of 0.5 kN is considered ‘noise’ and can be regarded as 0. Also, this figure shows that the creep load during step 4 is 5.0 kN.

The next step was the control of the deflections in order to see if faulty data were recorded. Figure 4-5 depicts the displacements of the 4 strain gauges attached to both faces of specimen 004 over the entire test time, which includes the creep period as well as load adjustment and removal.

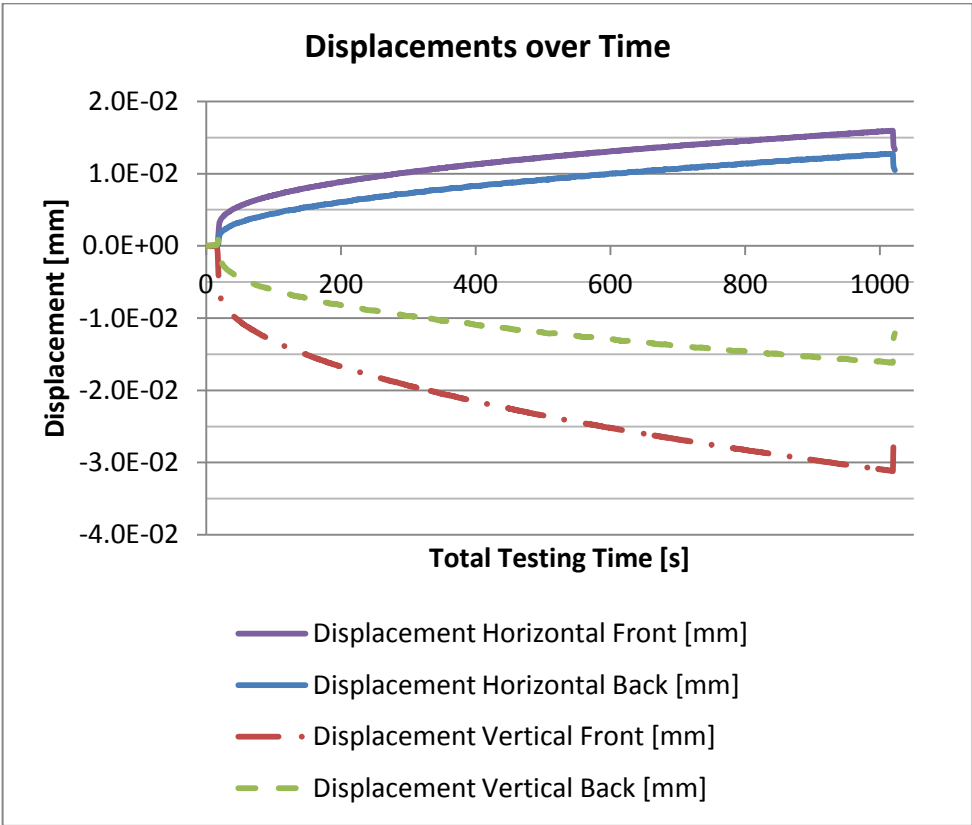


Figure 4-5 Displacements of both Axes on both Faces of Specimen 004 over Time

It can be observed that both horizontal deformations are approximately equal. This is a good result as it proves consistency within the specimen and the probability of

getting close to the “true” value is increased by calculating the average. The vertical displacements deviate a little more. This can be due to multiple reasons, starting from inhomogeneous material, influence of large or interlocked pieces of aggregate, or aggregate gaps on the path from the loading piston to the center of the specimen that are filled with binder or air voids. Also, sometimes the fault can lie within the strain gauges, although this is rather rare. Additionally, Figure 4-5 shows that the offset for all deflections is almost zero. One might argue that this must be the case automatically as a consequence of zeroing in step 1, but in one case initial measurements that varied from 0 significantly were observed. In such a case the error needs to be corrected by shifting all values of that curve by the error’s magnitude towards zero to compensate the inaccuracy.

Subsequently, the horizontal and vertical deformations of all specimens at the analyzed temperature were averaged and normalized in order to compare them. This was accomplished using Eq 4-1 and Eq 4-2 (AASHTO 2011).

$$\Delta X_{n,i,t} = \Delta X_{i,t} \cdot \frac{b_n}{b_{avg}} \cdot \frac{D_n}{D_{avg}} \cdot \frac{P_{avg}}{P_n} \quad \text{Eq 4-1}$$

$$\Delta Y_{n,i,t} = \Delta Y_{i,t} \cdot \frac{b_n}{b_{avg}} \cdot \frac{D_n}{D_{avg}} \cdot \frac{P_{avg}}{P_n} \quad \text{Eq 4-2}$$

where

$\Delta X_{n,i,t}$	normalized horizontal deformation of specimen $n$ for face $i$ at time $t$ [mm]
$\Delta Y_{n,i,t}$	normalized vertical deformation of specimen $n$ for face $i$ at time $t$ [mm]
$\Delta X_{i,t}$	measured horizontal deformation of specimen $n$ for face $i$ at time $t$ [mm]
$\Delta Y_{i,t}$	measured vertical deformation of specimen $n$ for face $i$ at time $t$ [mm]
$b_n, D_n, P_n$	thickness, diameter, creep load of specimen $n$
$b_{avg}, D_{avg}, P_{avg}$	average thickness, diameter, creep load of all replicate specimens at this temperature

Since all specimens have a diameter of 150.0 mm, the second fraction is 1. In the test method,  $\Delta X$  and  $\Delta Y$  are treated as arrays. In this study, this is achieved by calculating single values in a table in the spreadsheet software. After executing these equations, normalized deformations are obtained that enable the user to directly compare the deflections of all three specimens to one another. Figure 4-6 shows the normalized deflections of the HMA specimens at  $-10^{\circ}\text{C}$ .

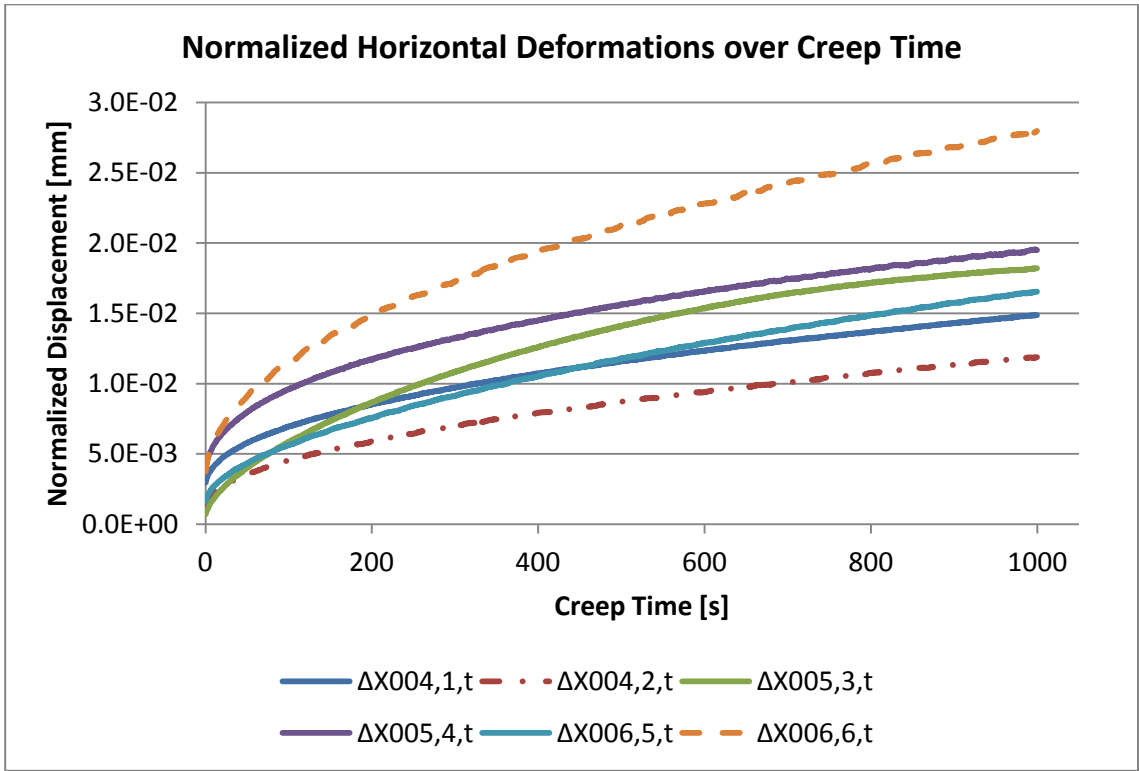


Figure 4-6 Normalized Horizontal Deformations of three HMA Specimens at  $-10^{\circ}\text{C}$

Only the graph for the HMA specimens at this temperature is shown here. All other results are shown in APPENDIX K. It can be seen in the above figure that the deflections fluctuate to a certain extent as it occurs in any kind of testing. Only the top and bottom curves show large discrepancies. If the average was determined with all 6 curves or arrays, the accuracy would decrease due to these two curves that deviate from

the mean value significantly. For this problem, the trimmed mean is used. A percentage of all measurements is chosen to be ‘cut off’ or trimmed from the top and bottom of the numerically ranked array before calculating the arithmetic mean.

The average horizontal and vertical deformations for every face are needed in order to determine the ratio of the horizontal to vertical deformations  $X/Y$ , Poisson’s ratio  $\nu$ , and a coefficient,  $C_{cpl}$ , needed for the calculation of the creep compliance. The average deformations occur after half the total creep time and are obtained using the Eq 4-3 and Eq 4-4 from the procedure of AASHTO T 322 (AASHTO 2011).

$$\Delta X_{a,i} = \Delta X_{n,i,t_{mid}} \quad \text{Eq 4-3}$$

where

$\Delta X_{a,i}$  average horizontal deformation for face  $i$   
 $\Delta X_{n,i,t}$  normalized horizontal deformation at a time corresponding to half the total creep test time for face  $i$ , here  $t = 500$  s

The vertical deformations were obtained by applying the same calculations to the  $\Delta Y$  values. Then, the trimmed mean of the deflections  $\Delta X_t$  and  $\Delta Y_t$  needed to be obtained. For this, the six  $\Delta X_{a,i}$  and  $\Delta Y_{a,i}$  values were ranked numerically and the highest and lowest values were disregarded. The average of the middle four values was determined, according to Eq 4-4.

$$\Delta X_t = \frac{\sum_{j=2}^5 \Delta X_{r,j}}{4} \quad \text{Eq 4-4}$$

where

$\Delta X_t$  trimmed mean of horizontal deformations  
 $\Delta X_{r,j}$   $\Delta X_{a,i}$  values in ascending order

The ratio of the horizontal to vertical deformations  $X/Y$  was computed according to Eq 4-5.



$$\frac{X}{Y} = \frac{\Delta X_t}{\Delta Y_t} \quad \text{Eq 4-5}$$

Consequently,  $C_{cpl}$  and  $\nu$  were determined using Eq 4-6 and Eq 4-8, respectively.

$$C_{cpl} = 0.6354 \cdot \left(\frac{X}{Y}\right)^{-1} - 0.332 \quad \text{Eq 4-6}$$

while Eq 4-7 must be true.

$$\left[ 0.704 - 0.213 \left(\frac{b_{avg}}{D_{avg}}\right) \right] \leq C_{cpl} \leq \left[ 1.566 - 0.195 \left(\frac{b_{avg}}{D_{avg}}\right) \right] \quad \text{Eq 4-7}$$

$$\nu = -0.10 + 1.480 \left(\frac{X}{Y}\right)^2 - 0.778 \left(\frac{b_{avg}}{D_{avg}}\right)^2 \left(\frac{X}{Y}\right)^2 \quad \text{Eq 4-8}$$

It may be noted that Poisson's ratio  $\nu$  should always be between 0.05 and 0.50 (AASHTO 2011). The calculations were carried out in a spreadsheet program (Microsoft Excel ©). They were performed for all temperatures for both mixtures. Table 4-3 shows the results for HMA at -10°C, while a summary of all calculations is provided in APPENDIX L.

Table 4-3 Calculations prior to Creep Compliance at -10°C (14°F)

-10 °C			
$\Delta X_{a,1} =$	1.16E-02	$\Delta Y_{a,1} =$	-2.22E-02
$\Delta X_{a,2} =$	8.71E-03	$\Delta Y_{a,2} =$	-1.13E-02
$\Delta X_{a,3} =$	1.41E-02	$\Delta Y_{a,3} =$	-1.35E-02
$\Delta X_{a,4} =$	1.56E-02	$\Delta Y_{a,4} =$	-3.96E-02
$\Delta X_{a,5} =$	1.18E-02	$\Delta Y_{a,5} =$	-1.77E-02
$\Delta X_{a,6} =$	2.13E-02	$\Delta Y_{a,6} =$	-3.19E-02
$\Delta X_t =$	1.33E-02	$\Delta Y_t =$	2.13E-02
$\frac{X}{Y} =$		0.62	
<b>0.69</b>			
0.644	$\leq C_{cmpl} \leq$		1.511
OK			OK
<b>v =</b>			
0.05	$\leq v \leq$		0.5
OK			OK

Based on the trimmed mean of the deflections (deflection arrays)  $\Delta X_{m,t}$  with respect to variable time  $t$  following the same numerical ranking for the average deformations in Eq 4-4, the creep compliance  $D(t)$  can finally be computed using Eq 4-9.

$$D(t) = \frac{\Delta X_{m,t} \cdot D_{avg} \cdot b_{avg}}{P_{avg} \cdot GL} \cdot C_{cmpl} \quad \text{Eq 4-9}$$

where

- $D(t)$  creep compliance [1/TPa]
- $GL$  gauge length (0.038 for 150 mm specimen)

This formula allows the computation of the creep compliance for any time recorded, in the present study every half-second. The simulation program, MEPDG,

requires the creep compliance only at certain time points. For greater precision of the requested data points  $\Delta X_{m,t}$  shown in Table 4-4, the results were averaged over the surrounding 5 time points in increments of 0.5 seconds. Also, the used version of the program only allows the input of the results in US customary units, while the test method consistently uses SI units. Therefore, the creep compliance is firstly calculated in [1/GPa] (SI unit) since it results from the calculations above. Technically, the obtained unit was [1/TPa], but by dividing by  $10^3$ , the unit [1/GPa] was obtained. Then the conversion factor of  $(145000)^{-1}$  was applied to obtain the customary unit of [1/psi].

Table 4-4 Creep Compliance of HMA at -10°C

creep time $t$ [s]	$\Delta X_{m,t}$ [mm]	$D(t)$ [1/GPa]	$D(t)$ [1/psi]
0	2.431E-03	5.999E-02	4.13707E-07
1	2.687E-03	6.630E-02	4.57243E-07
2	2.888E-03	7.127E-02	4.91514E-07
5	3.262E-03	8.049E-02	5.55092E-07
10	3.682E-03	9.087E-02	6.26694E-07
20	4.285E-03	1.057E-01	7.29301E-07
50	5.531E-03	1.365E-01	9.41392E-07
100	7.004E-03	1.728E-01	1.19195E-06

In summary, Table 4-5 and Table 4-6 were prepared as input material parameters for MEPDG analysis. It may be noted that the CIR mixture has a higher compliance than HMA does, as expected.

Table 4-5 Creep Compliance of HMA Mixture with Respect to Creep Time  $t$

creep time $t$ [s]	-20°C	-10°C	0°C
0	8.97389E-08	4.13707E-07	5.21493E-07
1	9.63726E-08	4.57243E-07	6.20040E-07
2	1.02322E-07	4.91514E-07	7.00792E-07
5	1.18006E-07	5.55092E-07	8.78080E-07
10	1.36596E-07	6.26694E-07	1.08040E-06
20	1.66465E-07	7.29301E-07	1.35649E-06
50	1.99880E-07	9.41392E-07	1.94403E-06
100	2.45938E-07	1.19195E-06	2.56138E-06

Table 4-6 Creep Compliance of CIR Mixture with Respect to Creep Time  $t$

creep time $t$ [s]	-20°C	-10°C	0°C
0	9.41206E-07	8.54305E-07	2.55396E-06
1	9.69910E-07	9.22309E-07	2.73292E-06
2	1.00329E-06	9.63768E-07	2.88960E-06
5	1.07410E-06	1.04849E-06	3.13043E-06
10	1.15122E-06	1.13398E-06	3.39047E-06
20	1.25605E-06	1.24203E-06	3.73268E-06
50	1.46296E-06	1.44683E-06	4.35663E-06
100	1.70172E-06	1.67104E-06	5.00597E-06

#### 4.3.2 TENSILE STRENGTH, $S$

The creep testing is not a destructive test; however permanent deformation is exhibited due to the viscoelastic reaction to a permanent load. The tensile strength test

destroys the specimen entirely which is why this test must, of course, be performed after the creep compliance test. AASHTO procedure T 322 schedules the strength test immediately after the creep compliance test but allows an unloading phase in between (AASHTO 2011). In the present study this was necessary to remove the strain gauges to prevent damage to them as a result of specimen collapse.

The specimen is aligned in the same way as for the compliance test, but this time the loading piston is to move at a constant speed of 12.5 mm/min. During testing only the sustained load is measured until a decrease is detected. This may or may not come along with a brittle collapse of the sample, but the maximum load is interpreted as the failure load and is used to determine the tensile strength.

When the failure load is known, Eq 4-10 allows computation of the tensile strength (AASHTO 2011).

$$S_{t,n} = \frac{2 \cdot P_{f,n}}{\pi \cdot b_n \cdot D_n} \quad \text{Eq 4-10}$$

where

$S_{t,n}$	tensile strength of specimen $n$ [GPa]
$P_{f,n}$	failure load of specimen $n$

Figure 4-7 visualizes the curve shape of the averaged tensile stress over testing time for the HMA mixture at all temperatures, while detailed data may be found in APPENDIX M. It can be seen how brittle the detected failure was at temperatures of -20 and -10°C which goes along with the observation of a sudden collapse of the specimen.

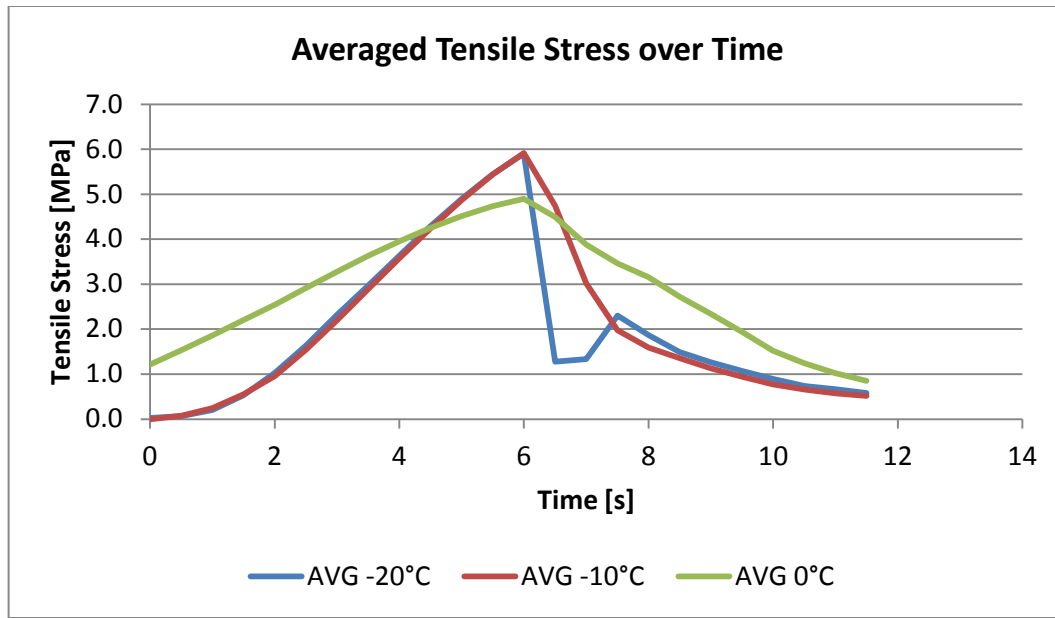


Figure 4-7 Averaged Tensile Stress over Time for HMA Material

As it can be seen, the temperature increase from -20 to -10°C does not affect the averaged tensile strength. It is rather consistent at a magnitude of 6.0 MPa. Even the increase in tension until failure seems to be linear when increasing, and both temperatures have an even steeper decline after failure.

Both samples at 0°C, however, behave differently. The increase in tension is slower, and both of them peak at about 4.4 MPa. This is due to the more ductile behavior of the binder as it allows more deformation with increasing temperatures, but it also leads to a lower strength. Table 4-7 shows the average tensile strengths for both mixtures at all temperatures.

Table 4-7 Average Tensile Strength  $S_t$  [psi] of both Mixtures

Temperature [°C]	HMA [psi]	CIR [psi]	Reduction by
-20	856.0	82.9	90%
-10	857.9	97.2	89%
0	637.3	96.6	85%

It is obvious that the tensile strength of CIR mixtures is reduced significantly. At all three temperatures,  $S_t$  is reduced to 10-15% of the HMA strength through the application of 100% RAP material. The data for all specimens at all temperatures for both mixtures as well as the behavior of the CIR mixture can be found in APPENDIX M.

Along with the results from the previous section which are shown in APPENDIX L, the tensile strength at a temperature of  $-10^{\circ}\text{C}$  ( $14^{\circ}\text{F}$ ) serves as input data for the prediction software. They are used to predict the low-temperature cracking for a fictional roadway project which is the topic of the following chapter.

## **5 PERFORMANCE PREDICTION OF BOTH MIXTURES**

This chapter's topic is the final step of performance prediction using the obtained data for a fictional project to evaluate the performance of the CIR mixture comparatively. It includes the input to the model and program for the selected boundary conditions of the site. Consequently, the outputs of the program would include resistance to low temperatures cracking and would be interpreted to formulate recommendations.

### **5.1 INPUT FOR TCMODEL AND MEPDG**

The software MEPDG offers a user-friendly input framework, characterized by a checklist layout. Each bullet point allows the adjustment of parameters for general information, traffic, climate, and pavement structure. This window is shown in Figure 5-1. MEPDG also includes several prediction models including TCMODEL for thermal cracking.

For this project a "minor arterial rural highway" was selected: Rhode Island Route 2 leads from South Kingstown to North Kingstown (Lee, Marcus, et al. 2003). A section of the road in the southern part of the State was chosen since from that area a report offers a variety of data for traffic and subgrade soil information. The study was conducted by a URI research team for the Rhode Island Department of Transportation (RIDOT).



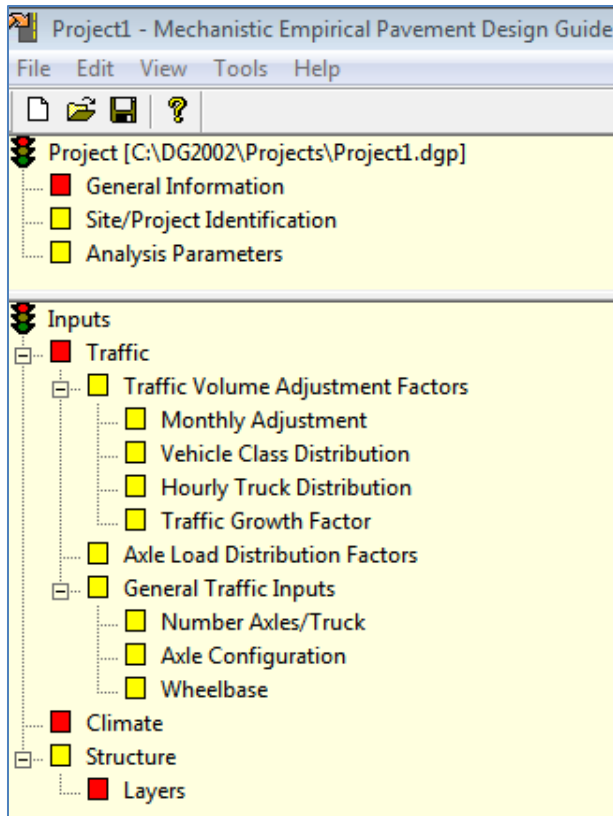


Figure 5-1 MEPDG Input Checklist

The first three items are about the project in general, i.e., the date of the construction and the analysis period. As road construction projects require proper weather conditions, the summer of 2012 was chosen. Also, the analysis period was set to be 20 years. This influences the time frame covered by the prediction and therefore affects the time required for the analysis and simulation.

The next window, “Analysis Parameters”, specifies the mathematical models required. In this case, only thermal cracking was of interest, therefore the mathematical models for longitudinal and alligator cracking (which are both load-related), rutting, and fatigue fracture were deactivated to reduce the amount of time for the computation.

The next inputs comprise the data for traffic amounts and distributions. It may be noted that thermal cracking is not load-related and does not depend on the amount of vehicles for this project. However, the programs requires a completed set of information for any project, so the traffic amount of 1,346 annual average daily truck traffic (AADTT) was entered (Lee, Marcus, et al. 2003). A summary of the traffic data is provided in APPENDIX N.

The climate plays a very important role for this distress. In MEPDG, the climate files are created based on the history that is known for weather stations in the vicinity of the project site. There are three stations in the State of Rhode Island: Westerly, Newport and Providence. Newport, RI, is located on an island, and is also rather far away from the planned location. In addition, climate data from stations in neighboring States were available and were used for improved accuracy. In total, the climate file was created through interpolation among 5 stations, as shown in Figure 5-2.

Next to the weather data, the location for which the data is to be interpolated needs to be entered. As shown, a position was chosen in the southern part of the State; its coordinates are N 41.52, E 71.55. The elevation is approximately 220 ft; both information were found using “Google Earth”. The depth of water table was entered as 10 ft (Esri 2011). A summary of the weather data is shown in APPENDIX N.

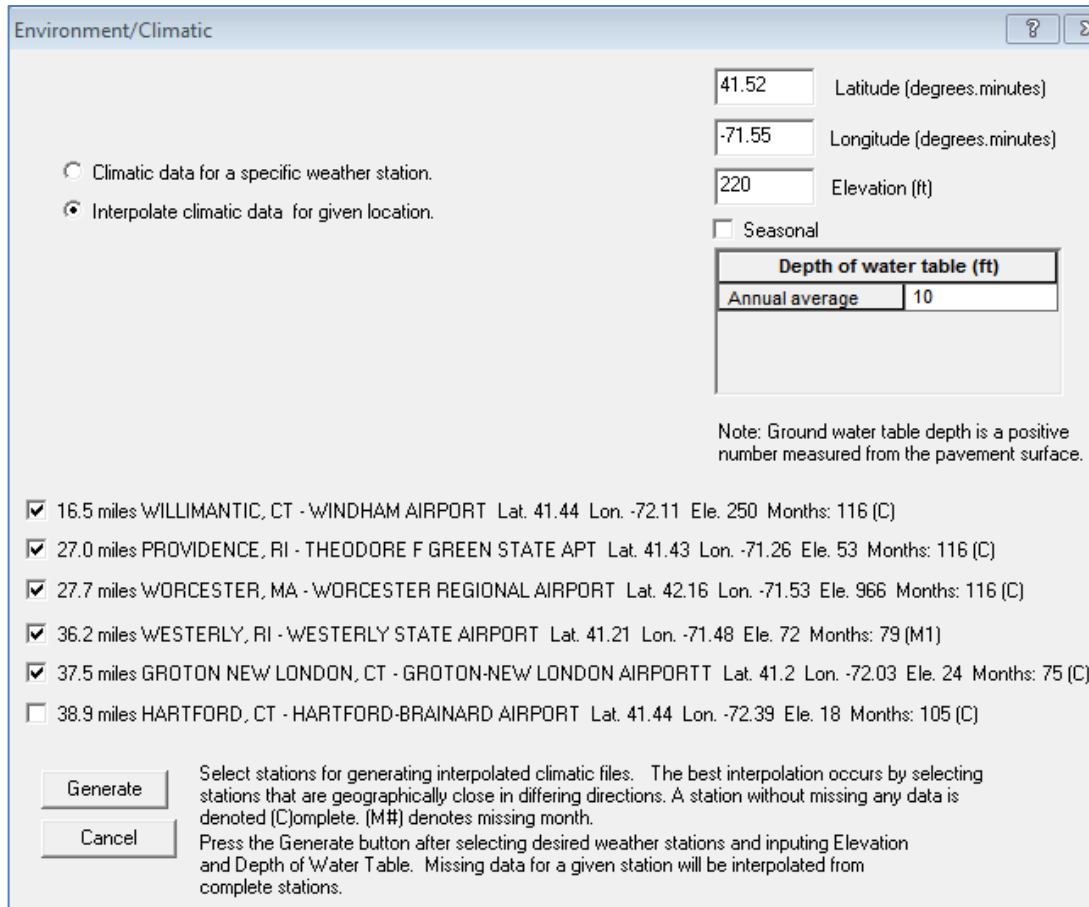


Figure 5-2 Climate File Generation via Interpolation

The next input is the pavement structure. The bottom layer is subgrade soil classified by AASHTO standards as A-1-b, i.e., that a maximum of 50 and 25% of the aggregate would pass the No. 40 and No. 200 sieves, respectively (Atkins 2002). The resilient modulus was 14,300 psi (Lee, Marcus, et al. 2003). It is semi-infinite while the above layers are assigned finite thicknesses. The layer above the subgrade is granular subbase with a thickness of 12 in., as it is common in Rhode Island for a fill or embankment section. In the case of cut or excavation section, 18 in. would be appropriate.

The base and surface courses need to be provided in the prediction software. This is the point where MEPDG, unfortunately, limits the possibilities to enter a

pavement that would accurately reflect the way CIR is supposed to be used in reality. After application of CIR and curing, protection is required for “the surface of the CIR-treated material by either a surface wearing course, such as a seal or HMA overlay” (FHWA 2005). Therefore, CIR would most likely be applied in combination with HMA. However, the program allows entering of only one set of creep compliance and strength test data for all bituminous layers of the entire setup, which prevents pavement structures that comprise layers of both HMA and CIR. So for comparison reasons, basically the two bituminous layers are entered with the creep compliance and tensile strength results from HMA in one case and from CIR in the other case. As it is practice in Rhode Island for deep strength pavements, the base and surface courses have thicknesses of 5 and 2 in., respectively. In addition, a third setup was simulated with a base course thickness of only 2 in. This, of course, must never be used in reality. However, it is intended to reveal how a very thin course of CIR mixture would perform in terms of thermal cracking. Figure 5-3 shows the three setups used in this study.

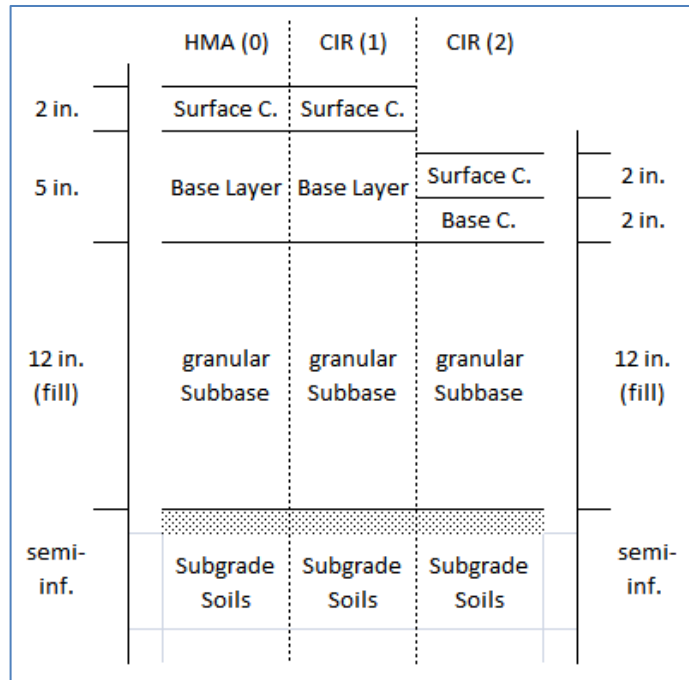


Figure 5-3 MEPDG Pavement Setups

The parameters to characterize HMA and CIR, the densities and percent of air voids must be entered into the program. The values are shown in Table 5-1.

Table 5-1 General Parameters for Bituminous Mixtures

Parameter	HMA	CIR
Performance Grading	64-28	64-28
Unit Weight [pcf]	130	127.2
Air Voids [%]	4	17.5

Figure 5-4 shows how the results from the IDT testing can be entered into the software. In this case, the values represent the results of HMA.

Thermal Cracking

Level 1  
 Level 2  
 Level 3

Average tensile strength at 14 °F (psi):

Loading Time sec	Creep Compliance (1/psi)		
	Low Temp (°F)	Mid Temp (°F)	High Temp (°F)
	-4	14	32
1	9.63726e-008	4.57243e-007	6.20040e-007
2	1.02322e-007	4.91514e-007	7.00792e-007
5	1.18006e-007	5.55092e-007	8.78080e-007
10	1.36596e-007	6.26694e-007	1.08040e-006
20	1.66465e-007	7.29301e-007	1.35649e-006
50	1.99880e-007	9.41392e-007	1.94403e-006
100	2.45938e-007	1.19195e-006	2.56138e-006

Compute mix coefficient of thermal contraction.

Mixture VMA (%):

Aggregate coefficient of thermal contraction:  ...

Mix coefficient of thermal contraction (in/in/°F):

Figure 5-4 Thermal Cracking Parameters Input Window

Input of the thermal cracking data completed the checklist required for inputs to MEPDG.

## 5.2 PREDICTION RESULTS AND INTERPRETATION

After simulating all three different cases, summaries of distresses revealed that none of the cases are expected to exhibit any distresses over the entire analysis period of 20 years. Not even the third case, where the pavement is by far too thin, showed any distresses. As an example, the output for the distresses of the pavement including CIR mixtures with a base course thickness of 5 in. (“CIR (1)”) is shown in Table 5-2.

Table 5-2 CIR (1) Simulation Output

Pavement Age		Month	Longitudinal Cracking	Alligator Cracking	Transverse Cracking	Total Rutting	IRI	IRI at Reliability
mo	yr		(ft/mi)	(%)	(ft/mi)	(in)	(in/mi)	(in/mi)
1	0.08	August	85	0.31	0	0.25	73.1	99.5
12	1.00	July	1600	2.38	0	0.38	79.7	108.9
24	2.00	July	3520	4.90	0	0.46	85.1	116.8
36	3.00	July	4740	6.95	0	0.51	88.6	121.6
48	4.00	July	5800	9.07	0	0.54	92.1	126.2
60	5.00	July	6490	11.00	0	0.58	95.6	130.9
72	6.00	July	7150	13.00	0	0.61	99.3	135.7
84	7.00	July	7670	15.00	0	0.64	102.6	140.0
96	8.00	July	8100	17.10	0	0.66	106.2	144.7
108	9.00	July	8450	19.10	0	0.68	109.7	149.2
120	10.00	July	8730	21.20	0	0.71	113.6	154.2
132	11.00	July	8920	22.80	0	0.73	116.9	158.5
144	12.00	July	9090	24.50	0	0.75	120.5	162.9
156	13.00	July	9220	26.10	0	0.77	124.1	167.5
168	14.00	July	9350	27.70	0	0.79	127.9	172.2
180	15.00	July	9470	29.30	0	0.80	131.5	176.8
192	16.00	July	9570	30.90	0	0.82	135.4	181.6
204	17.00	July	9660	32.60	0	0.83	139.3	186.4
216	18.00	July	9740	34.20	0	0.86	143.6	191.6
228	19.00	July	9800	35.50	0	0.87	147.4	196.3
240	20.00	July	9860	36.90	0	0.88	151.4	201.1

This is a rather unexpected result. Especially because of the observations about the texture which appeared weaker than the HMA, apparently this property does not affect the distress of thermal cracking. It can be expected to affect the performance for a variety of load-related distresses such as longitudinal or alligator cracking; however this

was not within the scope of this project but is rather recommended to be analyzed in future research.

The question of the performance cannot be answered entirely with the result that neither material will crack at the simulated weather conditions. Still, the result that CIR material performs very well in a climate found in the South of Rhode Island is more than desirable and supports this approach towards a more sustainable reconstruction practice immensely.

How can a CIR mixture with a tensile strength of less than 12% of HMA's strength perform just as well? Apparently, not only the tensile strength, but the material's behavior before failure plays a significant role for cracking. This distress is not load-, but temperature-related. The stresses do not arise from imposed loads that need to be sustained, but rather from (blocked) shrinkage. As mentioned earlier, the creep compliance is a measure of deflection over stress. The graphs of creep compliance over time reveal for both materials that CIR exhibits a more ductile behavior, i.e., allows more deflection. As both mixtures are exposed to the same climatic situations, they both do not show distresses, but behave differently. CIR mixtures reduce stresses by allowing higher deflections. HMA mixtures behave more brittle and deflect less, but do not fail because the tensile strength is higher than the actual stresses.

The results from MEPDG are shown in APPENDIX O. The output contains the magnitudes of the distress after every month, yet for clarity reasons only every full year is shown.

In summary, these results represent a more than desirable result for the analyzed problem. Thermal cracking of this type of recycled pavement material is of such a low



extent that it can be recommended, although more works in terms of performance regarding load-related distresses are necessary.

## 6 CONCLUSIONS AND RECOMMENDATIONS

The conclusions and recommendations based on the findings and observations of this study have been summarized below.

### 6.1 CONCLUSIONS

- (1) As an alternative to conventional roadway reconstruction practices, the Cold In-Place Recycling (CIR) possesses properties which meet conventional requirements.
- (2) Based on the Mix Design for CIR mixtures developed at URI, specimens were produced and tested. In comparison to conventional HMA, the texture of the CIR specimens appeared not to glue the particles to one another as thoroughly.
- (3) IDT testing revealed that the tensile strength is, in fact, reduced by up to 90%. However, also the creep deflection is increased, allowing the material to increase strain at a given load. This is expected to be a major reason for its very good performance.
- (4) The simulated results showed that no thermal cracking is expected to occur over the entire analysis period of 20 years.
- (5) The results of this study, however, support CIR as a viable option for roadway reconstruction. Through the reduced stresses to the environment and the people, CIR can provide a greener and more sustainable approach.

## 6.2 RECOMMENDATIONS

- (1) This positive result strongly supports the CIR technique as a rehabilitation strategy.
- (2) While the performed simulations were limited to exposure to Rhode Island climate, further investigations should be conducted for the severe weather conditions in other US states.
- (3) Further questions offer plenty of research possibilities regarding other types of distresses, variations for the additives and more.
- (4) Acquisition of newer RAP is recommended. CIR projects are often realized with recycling trains that perform the construction projects automatically. Retrieving RAP from such a train can reflect field conditions more accurately.
- (5) Concerning the sample production, two major improvements are recommended. One of them is the production of more specimens to obtain an increased statistical reliability. In this project, the scope was limited; however for future research projects more data is recommended. Also, a wet saw with a bigger blade is necessary. It should be able to cut specimens with a diameter of 150 mm in one motion, i.e., without having to turn the specimen during cutting.
- (6) For the prediction, the used software simplifies the problem as it applies linear elastic fracture mechanics. Newer software is recommended for future use, programs such as “LTC Model” contain non-linear approaches that contain a higher level of accuracy in representing the problem.

- (7) In addition, it is suggested to continue research in terms of different types of distresses, especially those depending on the amount and distribution of load applications, e.g., longitudinal and/or alligator cracking.

## REFERENCES

- AASHTO. Standard Method, Washington, D.C.: American Association of State Highway and Transportation Officials, 2011.
- Asphalt Institute, The. *mix design methods for asphalt concrete*. College Park, MD: The Asphalt Institute, 1984.
- Atkins, Harold N. *Highway Materials, Soils, and Concretes*. Prentice Hall, 2002.
- California Department of Transportation. "In-Place Recycling." *California Department of Transportation, Division of Maintenance*. February 19, 2008. <http://www.dot.ca.gov/hq/maint/FPMTAGChapter13-In-Place-Recycling.pdf> (accessed June 12, 2012).
- Coree, Brian J., and Kera VanDerHorst. "National Transportation Library." *SUPERPAVE® Compaction*. 1998. <http://ntl.bts.gov/lib/9000/9000/9079/264superpave.pdf> (accessed 12 15, 2011).
- Esri. *ArcGIS Rhode Island Soil Permeability and Depth to Water Table*. 2011. <http://www.arcgis.com/home/webmap/viewer.html?services=4ca8feb53f504b3c9c2b8bcefe0afd4d> (accessed June 20, 2012).
- FHWA. *Cold In-Place Asphalt Recycling Application Checklist*. Washington, D.C.: U.S. Department of Transportation, 2005.
- Lee, K. Wayne, Alan S. Marcus, Karissa Mooney, Sekhar Vajjhala, Edgar Kraus, and Kyungwon Park. *Development of Flexible Pavement Design Parameters for Use With The 1993 AASHTO Pavement Design Procedures*. FHWA-RIDOT-RTD-03-6, Providence, RI: Rhode Island Department of Transportation, 2003.
- Lee, K. Wayne, Todd E. Brayton, and Houston Milton. *Development of Performance Based Mix Design for Cold In-Place Recycling (CIR) of Bituminous Pavements Based on Fundamental Properties*. Washington, D.C.: Federal Highway Administration, 2002.
- Leon, Sofie, Eshan V. Dave, and Kyoungsoo Park. "Thermal Cracking Prediction Model and Software for Asphalt Pavements." *T&DI Congress 2011*. Chicago, IL: American Society of Civil Engineers, 2011. 667-676.

Mamlouk, Michael S., and John P. Zaniewski. *Materials for Civil and Construction Engineers*. Vol. Second Edition. Upper Saddle River, NJ: Pearson Prentice Hall, 2006.

Marasteanu, Mihai, et al. "Investigation of Low Temperature Cracking in Asphalt Pavements." Technical Report, St. Paul, MN, 2007.

Roque, Reynaldo, and William G. Buttlar. "The Development of a Measurement and Analysis System to accurately determine Asphalt Concrete Properties using the Indirect Tensile Mode." *Asphalt Paving Technology*. Charlestown, SC: Association of Asphalt Paving Technologies, 1992. 304-332.

Steen, Kristina. *Prediction of Rutting and Fatigue Cracking of Cold In-Place Recycling Asphalt Pavements Using the VESYS Computer Program*. Master Thesis, Kingston, RI: University of Rhode Island, 2001.

The Asphalt Institute. "Understanding Emulsified Asphalts." *Educational Series*, August 1979: 1-5.

Walker, Dwight. "Asphalt Emulsions 101." *Asphalt*, March 2012: 7-10.

## APPENDIX A

MODIFIED SUPERPAVE MIX DESIGN PROCEDURE FOR CIR MIXTURES

DEVELOPED BY THE URI RESEARCH TEAM

## APPENDIX A      MODIFIED SUPERPAVE MIX DESIGN FOR CIR MIXTURES

This section contains the modified mix design procedure for CIR mixtures. It was developed by a research team under leadership of the URI to establish a standard and reduce the variations in the practice of CIR applications.

### 1. Scope

1.1. This method covers the design of mixtures for cold in-place recycling (CIR) using the Superpave Gyrotory Compactor. The procedures presented are applicable only for mixtures containing asphalt emulsion and reclaimed asphalt pavement (RAP). This method consists of two parts. The first is the determination of the optimum emulsion content and the second is the determination of the optimum mixing water content.

### 2. Apparatus

2.1. See (AASHTO 2011)

### 3. Test Specimens

#### 3.1. Preparation of RAP

- 3.1.1. RAP samples shall be obtained from the roadway that will be recycled by taking cores to the specified depth. These cores will then be crushed in order to have representative samples.
- 3.1.2. Dry a portion of the RAP to a constant mass at 110° C (230° F) to determine the moisture content. Dry the remainder of the RAP to a constant mass at 60° C (140°F) to remove the existing water.
- 3.1.3. Separate the RAP into particle sizes according to Table A-1, by screening through a series of sieves. Eliminate the material retained on the 31.75 mm (1¼ in) sieve either by removing or crushing the material such that excess fines are not produced.

Table A-1 Sieve sizes for RAP gradation

+ 31.8 mm (1¼")
+ 25.0 mm (1")
+ 19.1 mm (¾")
+ 12.5 mm (½")
+ 9.5 mm (3/8")
+ 4.75 mm (# 4)
+ 2.36 mm (# 8)
+ 1.18 mm (# 16)
- 1.18 mm (# 16)

#### 3.2. Mixing and Compacting Temperatures



- 3.2.1. The mixing temperatures shall be  $25^{\circ}\text{C} \pm 2^{\circ}\text{C}$  ( $77^{\circ}\text{F} \pm 4^{\circ}\text{F}$ ) for the RAP and mixing water. The mixing temperature for the emulsion varies depending on the emulsion. Obtain the correct mixing temperature from the emulsion manufacturer.
- 3.2.2. The compaction temperature shall be  $25^{\circ}\text{C} \pm 2^{\circ}\text{C}$  ( $77^{\circ}\text{F} \pm 4^{\circ}\text{F}$ ).
- 3.3. Preparation of Mixtures
  - 3.3.1. The first part of the mix design involves the determination of the optimum emulsion content, while keeping the mixing water content constant. A minimum of two specimens shall be prepared for a minimum of four emulsion contents in 0.5 % increments. All specimens will be prepared with 3.0% mixing water (different water contents can be used based on experience). In addition, one loose sample shall be prepared for each additive content for determination of maximum theoretical specific gravity.
  - 3.3.2. Weigh into individual pans a sufficient amount of RAP (~ 4000 grams) based on the gradation determined in section 3.1.3 to fabricate specimens 150mm (6 in) in diameter and 115 mm (4.5 in) in height.
  - 3.3.3. Heat RAP samples at  $25^{\circ}\text{C} \pm 2^{\circ}\text{C}$  ( $77^{\circ}\text{F} \pm 4^{\circ}\text{F}$ ) for a minimum of one hour. In addition, heat emulsion at the specified temperature (Section 3.2.1) for one hour.
  - 3.3.4. Add mixing water to each sample and mix thoroughly for one minute. Mixing may be performed either by hand or through the use of a mechanical mixer.
  - 3.3.5. Add emulsion to each sample according to section 3.3.1 and mix thoroughly until the emulsion is uniformly dispersed but for no longer than two minutes. If the sample is not uniformly mixed after two minutes, additional mixing water may be required to improve emulsion dispersion. Otherwise, another emulsion type may be required.
  - 3.3.6. Spread the mixture in a pan and allow the sample to cure until it ‘breaks’ (when sample changes from a brown to a black color).
- 3.4. Compaction of Specimens
  - 3.4.1. Preheat the molds at  $60^{\circ}\text{C}$  ( $140^{\circ}\text{F}$ ) for a minimum of one hour.
  - 3.4.2. Apply load using the Superpave Gyrotory Compactor (SGC). The loading pressure shall be 600 kPa at an angle of gyration of  $1.25^{\circ}$ . The load shall be applied for the number of gyrations that will result in achieving densities similar to those found in the field.
  - 3.4.3. Remove specimens from their molds immediately after compaction.
  - 3.4.4. Oven-cure the specimens at  $60^{\circ}\text{C}$  ( $140^{\circ}\text{F}$ ) for 24 hours.
  - 3.4.5. Remove the specimens from the oven and allow to cool to room temperature.
- 3.5. Bulk Specific Gravity,  $G_{mb}$ 
  - 3.5.1. Perform testing according to T 166(AASHTO 2011).
  - 3.5.2. This test method should be used when the samples absorb less than 2 % of water by volume as determined by section 6.2 of T 166(AASHTO 2011). Otherwise use(AASHTO 2011).
  - 3.5.3. Determine maximum theoretical specific gravity for each emulsion content using (AASHTO 2011).

- 3.6. Determine Optimum Emulsion Content (OEC)
  - 3.6.1. Plot unit weight versus percent emulsion content for each emulsion content.
  - 3.6.2. Plot percent air voids versus percent emulsion content for each emulsion content
  - 3.6.3. OEC is the emulsion content at which the unit weight is at its maximum value.
  - 3.6.4. If a maximum unit weight is not achieved, the OEC should be the emulsion content at which the unit weight is the same as that found in the field.
- 3.7. Determine Optimum Mixing Water Content (OWC)
  - 3.7.1. OWC is determined by following steps 3.1 through 3.5, with the following exceptions.
  - 3.7.2. A minimum of two specimens will be prepared at the Optimum Emulsion Content (OEC) with each of four varying water contents, 0.5% and 1.0% above and below the mixing water content used in step 3.3.1.
  - 3.7.3. Plot unit weight versus percent water content for each water content.
  - 3.7.4. Plot percent air voids versus percent water content for each water content.
  - 3.7.5. OWC is the water content at which the unit weight is at its maximum value.
  - 3.7.6. If a maximum unit weight is not achieved, the OWC should be the water content at which the unit weight is the same as that found in the field.
- 3.8. Moisture Sensitivity
  - 3.8.1. Prepare six specimens at OEC and OWC, three for dry testing and three for conditioned testing and determine moisture sensitivity of the specimens in accordance with T 283(AASHTO 2011).
4. Report
  - 4.1. The report shall include the following:
    - 4.1.1. Type of Emulsion Used
    - 4.1.2. RAP Gradation
    - 4.1.3. Specimen Height
    - 4.1.4. Specimen Mass
    - 4.1.5. Specimen Bulk Specific Gravity
    - 4.1.6. Specimen Unit Weight
    - 4.1.7. Specimen Air Void Content
    - 4.1.8. Optimum Emulsion Content
    - 4.1.9. Optimum Mixing Water Content
    - 4.1.10. Moisture Sensitivity Results

## APPENDIX B

### DOCUMENTATION OF THE ACQUISITION FOR THE NEW IDT TESTING MACHINE

## APPENDIX B          NEW TEST MACHINE DOCUMENTATION

This Appendix contains the emails through which the parts that needed to be purchased were identified. Also, the quotation for the new equipment is included.s

On Fri, Jan 27, 2012 at 01:08 PM, Johnson, David <David\_Johnson@instron.com> wrote:

Hi Max,

Attached is a quotation for the BH2, VersaChannel conversion.

The 5900 electronics upgrade (attached) and the Expansion Channel Module would be around \$30K.

Would you like a formal quote for this, too?

Also, could you please provide the Merlin info (catalog number, serial number etc.)? I'm trying to figure out if it is custom Merlin software or not.

Regards,  
Dave

From: Max Mueller [mailto:max\_mueller@my.uri.edu]  
Sent: Thursday, January 26, 2012 11:38 AM  
To: Johnson, David  
Cc: K. Wayne Lee; Kevin Broccoli; Ajay Singh  
Subject: Re: Instron Model 5582

Hi Dave,

thank you for this elaborate answer.

Basically, what we need is an apparatus that can perform the required ISDCT test. So we would need a setup with 4 channels. I figure, that then a variety of other tests would be possible as well, which would come in great.

Considering your options, I would like to know how well Bluehill 2 performs in terms of reliability, user-friendliness and data recording.

Furthermore, for the decision I would like to know if you could give a quotation or an estimate of what expenses we are looking at. I assume that the least expensive option will be the very first one you mentioned will be BH 2 with the VersaChannel option in combination with 4 Channels. 4 channels would allow 4 displacements to be monitored, correct?

So a quotation for that would be extremely helpful.

In addition, how much would retrofitting the 5582 model to 5900 and the Expansion Channel Module be?

Thank you for your support! We will have a meeting this afternoon, so the more information I have, the better I can present it to my supervisor.

Max

On Thu, Jan 26, 2012 at 11:14 AM, Johnson, David <David\_Johnson@instron.com> wrote:

Hello Max,

After investigating this further, your current DAS system would NOT be compatible with the new Bluehill software platform (BH2 & BH3).

So, basically you have a couple of upgrade options.

Option 1: Upgrade to our Bluehill 2 software platform and purchase the VersaChannel option to connect up to 16 additional Input Channels.

2 Options:

4 Channel (4 Single Ended or 2 Differential)

16 Channel (16 Single Ended or 8 Differential)

Option 2: Retrofit existing 5582 system (5900 electronics), add the BH3 software, and expansion channel module.

The Expansion Channel Module is compatible only with 5900 electronics and BH3 software.

See link below:

[http://www.instron.us/wa/acc\\_catalog/detail.aspx?aid=5420](http://www.instron.us/wa/acc_catalog/detail.aspx?aid=5420)

Your thoughts?

Dave

From: max\_mueller@my.uri.edu [mailto:max\_mueller@my.uri.edu]

Sent: Wednesday, January 25, 2012 11:55 AM

To: Johnson, David

Cc: Prof. K. Wayne Lee; Kevin Broccolo; Ajay Singh

Subject: Re: Instron Model 5582

Hello David,

first of all, I would like to thank you for your answer.

I have been working on the machine with the purpose of making it work, but the data acquisition still refuses to operate as expected.

The problem is that this equipment is very old. After repairing measures, now the climate chamber picked up proper operation again, but without proper data acquisition testing is pointless.

I forwarded all our emails to my supervisor, Dr. K.W. Lee, and now he is considering proposing to the department the purchase of the Bluehill software. A decisive point for the decision will be if testing will then be possible as desired. As you pointed out, Bluehill software does seem to operate as desired. But for testing cooperation between

the software, the data acquisition system and the testing machine is vital. For your information, our Data Acquisition System (DAS) is "ATA 2001 LVDT Signal Conditioner" by Schaevitz. Now, could you please answer the following questions under the assumption of the URI purchasing the Bluehill 3 software?

Will the software work with our Instron testing machine?

Does that software still require a DAS? If so, will Bluehill require a new DAS?

Thank you very much and best regards,  
Max

From: Johnson, David  
Sent: Friday, January 20, 2012 8:44 AM  
To: max\_mueller@my.uri.edu  
Cc: Prof. K. Wayne Lee ; Kevin Broccolo  
Subject: RE: Instron Model 5582

Hi Max,  
Bluehill software has been our current selling product for the past 8 years so there will be no issues with this software conversion.

Regards,  
Dave

From: max\_mueller@my.uri.edu [mailto:max\_mueller@my.uri.edu]  
Sent: Thursday, January 19, 2012 4:24 PM  
To: Johnson, David  
Cc: Prof. K. Wayne Lee; Kevin Broccolo  
Subject: Re: Instron Model 5582

Hi David,  
thank you for the quotation.  
After discussion this option with my supervisor, Prof. Dr. Lee, we would like to know if you can assure us 100% functionality, assuming we will be able to purchase the Software Bluehill. Is that sure?  
Best regards and thank you,  
Max

From: Johnson, David  
Sent: Monday, December 19, 2011 8:49 AM  
To: max\_mueller@my.uri.edu  
Cc: Baker, Ron  
Subject: RE: Instron Model 5582

Hi Max,  
Per your request, attached is a quotation for the Bluehill 3 software conversion.  
Please contact me if you have any questions.

Thanks,

David Johnson  
Senior Account Rep  
tel: 781.575.5320 | david\_johnson@instron.com

From: max\_mueller@my.uri.edu [mailto:max\_mueller@my.uri.edu]  
Sent: Friday, December 16, 2011 2:51 PM  
To: Baker, Ron  
Cc: Prof. K. Wayne Lee; Ajay Singh; Kevin Broccolo  
Subject: Re: Instron Model 5582

Ron,  
thank you very much for your response.  
I think Mr. Broccolo tried to get in touch with you, but unfortunately he could only leave you a voicemail.  
We tried to narrow down the error possibilities, and the thermocouple appears to work fine, and so did the fuses.  
As for the software problem, we are still using the software Merlin. Could you also give advice for that software?  
Furthermore, we would like to know whether you could issue a quotation for the purchase of the software Bluehill, with an educational discount?  
Best regards,  
Max Müller

From: Baker, Ron  
Sent: Monday, December 12, 2011 10:27 AM  
To: mailto:max\_mueller@my.uri.edu  
Subject: Instron Model 5582

Max,  
The environmental chamber problem could be caused by a bad thermocouple probe, a bad connection or a bad solid state relay between the line voltage and the heaters in the chamber. If any of these problems occur the temperature will keep on climbing.  
You did not say what software you are using but I assume it is Bluehill. If it is, go into the method and under results1 click on strain and move strain 1 to the available channels to the right. If the LVDT is calibrated the software should now read it.  
The problem you are having with the chamber is probably going to require a service visit to determine what is wrong. I suggest arranging for an on site service visit to fix the chamber problem and look at the LVDT problem.  
If you would like on site service please call 1-800-473-7838 and select option 3 for technical support.  
Regards,  
Ron Baker  
Technical Support Systems Engineer

825 University Avenue, Norwood, MA 02062  
Tel: 1-800-473-7838  
E-mail: service\_support@instron.com

My name is Max Mueller and I am currently working with the Indirect Tensile testing machine made by Instron. Its model number is 5582.

Unfortunately I keep having difficulties while working with the machine. First of all, the climate chamber turns out not to work as intended. When the desired test temperature is entered according to the manual, the chamber will keep on heating up, although the desired temperature is exceeded.

Furthermore, the data acquisition system seems to malfunction in a way that although LVDTs are connected as described in the manual and can be read in the software, no real-time data are monitored during testing and no recordings are being stored.

I would be happy to receive an evaluation about likely malfunction and ideas to get the machine back to working properly. I am going to work on my Master thesis next semester and I rely on this machine to provide accurate test results.





## QUOTATION

Quote To:  
Max Mueller  
University of Rhode Island

Kingston, RI 2881  
Tel:  
Fax:

cc:

Date: 01/26/2012  
Quote# **INSQ78953**  
Reply To:  
Dave Johnson  
Instron  
825 University Avenue  
Norwood, MA 02062-2643  
Tel: 781-575-5320  
Fax: 781-575-5725  
Email: [david\\_johnson@instron.com](mailto:david_johnson@instron.com)

We are pleased to submit the following quotation for your consideration.

Qty.	Part Number	Price
------	-------------	-------

### Bluehill 2 Software Conversion for 5582 system

- 1 2410-420  
Bluehill 2 Materials Testing Software for 5500 systems. For Windows® 7 (32 bit) and XP (service pack 3) operating systems. Bluehill Materials Testing Software features a Window's based graphical userinterface designed for ease of use, power, and flexibility. The basic software provides a platform, which serves not only as basic materials measurement, test control, and report generation system, but also acts as the focal point of the software architecture to which other Bluehill modules are connected. The software provides up to four real time numerical displays (digital or analog) for test data as well as facilities for generating graphs and tables of processed test results. The use of simple memorable icons to represent system functions and features ensure rapid learning and make the system ideal for both infrequent and experienced users.

The basic software provides the following functionality and features:

- Set-up and configuration of the display screen and control panel
- Set-up of limits and gain controls
- Security with user passwords
- Automatic calibration and balancing of transducers
- User calculation creator for defining custom calculations
- Prompted Test Sequence Creator
- Live runtime test plots with automatic scaling and zoom-in/out
- Report generation with basic report templates included
- Monitoring of system and system service histories
- On-line help and reference guide
- API (Advanced Programming Interface) for data access or automation
- Specimen Protect (5500 and 5800 systems only)
- Automatic grip control (frame dependent)
- Saving and retrieval of test methods and data
- Example test methods included for easy test creation
- Interactive User Learning CD



Quote # INSQ78953  
Last modified 01/26/2012

Page 1

Quotation submitted subject to provisions included.

Figure B-1 Instron® Quotation for Test Machine Upgrades, page 1/5


Qty.	Part Number	Price
1	<p><b>2410-420Z1</b>            Complete Bluehill 2 Software Suite.            Includes Bluehill Software with:            - Tension, Compression, Flexure, Peel/Tear/Friction,            and Metals Applications Packages            - Enhanced Control            - TestProfiler            - Reports and Graphs Pack.            Requires basic 2410-420 platform.</p> <p><b>NEW Communication Device</b></p>	
1	<p><b>2424-500</b>            Ethernet Frame Interface (EFI).            - Includes Ethernet Frame Interface, PCI Ethernet Card and Cables.            - For all 3300, and 5500.            - Connects to PC Ethernet port</p> <p>EFI software compatibility :            Bluehill 3 (all versions)            Bluehill 2 version 2.15 or above            BH Lite version 2.15 or above            Partner version 8.2a or above</p>	
1	<p><b>OP565-47</b>            Firmware Upgrade for 5500 DSP Board</p> <p><b>VersaChannel</b></p>	
1	<p><b>2410-400V</b>            VersaChannel. - The VersaChannel option lets you create additional channels for your testing system and connect extra transducers to those channels. The VersaChannel Configuration screen displays to let you create and configure your additional channels. Set up the Name, Type (load, Strain, User defined), and Range for each channel. You can define the unit label for user transducers, e.g. Deg. C. Set channels to Single-ended or Differential, according to your needs.</p>	
1	<p><b>2410-400V3</b>            VersaChannel for 4 Single-ended or 2 Differential inputs via BNC.            Includes PC data acquisition board, BNC connection box, and cables. Signal conditioning not included.</p>	
<hr/> <div style="display: flex; justify-content: space-between; align-items: center;"> <div style="display: flex; align-items: center;">  <p><b>INSTRON</b></p> </div> <div style="font-size: small;"> <p>Quote # INSQ78953            Last modified 01/26/2012</p> </div> <div style="text-align: center;"> <p>Page 2</p> </div> <div style="text-align: right; font-size: small;"> <p>Quotation submitted subject to provisions included.</p> </div> </div>		

Figure B-2 Instron® Quotation for Test Machine Upgrades, page 2/5


Qty.	Part Number	Price
<b>Computer Integration</b>		
1	3781-625 On Site Integration of a customer supplied computer	
<b>Minimum required computer configuration for Bluehill software:</b>		
1	<p>Base Requirements:</p> <ul style="list-style-type: none"> <li>- Intel Pentium (Dual Core or Single Core) Processor: 2 GHz or faster clock speed</li> <li>- 1 GB RAM</li> <li>- Microsoft Windows 7 Professional (32 &amp; 64 bit) or Windows XP Professional with Service Pack 3</li> <li>- Microsoft Internet Explorer 7 or later</li> <li>- DVD Drive</li> <li>- Hard Drive: 1 GB Free Space</li> <li>- 1 Unused Ethernet port (Instron 3300/5500/5900 only - 2 Ethernet ports if network accessibility is required)</li> </ul>	
<b>Bluehill Training</b>		
1	<p>1450-056 BlueHill Upgrade Training - This introduction includes Test Method development and training for up to 3 operators on the customers supplied equipment and to pre-defined customer methods.</p> <p>Included in this item are:</p> <ul style="list-style-type: none"> <li>- Review user's application needs</li> <li>- Creation, if necessary, and the running of up to 5 user test methods</li> <li>- If required, conversion of up to 10 Instron Series IX test methods OR all Instron Merlin Test Methods</li> <li>- Set-up of Sample and Specimen Parameters</li> <li>- Set-up of Test Control Parameters</li> <li>- Results Calculations setup for applications</li> <li>- Review and set-up of report templates</li> <li>- Testing customer supplied specimens to validate/verify developed test methods</li> <li>- Instruction on simple modifications to Test Methods and Report Templates (if applicable)</li> </ul> <p>Note:</p> <p>1. The above service is expected to take a maximum of 4 hours</p>	
<b>Software Warranty</b>		
1	<p>1405-503 First Year Software Warranty - The first-year service and support agreement for this software under warranty includes the following services during the first year of ownership (see Instron Terms and Conditions for exact details, limitations and restrictions):</p> <ul style="list-style-type: none"> <li>- Technical Support: Includes the following:</li> <li>- Unlimited priority telephone support during normal business</li> </ul>	
 <span style="margin-left: 10px;">Quote # INSQ78953 Last modified 01/26/2012</span> <span style="margin-left: 100px;">Page 3</span> <span style="float: right;">Quotation submitted subject to provisions included.</span>		

Figure B-3 Instron® Quotation for Test Machine Upgrades, page 3/5


Qty.	Part Number	Price
	<ul style="list-style-type: none"> <li>- All software updates, but not upgrades, during the agreement period</li> <li>- Damaged CD replacement on warranted software</li> <li>- Web Support Agreement (WSA): Includes the following:</li> <li>- Allows access to a restricted website under one user log-in</li> <li>- FAQ's</li> <li>- Technical Literature</li> <li>- Priority Support web based help desk</li> <li>- 2 Instron Webinars providing application or product information or assistance</li> <li>- On-line access to calibration certificates</li> <li>- Software updates delivered via the web</li> </ul>	
	SubTotal:	\$13,896
1	Less Educational Discount:	-\$2,500
	Total:	\$11,396
<hr/>		
<b>Computer</b>		
1	<b>2490-681</b> HP Compaq Workstation PC with: <ul style="list-style-type: none"> <li>- Intel Core 2 Duo E8400 processor 3.00 GHz</li> <li>- Windows 7 Professional operating system option</li> <li>- 19 inch Flat Panel LCD Monitor</li> <li>- 2 Ethernet ports (1 on motherboard and 1 on a PCI card)</li> <li>- 1 GB DDR2 SDRAM</li> <li>- 80 GB SATA hard drive</li> <li>- 48 X 32 CDRW/DVD</li> <li>- HP ADD2 SDVO PCIe DVI-D graphics card</li> <li>- Three PCI expansion slots</li> <li>- One serial port</li> <li>- Minitower chassis</li> <li>- HP standard keyboard</li> <li>- HP 2-button optical scroll mouse</li> <li>- Internal chassis speakers</li> </ul> <p>PC specifications change on a regular basis. The above represents the minimum configuration that will be supplied.</p>	
	Computer Total:	\$1,000
<hr/>		
 <span style="font-size: small;">Quote # INSQ78953 Last modified 01/28/2012</span> <span style="float: right; margin-left: 100px;">Page 4    Quotation submitted subject to provisions included.</span>		

Figure B-4 Instron® Quotation for Test Machine Upgrades, page 4/5


Qty.	Part Number	Price
<p><b>DELIVERY</b> 30 - 45 days from receipt of order, subject to prior orders.</p>		
<p><b>TERMS</b> Net 30 days from date of shipment, subject to credit approval.</p>		
<p>DELIVERY: Ex-Works SHIP VIA: Most economical way FREIGHT: Prepaid and Add</p>		
<p>All Purchase Orders should be mailed to: Instron 825 University Avenue Norwood, MA 02062-2643 Or Faxed to: (781)575-5725 ATTN: Order Administration</p>		
<p>We accept Visa, Mastercard, and American Express Prices above are for U.S. destination. Warranty and service commitments only apply to instrumentation installed in the U.S.</p>		
<hr/>  <span data-bbox="527 1585 714 1627">Quote # INSQ78953 Last modified 01/26/2012</span> <span data-bbox="820 1596 901 1627">Page 5</span> <span data-bbox="950 1596 1404 1627">Quotation submitted subject to provisions included.</span>		

Figure B-5 Instron® Quotation for Test Machine Upgrades, page 5/5

## APPENDIX C

### GRADATION REQUIREMENTS FOR RHODE ISLAND CLASS I-1 GRADATION

APPENDIX C

GRADATION REQUIREMENTS FOR RI CLASS I-1

Table C-1 Gradation Required for Class I-1 classification

Sieve Size	Component										Total		RIDOT Specs.
	1/2" [21%]		3/8" [21%]		Screen [40%]		F. Sand [18%]						
	% Passing	% Retained	% Passing	% Retained	% Passing	% Retained	% Passing	% Retained	% Passing	% Retained	% Passing	% Retained	
3/4"	21.0	0.0	21.0	0.0	40.0	0.0	18.0	0.0	100.0	0.0	100.0	0.0	100.0
1/2"	18.3	2.7	21.0	0.0	40.0	0.0	18.0	0.0	97.3	2.7	80-100		
3/8"	3.4	14.9	19.7	1.3	40.0	0.0	18.0	0.0	81.1	16.2	70-90		
#4		3.4	4.2	15.5	39.2	0.8	18.0	0.0	61.4	19.7	50-70		
#8				4.2	27.6	11.6	17.8	0.2	45.4	16.0	35-50		
#30					10.4	17.2	16.6	1.2	27.0	18.4	18-29		
#50					6.0	4.4	13.7	2.9	19.7	7.3	13-23		
#100					3.2	2.8	6.5	7.2	9.7	10.0			
#200					1.6	1.6	1.4	5.1	3.0	6.7			3 to 8
Pan						1.6		1.4		3.0			
													100.0

Table C-2 Required Material Amounts for Preparation of Specimens

		1 -Specimen	2- Specimen	2 -Spec. + G <sub>mm</sub>
Sieve Size	wt. Retained	wt. Retained	Wt. Retained	For G <sub>mm</sub> also
3/4"	0.0	0.0	0.0	0.0
1/2"	2.7	124.2	248.4	275.4
3/8"	26.7	1228.2	2456.4	2723.4
#4	12.9	593.4	1186.8	1315.8
#8	12.8	588.8	1177.6	1305.6
#30	18.4	846.4	1692.8	1876.8
#50	7.3	335.8	671.6	744.6
#100	10.0	460.0	920.0	1020.0
#200	6.7	308.2	616.4	683.4
Pan	3.0	138.0	276.0	306.0
<b>Total (gms)</b>	<b>100.0</b>	<b>4600.0</b>	<b>9200.0</b>	<b>10200.0</b>
			↓	↓
		%	gms	gms
		5.5	535.4	593.7
		6.0	587.2	651.1
		6.5	639.6	709.1
		7.0	692.5	767.7



## APPENDIX D

### EXEMPLARY CALCULATIONS FOR THE COMPACTION OF ONE HMA SAMPLE

**APPENDIX D    EXEMPLARY COMPACTION CALCULATIONS FOR HMA SAMPLE**

Table D-1 Compaction Calculations for first 5.5% BC Sample

N	H [mm]	H [cm]	V [cm <sup>3</sup> ]	Gmb est	C	Gmb corr	% Gmm
0	116.3	11.63	2121.48	2.0529	1.041	2.1365	80.98%
1	111.6	11.16	2035.75	2.1394	1.041	2.2265	84.39%
2	109.3	10.93	1993.79	2.1844	1.041	2.2733	86.17%
3	107.9	10.79	1968.25	2.2127	1.041	2.3028	87.29%
4	106.8	10.68	1948.19	2.2355	1.041	2.3265	88.18%
5	105.9	10.59	1931.77	2.2545	1.041	2.3463	88.93%
6	105.2	10.52	1919.00	2.2695	1.041	2.3619	89.53%
7	104.6	10.46	1908.06	2.2825	1.041	2.3755	90.04%
8	104.1	10.41	1898.94	2.2935	1.041	2.3869	90.47%
9	103.7	10.37	1891.64	2.3024	1.041	2.3961	90.82%
10	103.3	10.33	1884.34	2.3113	1.041	2.4053	91.17%
11	102.9	10.29	1877.05	2.3203	1.041	2.4147	91.53%
12	102.6	10.26	1871.57	2.3270	1.041	2.4218	91.79%
13	102.3	10.23	1866.10	2.3339	1.041	2.4289	92.06%
14	102.1	10.21	1862.45	2.3384	1.041	2.4336	92.24%
15	101.8	10.18	1856.98	2.3453	1.041	2.4408	92.52%
16	101.6	10.16	1853.33	2.3499	1.041	2.4456	92.70%
17	101.4	10.14	1849.68	2.3546	1.041	2.4504	92.88%
18	101.2	10.12	1846.04	2.3592	1.041	2.4553	93.06%
19	101.0	10.10	1842.39	2.3639	1.041	2.4601	93.25%
20	100.9	10.09	1840.56	2.3662	1.041	2.4626	93.34%
21	100.7	10.07	1836.91	2.3709	1.041	2.4675	93.53%
22	100.6	10.06	1835.09	2.3733	1.041	2.4699	93.62%
23	100.5	10.05	1833.27	2.3757	1.041	2.4724	93.71%
24	100.3	10.03	1829.62	2.3804	1.041	2.4773	93.90%
25	100.2	10.02	1827.79	2.3828	1.041	2.4798	93.99%
26	100.1	10.01	1825.97	2.3852	1.041	2.4822	94.09%
27	100.0	10.00	1824.15	2.3875	1.041	2.4847	94.18%
28	99.9	9.99	1822.32	2.3899	1.041	2.4872	94.28%
29	99.8	9.98	1820.50	2.3923	1.041	2.4897	94.37%
30	99.7	9.97	1818.67	2.3947	1.041	2.4922	94.46%
31	99.7	9.97	1818.67	2.3947	1.041	2.4922	94.46%
32	99.6	9.96	1816.85	2.3971	1.041	2.4947	94.56%
33	99.5	9.95	1815.02	2.3995	1.041	2.4972	94.65%
34	99.5	9.95	1815.02	2.3995	1.041	2.4972	94.65%
35	99.4	9.94	1813.20	2.4020	1.041	2.4997	94.75%
36	99.3	9.93	1811.38	2.4044	1.041	2.5022	94.84%

Table above continued

N	H [mm]	H [cm]	V [cm <sup>3</sup> ]	Gmb est	C	Gmb corr	% Gmm
37	99.3	9.93	1811.38	2.4044	1.041	2.5022	94.84%
38	99.2	9.92	1809.55	2.4068	1.041	2.5048	94.94%
39	99.2	9.92	1809.55	2.4068	1.041	2.5048	94.94%
40	99.1	9.91	1807.73	2.4092	1.041	2.5073	95.04%
41	99.1	9.91	1807.73	2.4092	1.041	2.5073	95.04%
42	99.0	9.90	1805.90	2.4117	1.041	2.5098	95.13%
43	99.0	9.90	1805.90	2.4117	1.041	2.5098	95.13%
44	98.9	9.89	1804.08	2.4141	1.041	2.5124	95.23%
45	98.9	9.89	1804.08	2.4141	1.041	2.5124	95.23%
46	98.9	9.89	1804.08	2.4141	1.041	2.5124	95.23%
47	98.8	9.88	1802.26	2.4165	1.041	2.5149	95.32%
48	98.8	9.88	1802.26	2.4165	1.041	2.5149	95.32%
49	98.7	9.87	1800.43	2.4190	1.041	2.5175	95.42%
50	98.7	9.87	1800.43	2.4190	1.041	2.5175	95.42%
51	98.7	9.87	1800.43	2.4190	1.041	2.5175	95.42%
52	98.7	9.87	1800.43	2.4190	1.041	2.5175	95.42%
53	98.6	9.86	1798.61	2.4214	1.041	2.5200	95.52%
54	98.6	9.86	1798.61	2.4214	1.041	2.5200	95.52%
55	98.6	9.86	1798.61	2.4214	1.041	2.5200	95.52%
56	98.5	9.85	1796.78	2.4239	1.041	2.5226	95.62%
57	98.5	9.85	1796.78	2.4239	1.041	2.5226	95.62%
58	98.5	9.85	1796.78	2.4239	1.041	2.5226	95.62%
59	98.5	9.85	1796.78	2.4239	1.041	2.5226	95.62%
60	98.4	9.84	1794.96	2.4264	1.041	2.5251	95.71%
61	98.4	9.84	1794.96	2.4264	1.041	2.5251	95.71%
62	98.4	9.84	1794.96	2.4264	1.041	2.5251	95.71%
63	98.4	9.84	1794.96	2.4264	1.041	2.5251	95.71%
64	98.4	9.84	1794.96	2.4264	1.041	2.5251	95.71%
65	98.3	9.83	1793.13	2.4288	1.041	2.5277	95.81%
66	98.3	9.83	1793.13	2.4288	1.041	2.5277	95.81%
67	98.3	9.83	1793.13	2.4288	1.041	2.5277	95.81%
68	98.3	9.83	1793.13	2.4288	1.041	2.5277	95.81%
69	98.3	9.83	1793.13	2.4288	1.041	2.5277	95.81%
70	98.2	9.82	1791.31	2.4313	1.041	2.5303	95.91%
71	98.2	9.82	1791.31	2.4313	1.041	2.5303	95.91%
72	98.2	9.82	1791.31	2.4313	1.041	2.5303	95.91%
73	98.2	9.82	1791.31	2.4313	1.041	2.5303	95.91%
74	98.2	9.82	1791.31	2.4313	1.041	2.5303	95.91%

Table above continued

N	H [mm]	H [cm]	V [cm <sup>3</sup> ]	Gmb est	C	Gmb corr	% Gmm
75	98.2	9.82	1791.31	2.4313	1.041	2.5303	95.91%
76	98.1	9.81	1789.49	2.4338	1.041	2.5328	96.01%
77	98.1	9.81	1789.49	2.4338	1.041	2.5328	96.01%
78	98.1	9.81	1789.49	2.4338	1.041	2.5328	96.01%
79	98.1	9.81	1789.49	2.4338	1.041	2.5328	96.01%
80	98.1	9.81	1789.49	2.4338	1.041	2.5328	96.01%
81	98.1	9.81	1789.49	2.4338	1.041	2.5328	96.01%
82	98.1	9.81	1789.49	2.4338	1.041	2.5328	96.01%
83	98.0	9.80	1787.66	2.4363	1.041	2.5354	96.10%
84	98.0	9.80	1787.66	2.4363	1.041	2.5354	96.10%
85	98.0	9.80	1787.66	2.4363	1.041	2.5354	96.10%
86	98.0	9.80	1787.66	2.4363	1.041	2.5354	96.10%
87	98.0	9.80	1787.66	2.4363	1.041	2.5354	96.10%
88	98.0	9.80	1787.66	2.4363	1.041	2.5354	96.10%
89	98.0	9.80	1787.66	2.4363	1.041	2.5354	96.10%
90	98.0	9.80	1787.66	2.4363	1.041	2.5354	96.10%
91	97.9	9.79	1785.84	2.4388	1.041	2.5380	96.20%
92	97.9	9.79	1785.84	2.4388	1.041	2.5380	96.20%
93	97.9	9.79	1785.84	2.4388	1.041	2.5380	96.20%
94	97.9	9.79	1785.84	2.4388	1.041	2.5380	96.20%
95	97.9	9.79	1785.84	2.4388	1.041	2.5380	96.20%
96	97.9	9.79	1785.84	2.4388	1.041	2.5380	96.20%
97	97.9	9.79	1785.84	2.4388	1.041	2.5380	96.20%
98	97.9	9.79	1785.84	2.4388	1.041	2.5380	96.20%
99	97.9	9.79	1785.84	2.4388	1.041	2.5380	96.20%
100	97.9	9.79	1785.84	2.4388	1.041	2.5380	96.20%
101	97.8	9.78	1784.01	2.4412	1.041	2.5406	96.30%
102	97.8	9.78	1784.01	2.4412	1.041	2.5406	96.30%
103	97.8	9.78	1784.01	2.4412	1.041	2.5406	96.30%
104	97.8	9.78	1784.01	2.4412	1.041	2.5406	96.30%
105	97.8	9.78	1784.01	2.4412	1.041	2.5406	96.30%
106	97.8	9.78	1784.01	2.4412	1.041	2.5406	96.30%
107	97.8	9.78	1784.01	2.4412	1.041	2.5406	96.30%
108	97.8	9.78	1784.01	2.4412	1.041	2.5406	96.30%
109	97.8	9.78	1784.01	2.4412	1.041	2.5406	96.30%
110	97.8	9.78	1784.01	2.4412	1.041	2.5406	96.30%
111	97.8	9.78	1784.01	2.4412	1.041	2.5406	96.30%
112	97.8	9.78	1784.01	2.4412	1.041	2.5406	96.30%
113	97.7	9.77	1782.19	2.4437	1.041	2.5432	96.40%

Table above continued

N	H [mm]	H [cm]	V [cm <sup>3</sup> ]	Gmb est	C	Gmb corr	% Gmm
114	97.7	9.77	1782.19	2.4437	1.041	2.5432	96.40%
115	97.7	9.77	1782.19	2.4437	1.041	2.5432	96.40%
116	97.7	9.77	1782.19	2.4437	1.041	2.5432	96.40%
117	97.7	9.77	1782.19	2.4437	1.041	2.5432	96.40%
118	97.7	9.77	1782.19	2.4437	1.041	2.5432	96.40%
119	97.7	9.77	1782.19	2.4437	1.041	2.5432	96.40%
120	97.7	9.77	1782.19	2.4437	1.041	2.5432	96.40%
121	97.7	9.77	1782.19	2.4437	1.041	2.5432	96.40%
122	97.7	9.77	1782.19	2.4437	1.041	2.5432	96.40%
123	97.7	9.77	1782.19	2.4437	1.041	2.5432	96.40%
124	97.7	9.77	1782.19	2.4437	1.041	2.5432	96.40%
125	97.7	9.77	1782.19	2.4437	1.041	2.5432	96.40%
126	97.7	9.77	1782.19	2.4437	1.041	2.5432	96.40%
127	97.7	9.77	1782.19	2.4437	1.041	2.5432	96.40%
128	97.6	9.76	1780.37	2.4462	1.041	2.5458	96.50%
129	97.6	9.76	1780.37	2.4462	1.041	2.5458	96.50%
130	97.6	9.76	1780.37	2.4462	1.041	2.5458	96.50%
131	97.6	9.76	1780.37	2.4462	1.041	2.5458	96.50%
132	97.6	9.76	1780.37	2.4462	1.041	2.5458	96.50%
133	97.6	9.76	1780.37	2.4462	1.041	2.5458	96.50%
134	97.6	9.76	1780.37	2.4462	1.041	2.5458	96.50%
135	97.6	9.76	1780.37	2.4462	1.041	2.5458	96.50%
136	97.6	9.76	1780.37	2.4462	1.041	2.5458	96.50%
137	97.6	9.76	1780.37	2.4462	1.041	2.5458	96.50%
138	97.6	9.76	1780.37	2.4462	1.041	2.5458	96.50%
139	97.6	9.76	1780.37	2.4462	1.041	2.5458	96.50%
140	97.6	9.76	1780.37	2.4462	1.041	2.5458	96.50%
141	97.6	9.76	1780.37	2.4462	1.041	2.5458	96.50%
142	97.6	9.76	1780.37	2.4462	1.041	2.5458	96.50%
143	97.6	9.76	1780.37	2.4462	1.041	2.5458	96.50%
144	97.6	9.76	1780.37	2.4462	1.041	2.5458	96.50%
145	97.6	9.76	1780.37	2.4462	1.041	2.5458	96.50%
146	97.6	9.76	1780.37	2.4462	1.041	2.5458	96.50%
147	97.6	9.76	1780.37	2.4462	1.041	2.5458	96.50%
148	97.6	9.76	1780.37	2.4462	1.041	2.5458	96.50%
149	97.6	9.76	1780.37	2.4462	1.041	2.5458	96.50%
150	97.6	9.76	1780.37	2.4462	1.041	2.5458	96.50%
151	97.5	9.75	1778.54	2.4488	1.041	2.5484	96.60%

Table above continued

N	H [mm]	H [cm]	V [cm <sup>3</sup> ]	Gmb est	C	Gmb corr	% Gmm
152	97.5	9.75	1778.54	2.4488	1.041	2.5484	96.60%
153	97.5	9.75	1778.54	2.4488	1.041	2.5484	96.60%
154	97.5	9.75	1778.54	2.4488	1.041	2.5484	96.60%
155	97.5	9.75	1778.54	2.4488	1.041	2.5484	96.60%
156	97.5	9.75	1778.54	2.4488	1.041	2.5484	96.60%
157	97.5	9.75	1778.54	2.4488	1.041	2.5484	96.60%
158	97.5	9.75	1778.54	2.4488	1.041	2.5484	96.60%
159	97.5	9.75	1778.54	2.4488	1.041	2.5484	96.60%
160	97.5	9.75	1778.54	2.4488	1.041	2.5484	96.60%
161	97.5	9.75	1778.54	2.4488	1.041	2.5484	96.60%
162	97.5	9.75	1778.54	2.4488	1.041	2.5484	96.60%
163	97.5	9.75	1778.54	2.4488	1.041	2.5484	96.60%
164	97.5	9.75	1778.54	2.4488	1.041	2.5484	96.60%
165	97.5	9.75	1778.54	2.4488	1.041	2.5484	96.60%
166	97.5	9.75	1778.54	2.4488	1.041	2.5484	96.60%
167	97.5	9.75	1778.54	2.4488	1.041	2.5484	96.60%
168	97.5	9.75	1778.54	2.4488	1.041	2.5484	96.60%
169	97.5	9.75	1778.54	2.4488	1.041	2.5484	96.60%
170	97.5	9.75	1778.54	2.4488	1.041	2.5484	96.60%
171	97.5	9.75	1778.54	2.4488	1.041	2.5484	96.60%
172	97.5	9.75	1778.54	2.4488	1.041	2.5484	96.60%
173	97.5	9.75	1778.54	2.4488	1.041	2.5484	96.60%
174	97.5	9.75	1778.54	2.4488	1.041	2.5484	96.60%

Table D-2 Bulk SG Computations

G <sub>mb</sub>	dry	surface dry	under water	G <sub>mb</sub>	G <sub>mb</sub>
	A	B	C	measured	average
5.5	4354.0	4359.5	2651.0	2.5484	2.5499
	4379.5	4391.5	2675.0	2.5514	
6.0	4363.0	4367.0	2640.5	2.5271	2.5337
	4386.0	4391.0	2664.5	2.5404	
6.5	4385.0	4390.5	2637.5	2.5014	2.5021
	4388.5	4394.0	2640.5	2.5027	
7.0	4391.5	4394.0	2630.5	2.4902	2.4949
	4390.5	4393.5	2637.0	2.4996	

Table D-3 Theoretical Maximum SG Computations

G <sub>se</sub>	6.0%		2.9020
G <sub>mm</sub> -5.5	5.5		2.6382
G <sub>mm</sub> - 6.0	6.0		2.6166
G <sub>mm</sub> -6.5	6.5		2.5954
G <sub>mm</sub> -7.0	7.0		2.5744

## APPENDIX E

### ANALYSIS OF THE RECLAIMED ASPHALT PAVEMENT (RAP) MATERIAL



## APPENDIX E RAP MATERIAL ANALYSIS

Table E-1 shows the result of the moisture content determination.

Table E-1 Moisture Test

Object	Mass [g]
Bowl w/ wet sample	2,434.4
Bowl w/ dried sample	2,346.6
Bowl empty	272.2

Moisture content [g]:	87.8
Moisture content [%]:	<b>4.1%</b>
Dry mass	2,074.4

**Moisture Content**

A 3D pie chart titled "Moisture Content" showing the composition of the sample. The chart is divided into two segments: a small red segment representing "Moisture" at 4.1%, and a large blue segment representing "Dry mass" at 95.9%.

Category	Percentage
Moisture	4.1%
Dry mass	95.9%

Table E-2 Sieve Analysis Measurements

Sieve Size		Wt. retained single (two runs)		Wt. retained single sum	Wt. retained single sum	Wt. passing accum. sum	Wt. passing accum. sum
US	[mm]	[g]	[g]	[g]	[%]	[g]	[%]
5/4"	31.8	0.0	0.0	0.0	0%	1997.5	100%
1"	25.0	25.0	19.0	44.0	2%	1953.5	98%
3/4"	19.1	19.5	73.0	92.5	5%	1861.0	93%
1/2"	12.5	123.0	175.5	298.5	15%	1562.5	78%
3/8"	9.5	173.0	170.0	343.0	17%	1219.5	61%
#4	4.8	240.0	210.5	450.5	23%	769.0	38%
#8	2.4	136.5	113.0	249.5	12%	519.5	26%
#16	1.2	118.0	91.5	209.5	10%	310.0	16%
Pan	0.6	164.0	146.0	310.0	16%	0.0	0%
Σ:		999.0	998.5	1997.5			
Input Mass:		1000.0	1000.0	2000.0			
Loss [g]:		1.0	1.5	2.5			
Loss [%]:		0.1%	0.2%	0.1%			

## APPENDIX F

### DETERMINATION OF THE NECESSARY NUMBER OF GYRATIONS FOR THE COMPACTION OF CIR MIXTURES

**APPENDIX F    NECESSARY NUMBER OF GYRATIONS FOR CIR MATERIAL**

Table F-1 Calculations for Determination of Number of Gyration for CIR Materials

Specimen Characteristics:					
Shape:	cylindrical				
Diameter:	6	in	=	15.24	cm
Mass:	4136.5	g			
Emulsion content:	1.0%	%			
Water content:	3.0%	%			

Correction Factor					
$G_{mb}$ measured:	2.119				
C=	1.008				
Field density / $G_{mb,field}$ :	130.0	pcf	=	2.084	$g/cm^3$

Table F-2 Compaction for Determination of Number of Gyration for CIR Materials

Gyration Number	Specimen height [mm]	Volume [ $cm^3$ ]	$G_{mb}$ est. [ $g/cm^3$ ]	$G_{mb}$ corr. [ $g/cm^3$ ]	$G_{mb}$ corr./field %
0	135.2	2466.247	1.677	1.691	81.2%
1	131.9	2406.050	1.719	1.734	83.2%
2	129.8	2367.743	1.747	1.762	84.5%
3	128.1	2336.732	1.770	1.785	85.7%
4	126.7	2311.194	1.790	1.805	86.6%
5	125.6	2291.129	1.805	1.821	87.4%
6	124.7	2274.711	1.818	1.834	88.0%
7	123.9	2260.118	1.830	1.846	88.6%
8	123.2	2247.349	1.841	1.856	89.1%
9	122.6	2236.404	1.850	1.865	89.5%
10	122.1	2227.283	1.857	1.873	89.9%
11	121.6	2218.163	1.865	1.880	90.2%
12	121.1	2209.042	1.873	1.888	90.6%
13	120.7	2201.745	1.879	1.894	90.9%
14	120.3	2194.449	1.885	1.901	91.2%

Table above continued

Gyration Number	Specimen height [mm]	Volume [cm <sup>3</sup> ]	Gmb est. [g/cm <sup>3</sup> ]	Gmb corr. [g/cm <sup>3</sup> ]	Gmb corr./field %
15	119.9	2187.152	1.891	1.907	91.5%
16	119.5	2179.856	1.898	1.913	91.8%
17	119.2	2174.383	1.902	1.918	92.1%
18	118.9	2168.911	1.907	1.923	92.3%
19	118.6	2163.438	1.912	1.928	92.5%
20	118.4	2159.790	1.915	1.931	92.7%
21	118.1	2154.318	1.920	1.936	92.9%
22	117.8	2148.845	1.925	1.941	93.2%
23	117.6	2145.197	1.928	1.944	93.3%
24	117.4	2141.548	1.932	1.948	93.5%
25	117.2	2137.900	1.935	1.951	93.6%
26	116.9	2132.428	1.940	1.956	93.9%
27	116.8	2130.604	1.941	1.958	94.0%
28	116.6	2126.955	1.945	1.961	94.1%
29	116.4	2123.307	1.948	1.964	94.3%
30	116.2	2119.659	1.951	1.968	94.4%
31	116.0	2116.010	1.955	1.971	94.6%
32	115.9	2114.186	1.957	1.973	94.7%
33	115.7	2110.538	1.960	1.976	94.8%
34	115.6	2108.714	1.962	1.978	94.9%
35	115.4	2105.066	1.965	1.981	95.1%
36	115.3	2103.241	1.967	1.983	95.2%
37	115.1	2099.593	1.970	1.987	95.3%
38	115.0	2097.769	1.972	1.988	95.4%
39	114.9	2095.945	1.974	1.990	95.5%
40	114.7	2092.297	1.977	1.994	95.7%
41	114.6	2090.472	1.979	1.995	95.8%
42	114.5	2088.648	1.980	1.997	95.8%
43	114.4	2086.824	1.982	1.999	95.9%
44	114.3	2085.000	1.984	2.001	96.0%
45	114.1	2081.352	1.987	2.004	96.2%
46	114.0	2079.527	1.989	2.006	96.3%
47	113.9	2077.703	1.991	2.008	96.3%
48	113.8	2075.879	1.993	2.009	96.4%
49	113.7	2074.055	1.994	2.011	96.5%

Table above continued

Gyration Number	Specimen height [mm]	Volume [cm <sup>3</sup> ]	Gmb est. [g/cm <sup>3</sup> ]	Gmb corr. [g/cm <sup>3</sup> ]	Gmb corr./field %
50	113.6	2072.231	1.996	2.013	96.6%
51	113.5	2070.407	1.998	2.015	96.7%
52	113.4	2068.583	2.000	2.016	96.8%
53	113.3	2066.758	2.001	2.018	96.9%
54	113.2	2064.934	2.003	2.020	96.9%
55	113.2	2064.934	2.003	2.020	96.9%
56	113.1	2063.110	2.005	2.022	97.0%
57	113.0	2061.286	2.007	2.024	97.1%
58	112.9	2059.462	2.009	2.025	97.2%
59	112.8	2057.638	2.010	2.027	97.3%
60	112.7	2055.814	2.012	2.029	97.4%
61	112.7	2055.814	2.012	2.029	97.4%
62	112.6	2053.989	2.014	2.031	97.5%
63	112.5	2052.165	2.016	2.033	97.5%
64	112.4	2050.341	2.017	2.034	97.6%
65	112.4	2050.341	2.017	2.034	97.6%
66	112.3	2048.517	2.019	2.036	97.7%
67	112.2	2046.693	2.021	2.038	97.8%
68	112.1	2044.869	2.023	2.040	97.9%
69	112.1	2044.869	2.023	2.040	97.9%
70	112.0	2043.045	2.025	2.042	98.0%
71	111.9	2041.220	2.026	2.043	98.1%
72	111.9	2041.220	2.026	2.043	98.1%
73	111.8	2039.396	2.028	2.045	98.2%
74	111.7	2037.572	2.030	2.047	98.2%
75	111.7	2037.572	2.030	2.047	98.2%
76	111.6	2035.748	2.032	2.049	98.3%
77	111.6	2035.748	2.032	2.049	98.3%
78	111.5	2033.924	2.034	2.051	98.4%
79	111.4	2032.100	2.036	2.053	98.5%
80	111.4	2032.100	2.036	2.053	98.5%
81	111.3	2030.276	2.037	2.054	98.6%
82	111.3	2030.276	2.037	2.054	98.6%
83	111.2	2028.451	2.039	2.056	98.7%
84	111.2	2028.451	2.039	2.056	98.7%

Table above continued

Gyration Number	Specimen height [mm]	Volume [cm <sup>3</sup> ]	Gmb est. [g/cm <sup>3</sup> ]	Gmb corr. [g/cm <sup>3</sup> ]	Gmb corr./field %
85	111.1	2026.627	2.041	2.058	98.8%
86	111.0	2024.803	2.043	2.060	98.9%
87	111.0	2024.803	2.043	2.060	98.9%
88	110.9	2022.979	2.045	2.062	99.0%
89	110.9	2022.979	2.045	2.062	99.0%
90	110.8	2021.155	2.047	2.064	99.0%
91	110.8	2021.155	2.047	2.064	99.0%
92	110.7	2019.331	2.048	2.066	99.1%
93	110.7	2019.331	2.048	2.066	99.1%
94	110.6	2017.506	2.050	2.067	99.2%
95	110.6	2017.506	2.050	2.067	99.2%
96	110.5	2015.682	2.052	2.069	99.3%
97	110.5	2015.682	2.052	2.069	99.3%
98	110.4	2013.858	2.054	2.071	99.4%
99	110.4	2013.858	2.054	2.071	99.4%
100	110.4	2013.858	2.054	2.071	99.4%
101	110.3	2012.034	2.056	2.073	99.5%
102	110.3	2012.034	2.056	2.073	99.5%
103	110.2	2010.210	2.058	2.075	99.6%
104	110.2	2010.210	2.058	2.075	99.6%
105	110.1	2008.386	2.060	2.077	99.7%
106	110.1	2008.386	2.060	2.077	99.7%
107	110.0	2006.562	2.061	2.079	99.8%
108	110.0	2006.562	2.061	2.079	99.8%
109	110.0	2006.562	2.061	2.079	99.8%
110	109.9	2004.737	2.063	2.081	99.9%
111	109.9	2004.737	2.063	2.081	99.9%
112	109.8	2002.913	2.065	2.082	99.9%
113	109.8	2002.913	2.065	2.082	99.9%
114	109.8	2002.913	2.065	2.082	99.9%
115	109.7	2001.089	2.067	2.084	100.0%
116	109.7	2001.089	2.067	2.084	100.0%
117	109.6	1999.265	2.069	2.086	100.1%
118	109.6	1999.265	2.069	2.086	100.1%
119	109.6	1999.265	2.069	2.086	100.1%

Table above continued

Gyration Number	Specimen height [mm]	Volume [cm <sup>3</sup> ]	Gmb est. [g/cm <sup>3</sup> ]	Gmb corr. [g/cm <sup>3</sup> ]	Gmb corr./field %
120	109.5	1997.441	2.071	2.088	100.2%
121	109.5	1997.441	2.071	2.088	100.2%
122	109.5	1997.441	2.071	2.088	100.2%
123	109.4	1995.617	2.073	2.090	100.3%
124	109.4	1995.617	2.073	2.090	100.3%
125	109.4	1995.617	2.073	2.090	100.3%
126	109.3	1993.793	2.075	2.092	100.4%
127	109.3	1993.793	2.075	2.092	100.4%
128	109.3	1993.793	2.075	2.092	100.4%
129	109.2	1991.968	2.077	2.094	100.5%
130	109.2	1991.968	2.077	2.094	100.5%
131	109.2	1991.968	2.077	2.094	100.5%
132	109.1	1990.144	2.078	2.096	100.6%
133	109.1	1990.144	2.078	2.096	100.6%
134	109.1	1990.144	2.078	2.096	100.6%
135	109.0	1988.320	2.080	2.098	100.7%
136	109.0	1988.320	2.080	2.098	100.7%
137	109.0	1988.320	2.080	2.098	100.7%
138	108.9	1986.496	2.082	2.100	100.8%
139	108.9	1986.496	2.082	2.100	100.8%
140	108.9	1986.496	2.082	2.100	100.8%
141	108.9	1986.496	2.082	2.100	100.8%
142	108.8	1984.672	2.084	2.102	100.9%
143	108.8	1984.672	2.084	2.102	100.9%
144	108.8	1984.672	2.084	2.102	100.9%
145	108.7	1982.848	2.086	2.104	101.0%
146	108.7	1982.848	2.086	2.104	101.0%
147	108.7	1982.848	2.086	2.104	101.0%
148	108.6	1981.024	2.088	2.106	101.0%
149	108.6	1981.024	2.088	2.106	101.0%
150	108.6	1981.024	2.088	2.106	101.0%
151	108.6	1981.024	2.088	2.106	101.0%
152	108.5	1979.199	2.090	2.107	101.1%
153	108.5	1979.199	2.090	2.107	101.1%
154	108.5	1979.199	2.090	2.107	101.1%



Table above continued

Gyration Number	Specimen height [mm]	Volume [cm <sup>3</sup> ]	Gmb est. [g/cm <sup>3</sup> ]	Gmb corr. [g/cm <sup>3</sup> ]	Gmb corr./field %
155	108.5	1979.199	2.090	2.107	101.1%
156	108.4	1977.375	2.092	2.109	101.2%
157	108.4	1977.375	2.092	2.109	101.2%
158	108.4	1977.375	2.092	2.109	101.2%
159	108.3	1975.551	2.094	2.111	101.3%
160	108.3	1975.551	2.094	2.111	101.3%
161	108.3	1975.551	2.094	2.111	101.3%
162	108.3	1975.551	2.094	2.111	101.3%
163	108.2	1973.727	2.096	2.113	101.4%
164	108.2	1973.727	2.096	2.113	101.4%
165	108.2	1973.727	2.096	2.113	101.4%
166	108.2	1973.727	2.096	2.113	101.4%
167	108.1	1971.903	2.098	2.115	101.5%
168	108.1	1971.903	2.098	2.115	101.5%
169	108.1	1971.903	2.098	2.115	101.5%
170	108.1	1971.903	2.098	2.115	101.5%
171	108.0	1970.079	2.100	2.117	101.6%
172	108.0	1970.079	2.100	2.117	101.6%
173	108.0	1970.079	2.100	2.117	101.6%
174	107.9	1968.255	2.102	2.119	101.7%

## APPENDIX G

### DETERMINATION OF THE OPTIMUM EMULSION AND WATER CONTENTS OF CIR MIXTURES

**APPENDIX G          DETERMINATION OF OPTIMUM CONTENTS OF CIR MATERIAL**

The following Table G-1 through Table G-4 show the values measured and calculated in order to identify the optimum emulsion and water contents for CIR material.

Table G-1 Determination of Theoretical Maximum SG for OEC Determination

EC/ Sample name	Dry Sample only <i>A</i>	Masses [g]		$G_{mm}$ [-]
		Container w/ Water <i>D</i>	Container w/ Water and Sample <i>E</i>	
0.5% / <i>A</i>	1,192.5	7,327.5	8,041.5	2.492
1.0% / <i>B</i>	1,317.5		8,110.5	2.465
1.5% / <i>C</i>	1,232.0		8,056.5	2.449
2.0% / <i>D</i>	1,331.0		8,108.5	2.420

Table G-2 Bulk and Theoretical Maximum SG Results and Calculations for OEC Determination

Water content: 3.0%		Masses [g]			$G_{mb}$ [-]	$G_{mm}$ [-]	Air voids [%]	Unit weight [pcf]
Emulsion Content [%]	Specimen Number	in air A	in water C	SSD B				
0.5%	A I	3,869.0	2,076.0	3,928.5	2.089			
	A II	3,891.5	2,113.0	3,962.0	2.105			
	AVG(A)				<b>2.097</b>	<b>2.49</b>	<b>15.9%</b>	<b>130.9</b>
1.0%	B I	3,862.0	2,079.0	3,968.0	2.044			
	B II	3,858.5	2,072.5	3,931.5	2.076			
	AVG(B)				<b>2.060</b>	<b>2.46</b>	<b>16.4%</b>	<b>128.6</b>
1.5%	C I	3,905.0	2,114.0	4,013.5	2.056			
	C II	3,896.0	2,102.0	4,017.5	2.034			
	AVG(C)				<b>2.045</b>	<b>2.45</b>	<b>16.5%</b>	<b>127.7</b>
2.0%	D I	3,833.0	2,056.5	3,931.5	2.044			
	D II	3,813.5	2,042.0	3,932.5	2.017			
	AVG(D)				<b>2.031</b>	<b>2.42</b>	<b>16.1%</b>	<b>126.8</b>

**OEC= 0.7%**

Table G-3 Determination of Theoretical Maximum SG for OWC Determination

WC/ Sample name	Dry Sample only A	Masses [g]		$G_{mm}$ [-]
		Container w/ Water D	Container w/ Water and Sample E	
2.0% / E	1,218.5	7,327.5	8,054.5	2.479
2.5% / F	1,240.5		8,060.5	2.444
3.0% / G	1,201.0		8,042.0	2.469
3.5% / H	1,272.5		8,066.5	2.385

Table G-4 Bulk and Theoretical Maximum SG Results and Calculations for OWC Determination

Emulsion content:		0.7% (OEC)							
Water Content [%]	Specimen Number	Masses [g]			G <sub>mb</sub> [-]	G <sub>mm</sub> [-]	Air voids [%]	Unit weight [pcf]	
		in air A	in water C	SSD B					
2.0%	E I	3,886.5	2,063.5	4,002.0	2.005				
	E II	3,890.0	2,066.5	3,996.0	2.016				
	AVG(A)				<b>2.010</b>	<b>2.48</b>	<b>18.9%</b>	<b>125.5</b>	
2.5%	F I	3,881.5	2,048.5	4,008.0	1.981				
	F II	3,889.0	2,084.0	4,013.5	2.016				
	AVG(B)				<b>1.998</b>	<b>2.44</b>	<b>18.3%</b>	<b>124.7</b>	
3.0%	G I	3,875.5	2,134.5	4,042.5	2.031				
	G II	3,873.0	2,122.5	4,019.0	2.042				
	AVG(C)				<b>2.037</b>	<b>2.47</b>	<b>17.5%</b>	<b>127.2</b>	
3.5%	H I	3,858.0	2,056.5	4,000.0	1.985				
	H II	3,853.0	2,046.5	3,993.5	1.979				
	AVG(D)				<b>1.982</b>	<b>2.39</b>	<b>16.9%</b>	<b>123.7</b>	

**OWC= 3.0%**

## APPENDIX H

### MASSES OF THE INGREDIENTS OF PRODUCED CIR SPECIMENS

**APPENDIX H      MASSES OF INGREDIENTS FOR PRODUCED CIR SPECIMENS**

Table H-1 Required Masses of Ingredients for CIR Specimen Production

Mass of RAP:	<b>9,000</b>	<b>g</b>
--------------	--------------	----------

OEC Determination

Water content:	<b>3.0%</b>
----------------	-------------

Emulsion contents:	0.5%	1.0%	1.5%	2.0%
Emulsion mass [g]:	<b>46.6</b>	<b>93.8</b>	<b>141.4</b>	<b>189.5</b>
Water mass [g]:	279.8	281.3	282.7	284.2
Mass of specimen [g]:	9326.4	9375.0	9424.1	9473.7

OWC Determination

Emulsion content:	<b>0.7%</b>	(OEC)
-------------------	-------------	-------

Water content:	2.0%	2.5%	3.0%	3.5%
Water mass [g]:	<b>185.0</b>	<b>232.4</b>	<b>280.4</b>	<b>328.8</b>
Emulsion mass [g]:	64.7	65.1	65.4	65.8
Mass of specimen [g]:	9249.7	9297.5	9345.8	9394.6

Specimens for IDT Testing

Mass of RAP:	<b>8,000</b>	<b>g</b>
--------------	--------------	----------

Water content:	<b>3.0%</b>	(OWC)
Emulsion content:	<b>0.7%</b>	(OEC)

Water mass [g]:	<b>249.2</b>
Emulsion mass [g]:	<b>58.2</b>
Mass of specimen [g]:	8307.4

## APPENDIX I

### TESTING SCHEDULE FOR IDT TESTING



## APPENDIX I PLANNED TESTING SCHEDULE

The following Figure I-1 shows the planned testing schedule for one material in one day. Of course, testing rarely works as planned, however rough planning should at least be attempted to get an idea of the approximate time frames.

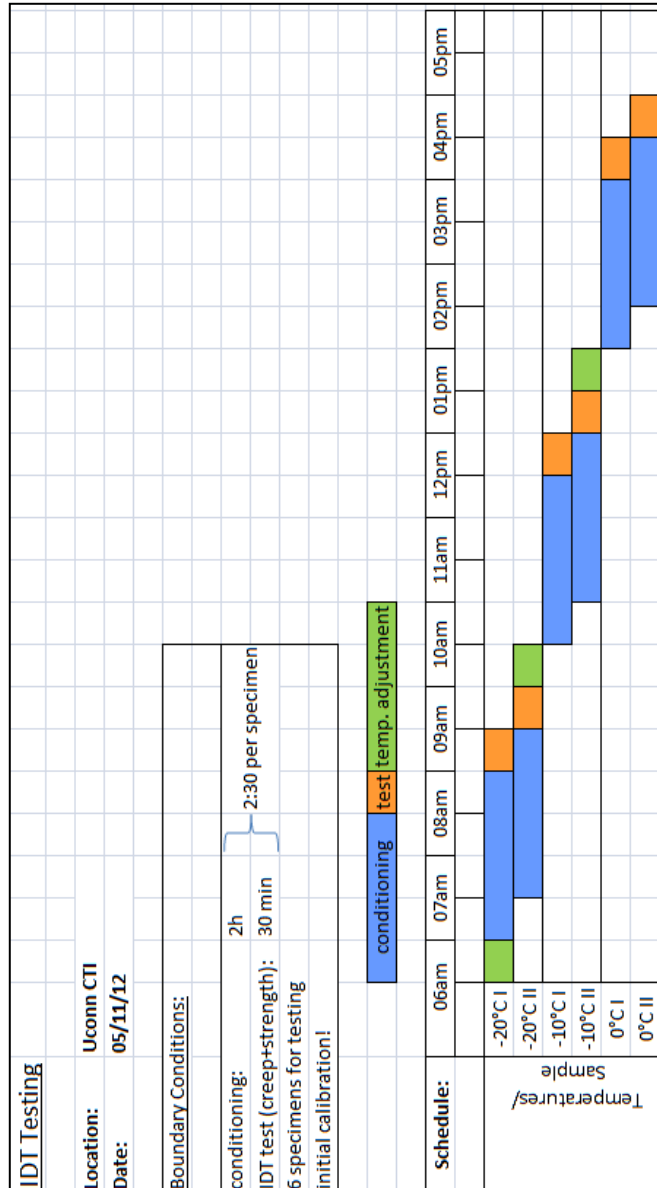


Figure I-1 Planned Testing Schedule

## APPENDIX J

### LABELS FOR THE PRODUCED SPECIMENS OF BOTH MATERIALS

**APPENDIX J SPECIMEN LABELS**

Table J-1 Specimen Labels

Specimen ID	Material	Temperature [°C]	Avg. Thickness [mm]	Front Face Number	Back Face Number
001	HMA	-20	42.21	1	2
002	HMA	-20	42.28	3	4
003	HMA	-20	42.26*	-	-
004	HMA	-10	42.38	1	2
005	HMA	-10	42.42	3	4
006	HMA	-10	42.44	5	6
007	HMA	0	42.18	1	2
008	HMA	0	42.33	3	4
011	CIR	-20	-*	-	-
012	CIR	-20	42.13	1	2
013	CIR	-20	42.85	3	4
014	CIR	-10	41.80	1	2
015	CIR	-10	42.62	3	4
016	CIR	-10	41.99	5	6
017	CIR	0	42.38	1	2
018	CIR	0	42.10	3	4

\*This specimen failed early and was therefore not used for analysis purposes.

Due to the exact dimensions of the mold, every specimen's diameter was 150.0 mm with deviations below 0.03 mm.

## APPENDIX K

SUMMARY OF THE NORMALIZED HORIZONTAL DEFORMATIONS DURING  
CREEP COMPLIANCE TESTING OF ALL SPECIMENS

## APPENDIX K NORMALIZED HORIZONTAL DEFORMATIONS

The following shows a summary of the normalized horizontal deformations of all specimens made from both materials.

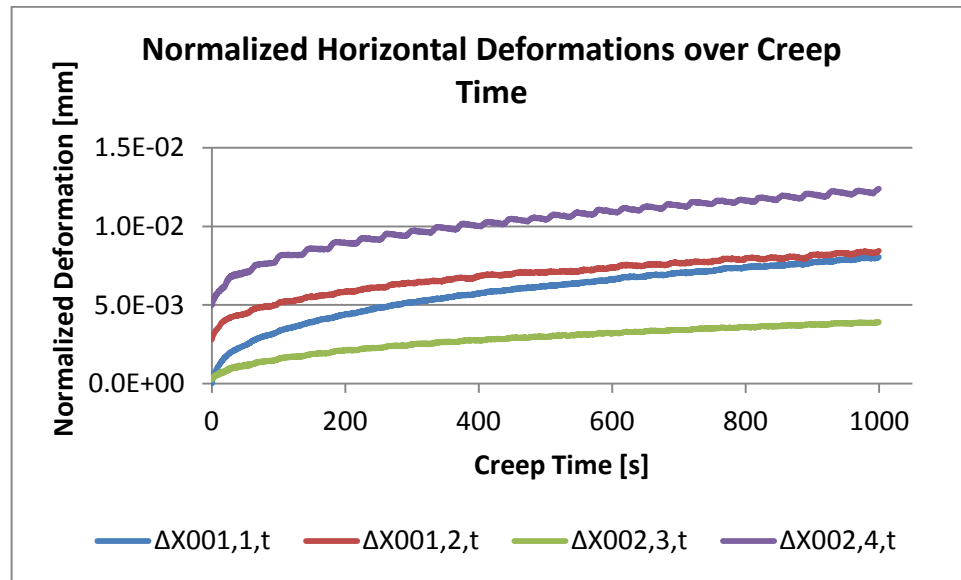


Figure K-1 Normalized Horizontal Deformations of HMA Specimens at -20 °C

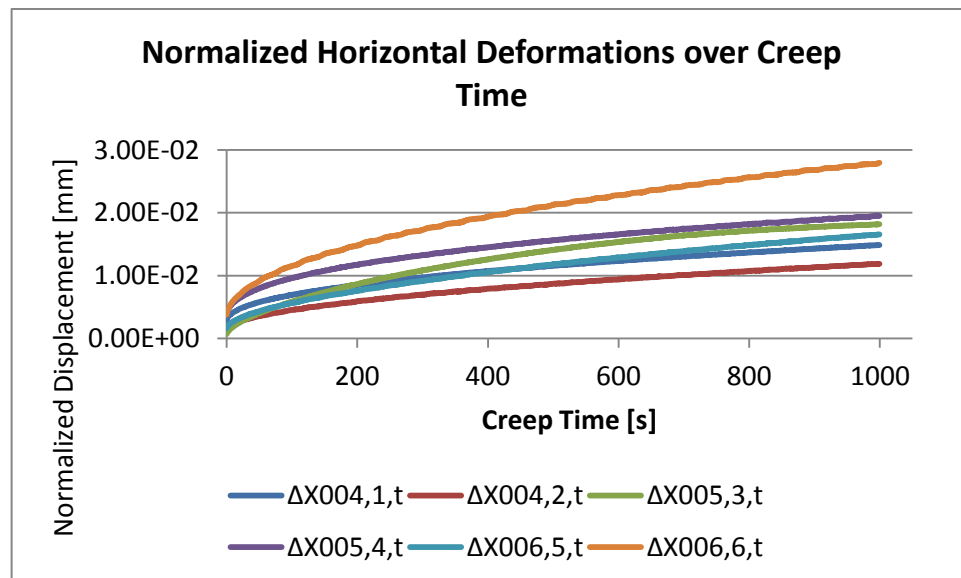


Figure K-2 Normalized Horizontal Deformations of HMA Specimens at -10 °C

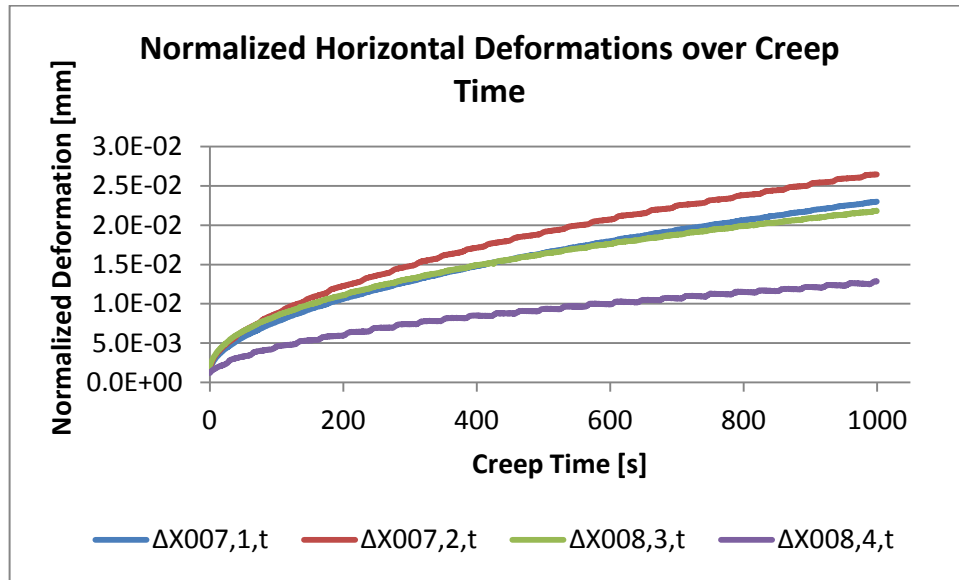


Figure K-3 Normalized Horizontal Deformations of HMA Specimens at 0 °C

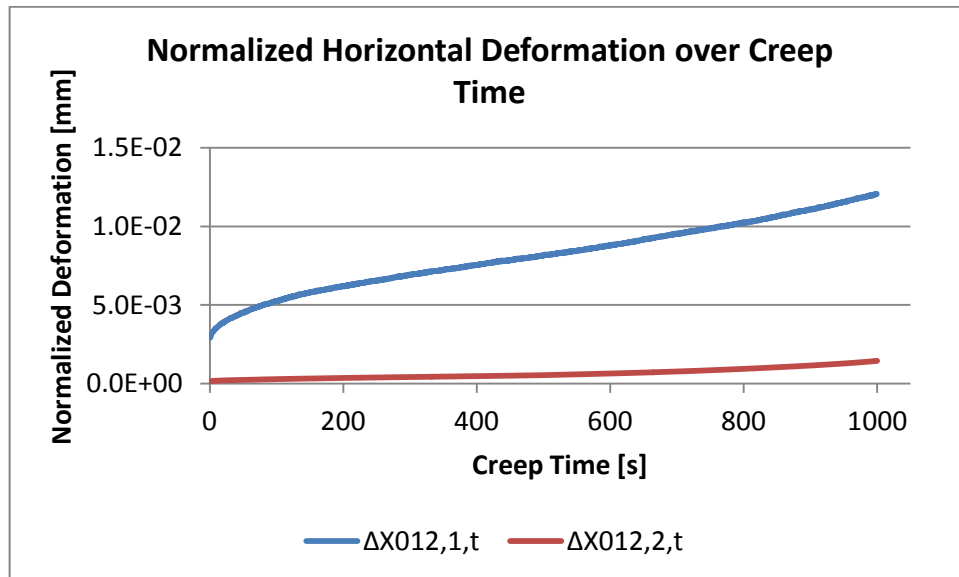


Figure K-4 Normalized Horizontal Deformations of CIR Specimens at -20 °C

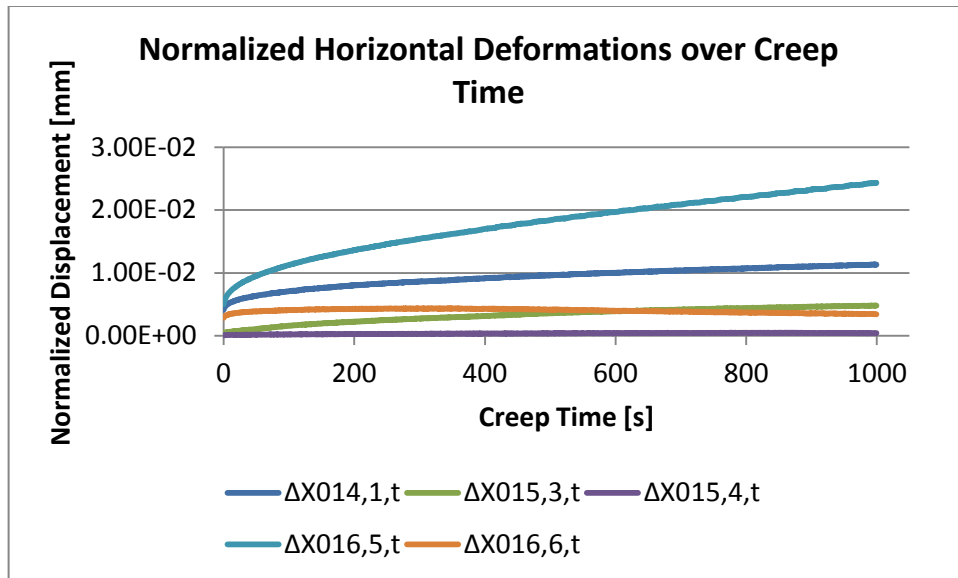


Figure K-5 Normalized Horizontal Deformations of two CIR Specimens at -10 °C

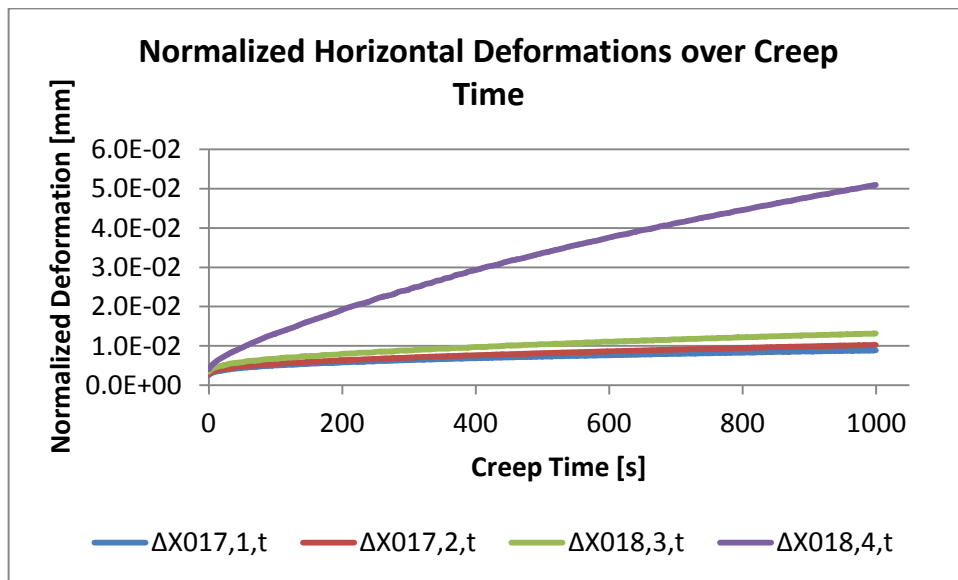


Figure K-6 Normalized Horizontal Deformations of two CIR Specimens at 0 °C

## APPENDIX L

SUMMARY OF THE RESULTS OF THE DATA ANALYSIS OF CREEP COMPLIANCE

TESTING



## APPENDIX L      CREEP COMPLIANCE SUMMARY

In this section, the dimensions and loads for all tested specimens are shown in Figure L-1 and Figure L-2. Consequently, Figure L-3 and Figure L-4 depict the summarizing calculations for the creep compliance determination.

Specimen	Temperature	Thicknesses $b$ [mm]						Loads $P$ [kN]		Diameter [mm] $D_{avg}$ :	Gauge Length [m] $GL$ :
		a	b	c	$b_j$	$b_{avg}$	$P_n$	$P_{avg}$			
001	-20°C	42.31	42.14	42.19	42.21	42.25	10.00	12.50	150.0	0.038	
002		42.15	42.35	42.33	42.28		15.00				
003		42.58	42.10	42.09	42.26	-	-				
004	-10°C	42.30	42.17	42.68	42.38	42.41	5.00	4.67			
005		42.44	42.32	42.50	42.42		4.50				
006		42.38	42.53	42.41	42.44	4.50					
007	±0°C	42.06	42.20	42.28	42.18	42.26	1.75	1.50			
008		42.22	42.20	42.57	42.33		1.25				

Figure L-1 Specimen Dimensions for HMA Mixture

Specimen	Temperature	Thicknesses $b$ [mm]						Loads $P$ [kN]		Diameter [mm]	Gauge Length [m]
		$a$	$b$	$c$	$b_i$	$b_{avg}$	$P_n$	$P_{avg}$			
011	-20°C	-	-	-	-	-	-	-	<b>150.0</b>	<b>0.038</b>	
012		42.19	41.91	42.28	42.13	<b>42.13</b>	5.00	<b>5.00</b>			
013		43.67	42.25	42.64	42.85	-	-	-			
014	-10°C	42.00	41.91	41.49	41.80	<b>42.13</b>	2.50	<b>3.17</b>			
015		42.70	42.56	42.59	42.62		3.50				
016		41.82	42.02	42.12	41.99		3.50				
017	±0°C	42.33	42.45	42.37	42.38	<b>42.24</b>	1.50	<b>1.50</b>			
018		41.92	42.11	42.28	42.10		1.50				

Figure L-2 Specimen Dimensions for CIR Mixture

face	-20°C			-10 °C			±0°C		
	$\Delta X_{\sigma,1}$	$\Delta Y_{\sigma,1}$	$\Delta Y_{\sigma,1}$	$\Delta X_{\sigma,1}$	$\Delta Y_{\sigma,1}$	$\Delta Y_{\sigma,1}$	$\Delta X_{\sigma,1}$	$\Delta Y_{\sigma,1}$	$\Delta Y_{\sigma,1}$
1	6.20E-03	-2.21E-02	-2.21E-02	1.16E-02	-2.22E-02	-2.22E-02	1.65E-02	-2.07E-02	-2.07E-02
2	7.07E-03	-1.02E-02	-1.02E-02	8.71E-03	-1.13E-02	-1.13E-02	1.91E-02	-1.74E-02	-1.74E-02
3	3.13E-03	-6.28E-03	-6.28E-03	1.41E-02	-1.35E-02	-1.35E-02	1.64E-02	-2.44E-02	-2.44E-02
4	1.04E-02	-9.92E-03	-9.92E-03	1.56E-02	-3.96E-02	-3.96E-02	7.77E-03	-1.78E-02	-1.78E-02
5				1.18E-02	-1.77E-02	-1.77E-02			
6				2.13E-02	-3.19E-02	-3.19E-02			
Trimmed mean	$\Delta X_i$	$\Delta Y_i$	$\Delta Y_i$	$\Delta X_i$	$\Delta Y_i$	$\Delta Y_i$	$\Delta X_i$	$\Delta Y_i$	$\Delta Y_i$
Ratio of horiz. to vert. defl.	$\frac{X}{Y}$	=	0.66	$\frac{X}{Y}$	=	0.62	$\frac{X}{Y}$	=	0.85
$C_{empl}$	0.63								
$C_{empl}$ check	0.644	$\leq C_{empl}$	1.511	0.644	$\leq C_{empl}$	1.511	0.644	$\leq C_{empl}$	1.511
Poisson's ratio	$\nu$	=	0.52	$\nu$	=	0.45	$\nu$	=	0.93
v check	0.05	$\leq \nu$	0.50	0.05	$\leq \nu$	0.50	0.05	$\leq \nu$	0.50
Creep Compliance	creep time t [s]	$\Delta X_{m,t}$ [mm]	$D(t)$ [1/GPa]	creep time t [s]	$\Delta X_{m,t}$ [mm]	$D(t)$ [1/GPa]	creep time t [s]	$\Delta X_{m,t}$ [mm]	$D(t)$ [1/GPa]
	0	1.542E-03	1.301E-02	0	2.431E-03	5.999E-02	0	1.645E-03	7.562E-02
	1	1.656E-03	1.397E-02	1	2.687E-03	6.630E-02	1	1.956E-03	8.991E-02
	2	1.759E-03	1.484E-02	2	2.888E-03	7.127E-02	2	2.211E-03	1.016E-01
	5	2.028E-03	1.711E-02	5	3.262E-03	8.049E-02	5	2.770E-03	1.273E-01
	10	2.348E-03	1.981E-02	10	3.682E-03	9.087E-02	10	3.409E-03	1.567E-01
	20	2.861E-03	2.414E-02	20	4.285E-03	1.057E-01	20	4.280E-03	1.967E-01
	50	3.436E-03	2.898E-02	50	5.531E-03	1.365E-01	50	6.133E-03	2.819E-01
	100	4.227E-03	3.566E-02	100	7.004E-03	1.728E-01	100	8.081E-03	3.714E-01
ME PDG Input									

Figure L-3 Creep Compliance Calculations for HMA Specimens

face	-20°C			-10 °C			±0°C		
	$\Delta X_{o,t}$	$\Delta Y_{o,t}$	$\Delta Y_{o,t} = \frac{\Delta X_{o,t}}{\Delta Y_{o,t}}$	$\Delta X_{o,t}$	$\Delta Y_{o,t}$	$\Delta Y_{o,t} = \frac{\Delta X_{o,t}}{\Delta Y_{o,t}}$	$\Delta X_{o,t}$	$\Delta Y_{o,t}$	$\Delta Y_{o,t} = \frac{\Delta X_{o,t}}{\Delta Y_{o,t}}$
1	8.16E-03	-2.06E-02	0.36	9.64E-03	-2.55E-02	0.49	7.28E-03	-1.53E-02	0.45
2	5.34E-04	-3.26E-03			-5.12E-03		8.16E-03	-1.17E-02	
3				3.57E-03	-1.76E-03		1.04E-02	-2.58E-02	
4				3.50E-04	-8.22E-03		3.37E-02	-3.09E-02	
5				1.84E-02	-4.03E-02				
6				4.12E-03	-1.96E-02				
Trimmed mean	4.35E-03	1.19E-02		7.21E-03	1.46E-02		9.29E-03	2.06E-02	
Ratio of horiz. to vert. defl.			0.36			0.49			0.45
$C_{empl}$			1.41			0.95			1.08
$C_{empl}$ check	0.644	$\leq C_{empl}$	1.511	0.644	$\leq C_{empl}$	1.511	0.644	$\leq C_{empl}$	1.511
Poisson's ratio			0.09			0.25			0.19
v check	0.05	$\leq v \leq$	0.50	0.05	$\leq v \leq$	0.50	0.05	$\leq v \leq$	0.50
Creep Compliance			OK			OK			OK
ME PDG Input	creep time t [s]	$\Delta X_{m,t}$ [mm]	$D(t)$ [1/GPa]	creep time t [s]	$\Delta X_{m,t}$ [mm]	$D(t)$ [1/GPa]	creep time t [s]	$\Delta X_{m,t}$ [mm]	$D(t)$ [1/GPa]
	0	2.907E-03	1.365E-01	0	2.472E-03	1.239E-01	0	3.099E-03	3.703E-01
	1	2.996E-03	1.406E-01	1	2.669E-03	1.337E-01	1	3.316E-03	3.963E-01
	2	3.099E-03	1.455E-01	2	2.789E-03	1.397E-01	2	3.506E-03	4.190E-01
	5	3.317E-03	1.557E-01	5	3.034E-03	1.520E-01	5	3.799E-03	4.539E-01
	10	3.556E-03	1.669E-01	10	3.281E-03	1.644E-01	10	4.114E-03	4.916E-01
	20	3.879E-03	1.821E-01	20	3.594E-03	1.801E-01	20	4.529E-03	5.412E-01
	50	4.519E-03	2.121E-01	50	4.186E-03	2.098E-01	50	5.287E-03	6.317E-01
	100	5.256E-03	2.467E-01	100	4.835E-03	2.423E-01	100	6.075E-03	7.259E-01

Figure L-4 Creep Compliance Calculations for CIR Specimens

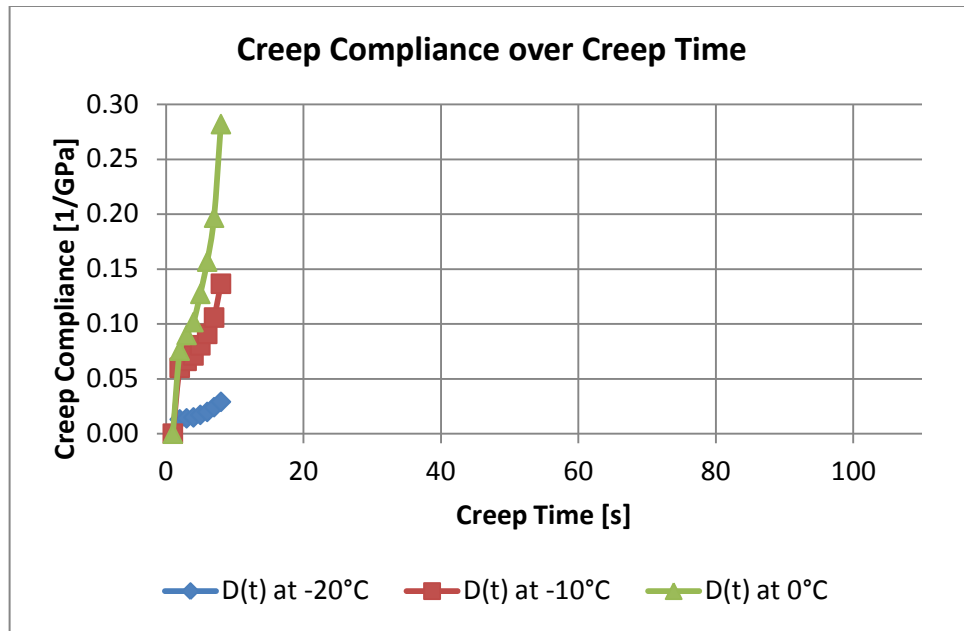


Figure L-5 Creep Compliance of HMA for Superpave Software Input

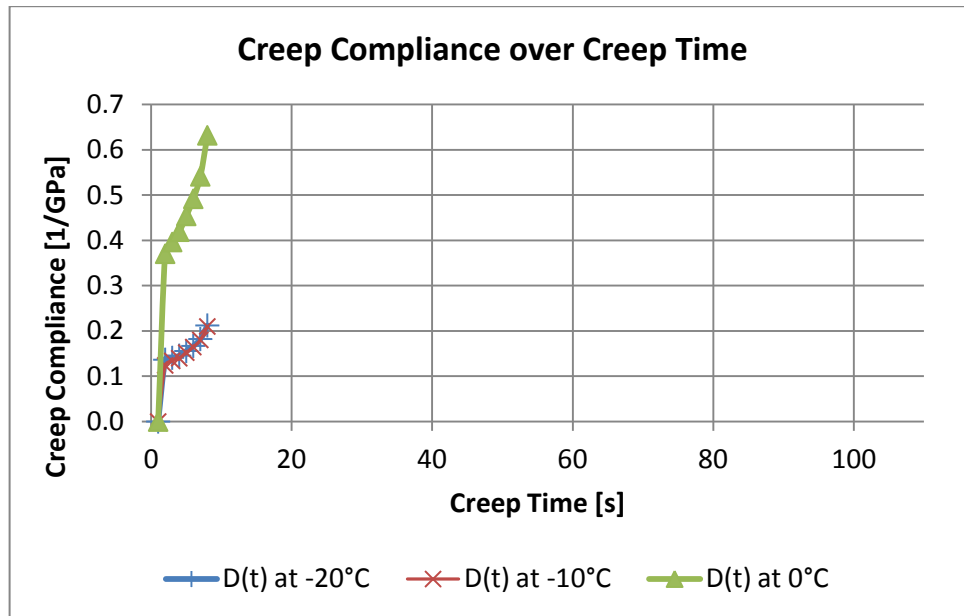


Figure L-6 Creep Compliance of CIR for Superpave Software Input

## APPENDIX M

### SUMMARY OF THE RESULTS OF THE TENSILE STRENGTH TESTING

**APPENDIX M TENSILE STRENGTH SUMMARY**

This section of the Appendix contains the results from the tensile strength testing of both materials. Complementing Figure 4-7 in section 4.3.2, the equivalent graph for CIR (Figure M-1) will be shown in this section.

Table M-1 Tensile Strength Test Results for HMA

Specimen	Temperature [°C]	Tensile Stress [MPa]	Avg. Tensile Strength [MPa]	Avg. Tensile Strength [psi]
001	-20	6.03	5.90	856.04
002	-20	6.16		
003	-20	5.52		
004	-10	6.13	5.92	857.90
005	-10	5.85		
006	-10	5.77		
007	0	4.48	4.40	637.28
008	0	4.31		

Table M-2 Tensile Strength Test Results for CIR

Specimen	Temperature [°C]	Tensile Stress [MPa]	Avg. Tensile Strength [MPa]	Avg. Tensile Strength [psi]
011	-20	-	(disregarded*)	
012	-20	0.74	0.57	82.93
013	-20	0.40	(disregarded*)	
014	-10	0.91	0.67	97.21
015	-10	0.44		
016	-10	0.65		
017	0	0.59	0.67	96.57
018	0	0.75		

\* These specimens broke early in the creep test and could therefore not be used in this analysis.

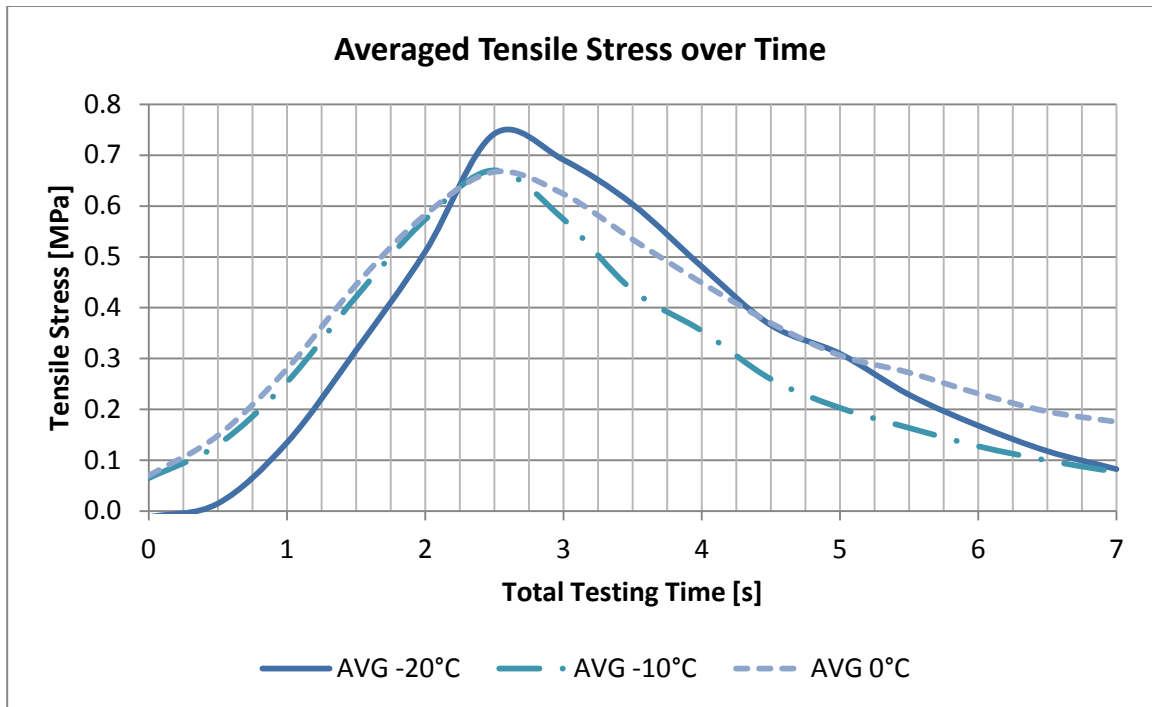


Figure M-1 Averaged Tensile Stress over Time for CIR Mixture

\* Values taken from failed creep test for display only.

While Figure 4-7 and Figure M-1 portray the averaged results for tensile strength testing, Figure M-2 and Figure M-3 show the detailed data of all tested specimens.



Total Time (s)	Specimen 001(-20 C)			Specimen 002(-20 C)			Specimen 003(-20 C)			Specimen 004(-10 C)			Specimen 005(-10 C)			Specimen 006(-10 C)			Specimen 007(+0 C)			Specimen 008(+0 C)			
	Load raw [kN]	Load mod [kN]	Tensile Stress [MPa]	Load raw [kN]	Load mod [kN]	Tensile Stress [MPa]	Load raw [kN]	Load mod [kN]	Tensile Stress [MPa]	Load raw [kN]	Load mod [kN]	Tensile Stress [MPa]	Load raw [kN]	Load mod [kN]	Tensile Stress [MPa]	Load raw [kN]	Load mod [kN]	Tensile Stress [MPa]	Load raw [kN]	Load mod [kN]	Tensile Stress [MPa]	Load raw [kN]	Load mod [kN]	Tensile Stress [MPa]	
0.0	-1.18	1.18	0.12	0.21	-0.21	-0.03	0.02	0.19	-0.19	-0.02	0.02	0.25	0.25	0.02	0.07	-0.07	-0.01	0.00	-13.04	13.04	1.31	-23.31	23.31	2.34	1.22
0.5	-1.93	1.93	0.19	0.10	-0.10	-0.01	0.01	0.07	-0.09	-0.01	0.07	0.76	0.76	0.08	-1.50	1.50	0.15	0.07	-18.54	18.54	1.87	-26.48	26.48	2.66	1.53
1.0	-3.26	3.26	0.33	-0.82	0.82	0.08	0.20	2.24	-2.24	0.22	-1.74	1.74	0.17	3.31	-3.31	0.33	0.24	0.24	-23.76	23.76	2.39	-29.41	29.41	2.95	1.86
1.5	-5.87	5.87	0.59	-3.79	3.79	0.36	0.62	-5.61	5.61	0.56	-4.69	4.69	0.47	6.32	-6.32	0.63	0.55	-28.33	28.33	2.85	-31.97	31.97	3.21	2.20	
2.0	-9.63	9.63	0.99	-9.28	9.28	0.93	1.16	-11.59	11.59	1.16	1.03	8.62	8.62	0.86	-10.23	10.23	1.02	0.96	-32.28	32.28	3.25	-34.20	34.20	3.43	2.54
2.5	-15.63	15.63	1.57	-15.71	15.71	1.58	2.46	-17.51	17.51	1.76	1.64	-15.62	15.62	1.56	-13.85	13.85	1.39	1.54	-35.68	35.68	3.59	-36.09	36.09	3.62	2.92
3.0	-21.84	21.84	2.20	-22.88	22.88	2.30	4.46	-24.47	24.47	4.26	4.29	-43.18	43.18	4.32	-40.49	40.49	4.05	4.24	-43.41	43.41	4.37	-41.37	41.37	4.15	4.25
3.5	-28.12	28.12	2.83	-29.97	29.97	3.01	3.07	-30.61	30.61	3.07	2.97	-29.15	29.15	2.92	-26.77	26.77	2.68	3.07	-30.74	30.74	3.07	-32.85	32.85	3.32	3.63
4.0	-34.67	34.67	3.49	-37.11	37.11	3.73	3.69	-36.75	36.75	3.69	3.63	-33.64	33.64	3.37	-33.64	33.64	3.37	3.58	-42.25	42.25	4.25	-40.27	40.27	4.04	3.95
4.5	-41.46	41.46	4.17	-44.15	44.15	4.43	4.78	-47.55	47.55	4.78	4.90	-49.82	49.82	4.99	-47.15	47.15	4.72	4.90	-48.97	48.97	4.90	-44.14	44.14	4.44	4.51
5.0	-48.15	48.15	4.84	-50.63	50.63	5.06	5.06	-50.63	50.63	5.06	5.45	-56.03	56.03	5.61	-53.32	53.32	5.33	5.44	-44.48	44.48	4.48	-42.71	42.71	4.28	4.73
5.5	-54.39	54.39	5.47	-56.51	56.51	5.67	5.21	-51.87	51.87	5.21	5.45	-56.03	56.03	5.61	-53.32	53.32	5.33	5.44	-44.48	44.48	4.48	-42.71	42.71	4.28	4.73
6.0	-53.95	53.95	6.03	-61.36	61.36	6.16	5.52	-54.99	54.99	5.52	5.90	-61.24	61.24	6.13	-58.49	58.49	5.85	5.77	-44.48	44.48	4.48	-43.03	43.03	4.31	4.30
6.5	-1.64	1.64	0.16	0.21	-0.21	-0.02	0.02	-26.76	26.76	2.69	1.33	-28.45	28.45	2.85	-28.68	28.68	2.87	3.34	-33.41	33.41	3.34	-42.20	42.20	4.23	3.88
7.0	0.24	-0.24	-0.02				2.30	-9.10	9.10	0.91	2.08	-29.31	29.31	2.93	1.97	-42.70	42.70	4.30	-40.98	40.98	4.11	-40.98	40.98	4.11	3.46
8.0							2.30	-18.59	18.59	1.87	1.87	-5.31	5.31	0.53	-16.33	16.33	1.63	2.61	-26.05	26.05	2.61	-40.41	40.41	4.07	3.16
8.5							2.30	-14.87	14.87	1.49	1.49	-3.76	3.76	0.36	-13.39	13.39	1.34	2.35	-23.52	23.52	2.35	-33.84	33.84	3.41	2.72
9.0							2.30	-12.56	12.56	1.26	1.26	-2.43	2.43	0.24	-9.99	9.99	1.00	2.15	-21.46	21.46	2.15	-27.99	27.99	2.82	2.34
9.5							2.30	-10.64	10.64	1.07	1.07	-1.57	1.57	0.16	-6.42	6.42	0.64	2.03	-20.25	20.25	2.03	-20.95	20.95	2.11	1.94
10.0							2.30	-8.93	8.93	0.90	0.90	-1.03	1.03	0.10	-3.44	3.44	0.34	1.86	-18.78	18.78	1.86	-13.34	13.34	1.34	1.52
10.5							2.30	-7.36	7.36	0.74	0.74	-0.68	0.68	0.07	-1.66	1.66	0.17	1.74	-17.41	17.41	1.74	-9.18	9.18	0.92	1.24
11.0							2.30	-6.63	6.63	0.67	0.67	-0.41	0.41	0.04	-0.62	0.62	0.06	1.61	-16.08	16.08	1.61	-6.26	6.26	0.63	1.02
11.5							2.30	-5.78	5.78	0.58	0.58	-0.13	0.13	0.01	-0.24	0.24	0.02	1.51	-15.10	15.10	1.51	-4.45	4.45	0.45	0.85

Figure M-2 Detailed Strength Test Data for HMA Mixtures

Total Time (s)	Specimen 012 (~20°C)			Specimen 013* (~20°C)			Specimen 014 (~10°C)			Specimen 015 (~10°C)			Specimen 016 (~10°C)			Specimen 017 (0°C)			Specimen 018 (0°C)			AVG 0°C Tensile Stress [MPa]
	Load raw [kN]	Load mod [kN]	Tensile Stress [MPa]	Load raw [kN]	Load mod [kN]	Tensile Stress [MPa]	Load raw [kN]	Load mod [kN]	Tensile Stress [MPa]	Load raw [kN]	Load mod [kN]	Tensile Stress [MPa]	Load raw [kN]	Load mod [kN]	Tensile Stress [MPa]	Load raw [kN]	Load mod [kN]	Tensile Stress [MPa]	Load raw [kN]	Load mod [kN]	Tensile Stress [MPa]	
0.0	0.11941	-0.12	-0.01	-0.2215	0.22	0.02	0.0048	0.00	0.00	1.41	0.14	-0.546	0.55	0.06	-1.518	1.52	0.15	0.0667	-0.07	-0.01	0.07	
0.5	-0.1482	0.15	0.01	-0.303	0.30	0.03	-0.583	0.58	0.06	-2.08	2.08	-1.245	1.25	0.13	-2.988	3.00	0.30	-0.156	0.16	0.02	0.15	
1.0	-1.3372	1.34	0.13	-0.4079	0.41	0.04	-2.614	2.61	0.27	-2.741	2.74	-2.211	2.21	0.22	-4.07	4.07	0.41	-1.771	1.77	0.18	0.28	
1.5	-3.1391	3.14	0.32	-1.3174	1.32	0.13	-5.169	5.17	0.52	-3.63	3.63	-3.754	3.75	0.38	-4.965	4.96	0.50	-4.144	4.14	0.42	0.45	
2.0	-5.064	5.06	0.51	-1.3174	1.32	0.13	-7.319	7.32	0.74	-4.403	4.40	-5.339	5.34	0.54	-5.623	5.62	0.56	-6.077	6.08	0.61	0.58	
2.5	-7.3646	7.36	0.74	-4.0578	4.06	0.40	-8.399	9.00	0.91	-4.468	4.47	-6.456	6.46	0.65	-5.853	5.85	0.59	-7.399	7.40	0.75	0.67	
3.0	-6.8548	6.85	0.69	0.1208	-0.12	-0.01	-7.376	7.38	0.75	-3.5	3.50	-6.187	6.19	0.63	-5.807	5.81	0.58	-7.106	7.11	0.72	0.62	
3.5	-5.987	5.99	0.60				-5.246	5.25	0.53	-2.211	2.21	-4.863	4.86	0.49	-5.375	5.37	0.54	-6.254	6.25	0.63	0.53	
4.0	-4.7729	4.77	0.48				-4.291	4.29	0.44	-1.375	1.38	-4.863	4.86	0.49	-4.368	4.37	0.44	-5.51	5.51	0.56	0.45	
4.5	-3.6237	3.63	0.37				-3.136	3.14	0.32	-0.957	0.96	-3.617	3.62	0.37	-3.718	3.72	0.37	-4.746	4.75	0.48	0.37	
5.0	-3.0718	3.07	0.31				-2.5	2.50	0.25	-0.689	0.70	-2.831	2.83	0.29	-3.256	3.26	0.33	-3.869	3.87	0.39	0.31	
5.5	-2.2707	2.27	0.23				-2.072	2.07	0.21	-0.469	0.47	-2.317	2.32	0.23	-3.197	3.20	0.32	-3.313	3.31	0.33	0.27	
6.0	-1.6673	1.67	0.17				-1.558	1.56	0.16	-0.155	0.15	-2.073	2.07	0.21	-2.818	2.82	0.28	-2.82	2.82	0.28	0.23	
6.5	-1.1639	1.17	0.12				-1.125	1.13	0.11	0.0201	-0.02	-1.847	1.85	0.19	-2.577	2.58	0.26	-2.289	2.29	0.23	0.20	
7.0	-0.8166	0.82	0.08				-0.862	0.86	0.09	0.074	-0.07	-1.491	1.49	0.15	-2.512	2.51	0.25	-1.97	1.97	0.20	0.18	

Figure M-3 Detailed Strength Test Data for CIR Mixtures

## APPENDIX N

### DATA OF THE TRAFFIC AND CLIMATE FOR RHODE ISLAND ROUTE 2

**APPENDIX N            TRAFFIC AND WEATHER DATA FOR CONSTRUCTION SITE**

Table N-1 below shows the traffic amounts of Route 2. An annual growth rate of 1.25% will lead to an 18-kip-ESAL amount of 10,549,906 after the analysis period of 20 years (Lee, Marcus, et al. 2003).

Table N-1 Traffic Amount and Distribution for Route 2

FHWA Vehicle Class.	FHWA Vehicle Types	Current Traffic	Percentage	ESAL factor	Total ESAL
4	Busses	50	3.7%	1.67	30,478
5	2Ax-6Tr	644	47.8%	1.67	392,550
6	3Ax	176	13.1%	1.28	82,227
8	4Ax and more	134	10.0%	2.86	139,883
9	5Ax	326	24.2%	2.24	266,538
10	6Ax and more	8	0.6%	1.95	5,694
11	5Ax or less	8	0.6%	6.09	17,783
Sum of ESAL in 1st year on Rt. 2:					935,152

The following information contains information concerning the climate conditions the software used to predict the performance.

**Climate Station File:**

C:\Users\Al Capone\Documents\Studium\Fachsem 10\Master Thesis\ME PDG\HMA  
(default)\route2\_1.icm

**Climate station(s) used in analysis:**

1. 16.5 miles WILLIMANTIC, CT - WINDHAM AIRPORT Lat. 41.44 Lon. -72.11  
Ele. 250 Months: 116 (C)
2. 27.0 miles PROVIDENCE, RI - THEODORE F GREEN STATE APT Lat. 41.43  
Lon. -71.26 Ele. 53 Months: 116 (C)
3. 27.7 miles WORCESTER, MA - WORCESTER REGIONAL AIRPORT Lat. 42.16  
Lon. -71.53 Ele. 966 Months: 116 (C)
4. 36.2 miles WESTERLY, RI - WESTERLY STATE AIRPORT Lat. 41.21 Lon. -  
71.48 Ele. 72 Months: 79 (M1)
5. 37.5 miles GROTON NEW LONDON, CT - GROTON-NEW LONDON  
AIRPORTT Lat. 41.2 Lon. -72.03 Ele. 24 Months: 75 (C)

**Table N-2 Annual Climate Statistics**

<b>Mean annual air temperature (°F):</b>	50.37
<b>Mean annual rainfall (in):</b>	41.98
<b>Freezing index (°F-days):</b>	508.45
<b>Average Annual Number of Freeze/Thaw Cycles:</b>	81

Table N-3 Average Monthly Quintile Temperatures - Surface

Month	1st	2nd	3rd	4th	5th	Mean	Std.
	Quintile	Quintile	Quintile	Quintile	Quintile	Temp.	Dev.
	(°F)	(°F)	(°F)	(°F)	(°F)	(°F)	(°F)
January	16	24.6	30.7	36.4	45.4	30.6	10.5
February	20.8	29.3	35.1	42.1	52.9	36	11.6
March	27.3	35.6	41.8	49.7	64	43.7	13.2
April	38	46	53.4	63.3	80.4	56.2	15.3
May	48.7	56.8	64.2	75.1	93	67.6	16
June	57.3	66.5	75	87.7	103.3	78	16.7
July	62.6	70.5	79.7	93.4	106.2	82.5	16.1
August	62.2	70	77	89.8	103.9	80.6	15.2
September	52.6	62.2	69.3	79.3	94.1	71.5	14.8
October	39.2	48	55.3	63.1	77.9	56.7	13.8
November	31.1	39.6	45.7	51.9	61.9	46	11
December	22.1	30.1	35.6	41.2	51	36	10.3

Table N-4 Average Monthly Quintile Temperatures - Sublayer 1

Month	1st	2nd	3rd	4th	5th	Mean	Std.
	Quintile	Quintile	Quintile	Quintile	Quintile	Temp.	Dev.
	(°F)	(°F)	(°F)	(°F)	(°F)	(°F)	(°F)
January	16.5	24.8	30.7	36.3	44.8	30.6	10.2
February	21.2	29.5	35.1	41.8	52.1	36.0	11.1
March	27.8	35.8	41.9	49.5	63.1	43.6	12.7
April	38.6	46.5	53.5	63	79.3	56.2	14.7
May	49.4	57.2	64.3	74.7	91.9	67.5	15.4
June	58.0	67.0	75.1	87.2	102.3	77.9	16.0
July	63.4	71.1	79.8	92.8	105.1	82.5	15.4
August	62.9	70.5	77.3	89.3	102.8	80.6	14.5
September	53.3	62.7	69.5	78.9	93.1	71.5	14.2
October	39.8	48.4	55.5	63.0	77.0	56.7	13.3
November	31.6	39.9	45.8	51.7	61.3	46.1	10.6
December	22.5	30.3	35.6	41.0	50.4	36.0	9.9

Table N-5 Average Monthly Quintile Temperatures - Sublayer 2

Month	1st	2nd	3rd	4th	5th	Mean	Std.
	Quintile	Quintile	Quintile	Quintile	Quintile	Temp.	Dev.
	(°F)	(°F)	(°F)	(°F)	(°F)	(°F)	(°F)
January	17.4	25.3	30.9	36	43.8	30.7	9.5
February	22.1	29.9	35.2	41.2	50.5	35.8	10.2
March	28.7	36.4	42	49	61.4	43.5	11.8
April	39.7	47.2	53.9	62.4	77.4	56.1	13.6
May	50.6	58.1	64.6	73.9	89.8	67.4	14.1
June	59.2	68	75.4	86.2	100.2	77.8	14.8
July	64.8	72.2	80.1	91.7	103.1	82.4	14
August	64.2	71.5	77.7	88.4	100.8	80.5	13.3
September	54.6	63.6	69.9	78.3	91.3	71.5	13
October	40.9	49.2	55.9	62.7	75.3	56.8	12.3
November	32.5	40.5	46	51.4	60.2	46.1	9.9
December	23.4	30.8	35.8	40.7	49.4	36	9.2

Table N-6 Monthly Rainfall Statistics

Month	Mean	Std.
	Rainfall	Dev.
	(in)	(in)
January	2.76	1.1
February	4.38	0.93
March	3.82	1.83
April	3.84	1.02
May	4.07	2.83
June	2.87	1.21
July	3.62	1.14
August	4.04	1.62
September	2.88	1.57
October	3.2	1.72
November	3.15	1.12

## APPENDIX O

RESULTS OF THE SIMULATIONS OF

THREE DIFFERENT PAVEMENT STRUCTURES



## APPENDIX O SIMULATION RESULTS

This Appendix contains the simulation results for all three pavement structures. The results were stripped as the original shows the distress magnitudes after every month which is not suitable here. Instead, the results after every year are shown for the HMA pavement (“HMA”), CIR with 5 in. of base material (“CIR (1)”), and CIR with 2 in. of base material (“CIR (2)”).

Table O-1 HMA Simulation Output

Pavement Age		Month	Longitudinal Cracking	Alligator Cracking	Transverse Cracking	Total Rutting	IRI	IRI at Reliability
mo	yr		(ft/mi)	(%)	(ft/mi)	(in)	(in/mi)	(in/mi)
1	0.08	August	0.04	0.0011	0	0.162	69.5	94.36
12	1.00	July	0.39	0.0067	0	0.233	72.6	98.79
24	2.00	July	1.19	0.0147	0	0.272	74.8	101.84
36	3.00	July	1.88	0.0211	0	0.292	76.4	104.00
48	4.00	July	2.77	0.0279	0	0.308	77.9	106.13
60	5.00	July	3.75	0.0349	0	0.322	79.5	108.36
72	6.00	July	4.84	0.0421	0	0.336	81.2	110.68
84	7.00	July	5.98	0.0493	0	0.346	82.8	112.92
96	8.00	July	7.34	0.0570	0	0.356	84.5	115.29
108	9.00	July	8.82	0.0649	0	0.364	86.3	117.67
120	10.00	July	10.70	0.0738	0	0.375	88.2	120.24
132	11.00	July	12.00	0.0811	0	0.382	90.0	122.72
144	12.00	July	13.70	0.0890	0	0.388	91.9	125.28
156	13.00	July	15.30	0.0971	0	0.396	93.9	127.95
168	14.00	July	17.10	0.1050	0	0.403	96.0	130.70
180	15.00	July	19.00	0.1140	0	0.409	98.0	133.43
192	16.00	July	21.10	0.1220	0	0.415	100.2	136.28
204	17.00	July	23.30	0.1310	0	0.421	102.4	139.13
216	18.00	July	26.00	0.1420	0	0.428	104.7	142.14
228	19.00	July	28.00	0.1500	0	0.433	106.9	145.08
240	20.00	July	30.30	0.1590	0	0.438	109.3	148.08

Table O-2 CIR (1) Simulation Output

Pavement Age		Month	Longitudinal Cracking	Alligator Cracking	Transverse Cracking	Total Rutting	IRI	IRI at Reliability
mo	yr		(ft/mi)	(%)	(ft/mi)	(in)	(in/mi)	(in/mi)
1	0.08	August	85	0.31	0	0.25	73.1	99.5
12	1.00	July	1600	2.38	0	0.38	79.7	108.9
24	2.00	July	3520	4.90	0	0.46	85.1	116.8
36	3.00	July	4740	6.95	0	0.51	88.6	121.6
48	4.00	July	5800	9.07	0	0.54	92.1	126.2
60	5.00	July	6490	11.00	0	0.58	95.6	130.9
72	6.00	July	7150	13.00	0	0.61	99.3	135.7
84	7.00	July	7670	15.00	0	0.64	102.6	140.0
96	8.00	July	8100	17.10	0	0.66	106.2	144.7
108	9.00	July	8450	19.10	0	0.68	109.7	149.2
120	10.00	July	8730	21.20	0	0.71	113.6	154.2
132	11.00	July	8920	22.80	0	0.73	116.9	158.5
144	12.00	July	9090	24.50	0	0.75	120.5	162.9
156	13.00	July	9220	26.10	0	0.77	124.1	167.5
168	14.00	July	9350	27.70	0	0.79	127.9	172.2
180	15.00	July	9470	29.30	0	0.80	131.5	176.8
192	16.00	July	9570	30.90	0	0.82	135.4	181.6
204	17.00	July	9660	32.60	0	0.83	139.3	186.4
216	18.00	July	9740	34.20	0	0.86	143.6	191.6
228	19.00	July	9800	35.50	0	0.87	147.4	196.3
240	20.00	July	9860	36.90	0	0.88	151.4	201.1

Table O-3 CIR (2) Simulation Output

Pavement Age		Month	Longitudinal Cracking	Alligator Cracking	Transverse Cracking	Total Rutting	IRI	IRI at Reliability
mo	yr		(ft/mi)	(%)	(ft/mi)	(in)	(in/mi)	(in/mi)
1	0.08	August	88.9	1.89	0	0.33	77.8	106.6
12	1	July	3970	22.7	0	0.514	98.5	134.72
24	2	July	7050	40.3	0	0.629	118.1	159.83
36	3	July	8220	50.7	0	0.686	132.9	178.38
48	4	July	8920	58.8	0	0.733	148.5	197.45
60	5	July	9230	64.3	0	0.776	162.4	214.23
72	6	July	9550	69.0	0	0.82	177.7	232.32
84	7	July	9770	73.1	0	0.853	193.8	251.22
96	8	July	9930	76.3	0	0.886	210.1	270.04
108	9	July	10000	79.0	0	0.913	226.6	288.91
120	10	July	10100	81.3	0	0.947	244.2	308.95
132	11	July	10200	82.9	0	0.97	259.1	325.69
144	12	July	10200	84.3	0	0.992	274.8	343.29
156	13	July	10300	85.5	0	1.016	289.9	360.04
168	14	July	10300	86.6	0	1.042	305.9	377.76
180	15	July	10300	87.6	0	1.062	323.3	396.95
192	16	July	10300	88.5	0	1.084	340.5	415.78
204	17	July	10400	89.4	0	1.103	358.8	435.76
216	18	July	10400	90.1	0	1.128	377.8	456.42
228	19	July	10400	90.7	0	1.145	394.1	474.12
240	20	July	10400	91.3	0	1.162	411.7	493.12

## **BIBLIOGRAPHY**

AASHTO. Standard Method, Washington, D.C.: American Association of State Highway and Transportation Officials, 2011.

Asphalt Institute, The. *mix design methods for asphalt concrete*. College Park, MD: The Asphalt Institute, 1984.

Atkins, Harold N. *Highway Materials, Soils, and Concretes*. Prentice Hall, 2002.

California Department of Transportation. "In-Place Recycling." *California Department of Transportation, Division of Maintenance*. February 19, 2008. <http://www.dot.ca.gov/hq/maint/FPMTAGChapter13-In-Place-Recycling.pdf> (accessed June 12, 2012).

Coree, Brian J., and Kera VanDerHorst. "National Transportation Library." *SUPERPAVE® Compaction*. 1998. <http://ntl.bts.gov/lib/9000/9000/9079/264superpave.pdf> (accessed 12 15, 2011).

Esri. *ArcGIS Rhode Island Soil Permeability and Depth to Water Table*. 2011. <http://www.arcgis.com/home/webmap/viewer.html?services=4ca8feb53f504b3c9c2b8bcefe0afd4d> (accessed June 20, 2012).

FHWA. *Cold In-Place Asphalt Recycling Application Checklist*. Washington, D.C.: U.S. Department of Transportation, 2005.

Lee, K. Wayne, Alan S. Marcus, Karissa Mooney, Sekhar Vajjhala, Edgar Kraus, and Kyungwon Park. *Development of Flexible Pavement Design Parameters for Use With The 1993 AASHTO Pavement Design Procedures*. FHWA-RIDOT-RTD-03-6, Providence, RI: Rhode Island Department of Transportation, 2003.

Lee, K. Wayne, Todd E. Brayton, and Houston Milton. *Development of Performance Based Mix Design for Cold In-Place Recycling (CIR) of Bituminous Pavements Based on Fundamental Properties*. Washington, D.C.: Federal Highway Administration, 2002.

Leon, Sofie, Eshan V. Dave, and Kyoungsoo Park. "Thermal Cracking Prediction Model and Software for Asphalt Pavements." *T&DI Congress 2011*. Chicago, IL: American Society of Civil Engineers, 2011. 667-676.

Mamlouk, Michael S., and John P. Zaniewski. *Materials for Civil and Construction Engineers*. Vol. Second Edition. Upper Saddle River, NJ: Pearson Prentice Hall, 2006.

Marasteanu, Mihai, et al. "Investigation of Low Temperature Cracking in Asphalt Pavements." Technical Report, St. Paul, MN, 2007.

Roque, Reynaldo, and William G. Buttlar. "The Development of a Measurement and Analysis System to accurately determine Asphalt Concrete Properties using the Indirect Tensile Mode." *Asphalt Paving Technology*. Charlestown, SC: Association of Asphalt Paving Technologies, 1992. 304-332.

Steen, Kristina. *Prediction of Rutting and Fatigue Cracking of Cold In-Place Recycling Asphalt Pavements Using the VESYS Computer Program*. Master Thesis, Kingston, RI: University of Rhode Island, 2001.

The Asphalt Institute. "Understanding Emulsified Asphalts." *Educational Series*, August 1979: 1-5.

Walker, Dwight. "Asphalt Emulsions 101." *Asphalt*, March 2012: 7-10.